Department of Chemistry

Investigation of the Impact of Nitrate Injection to Control Souring Problem in Oil Reservoir: Benefit and Side Effects on Steel Materials

Amalia Yunita Halim

This thesis is presented for the Degree of

Master of Philosophy

of

Curtin University

August 2011

Declaration

To the best of my knowledge and belief this thesis contains no material previously published by any other person except where due acknowledgment has been made.

This thesis contains no material which has been accepted for the award of any other degree or diploma in any university.

Signature: …….

Date: ……...

Abstract

The successful control of reservoir souring by nitrate injection has been well documented in the literature. Recent interest has centred on how nitrate application can increase the corrosion risk in pipelines and metal equipment. This study was conducted to observe the impact of nitrate reducing bacteria (NRB) and sulphate reducing bacteria (SRB) on the extent of corrosion on UNS S31603 and ASTM-A572-50 carbon steel, two commonly used materials in the oil and gas industry. The bacteria used in this experimental study were indigenous bacteria, isolated from the crude oil and production water samples of an oil field off the northwest of Western Australia. The NRB were isolated using nitrate broth, targeting nitrate reducers while SRB were isolated using Starkey media, targeting lactate utilizing bacteria (Desulfotomaculum and Desulfovibrio). In this study, a mixture of corrosive production water which contains a high level of chloride (21000 mg/L) supplemented with 10% (v/v) crude oil was used as the testing solution. The crude oil was taken into account because in the oil field it serves as the carbon source for the bacterial growth and it may also influence the corrosion behaviour of any steel material. However, this study has limited its scope to observe the impact of SRB and NRB using electrochemical techniques in a closed batch culture system without any water/nutrient renewal.

The basic experimental design for the two materials investigated, UNS S31603 and the ASTM-A572-50 carbon steel were similar. The experiments were conducted at 50°C in electrochemical cells containing 10% (v/v) crude oil in 700mL production water and purged with filter-sterilized nitrogen to keep the oxygen level as low as possible. Each of the two materials were evaluated under four different conditions: (1) control cell (no bacteria), (2) NRB inoculated cell, (3) SRB inoculated cell, and (4) mixed bacteria (NRB+SRB) inoculated cell. A small amount of 5 mM $NaNO_3$, was added as the growth nutrient for the bacteria. The open circuit potential (E_{corr}) of the corrosion coupons, and the redox potential (E_h) of the solution were monitored throughout the experiments. Additionally, the microbial populations were counted by Most Probable Number (MPN) method and direct counting method using a Helber Counting Chamber Z30000. A production water analytical analysis (nitrate, nitrite, sulphate and sulphide) was conducted before and after the experiment.

However, the exposure time in the corrosive media and the electrochemical analysis were different for each of the two materials tested. The immersion time for the UNS S31603 was 28 days and at the end of the immersion period, Linear Polarization Resistance (LPR) and Cyclic Polarization Scan (CPS) were carried out to determine the uniform and localized corrosion behaviour, respectively. The immersion time for the ASTM-A572-50 carbon steel was 21 days; LPR and electrochemical impedance spectroscopy (EIS) were conducted at an interval of every five days to monitor the biofilm formation, corrosion product formation and corrosion rate changes.

The results for both UNS S31603 and ASTM-A572-50 carbon steel demonstrated that: (1) The addition of nitrate, promoted the growth of NRB and suppressed the growth of SRB, hence H_2S production can be eliminated; (2) The NRB was able to oxidize the sulphide and also maintain a redox potential of above -100 mV, a level which inhibits the growth of SRB; (3) An increase in E_{corr} was observed in the presence and absence of bacteria.

The results from the UNS S31603 investigation show that: (1) NRB forms patchy biofilms on the UNS S31603 surfaces that weaken steel passivity and decrease its Critical Pitting Potential (CPP) to a greater extent than SRB after 28 days, (2) On the contrary, the corrosion rate of the UNS S31603 in the SRB inoculated cell is higher than the corrosion rate of the coupons in the NRB inoculated cell. This can be due to the formation of metastable pits as observed in the non-polarized corrosion coupon of the SRB inoculated cell after 28 days. (3) In order to study the effect of immersion time on the NRB and mixed bacteria (NRB+SRB), additional tests were conducted in the same manner for a short period of seven days of exposure. The results show that the CPP for the corrosion coupons in both the NRB inoculated cell and the mixed bacteria inoculated cell is higher than the corrosion coupons in the control cell. Therefore, it is postulated that, in this particular corrosive biochemical environment (high chloride level), the NRB and the mixed bacteria (NRB+SRB), may give beneficial protection to UNS S31603 for a short immersion time, and may give detrimental effects in longer exposure times.

The results from ASTM-A572-50 carbon steel investigation show that: (1) the EIS technique can be used to monitor the formation of biofilm and/or corrosion products

layers on the steel surface, (2) LPR, EIS and weight loss results show that in the tested corrosive environment, the presence of bacteria give lower rate of corrosion of ASTM-A572-50 carbon steel coupons compared to the corrosion coupons in the control cell. This indicates the corrosion inhibition activity of bacteria in this particular environment. (3) However, in the presence of bacteria, localized corrosion is inevitable as pits may form underneath bacterial biofilm.

In general, it is important to examine the corrosion impact of nitrate application on case by case basis because it is a complex mechanism and cannot be simply predicted based on electrochemical techniques alone. Further work is required to understand the biological materials that were produced by NRB, especially in the presence of other bacteria, which in a real situation in an oil reservoir may not only be SRB. Such studies can aid in understanding the fundamentals of the biochemistry of nitrate injection, thus resulting in important information for the process and design of field applications.

Table of Contents

List of Figures

List of Tables

Publications

The works performed during my research have so far led to two publications. Part of the work in Chapter 4 concerning the impact of nitrate injection on UNS S31603 has resulted in the following conference papers:

Halim A, Gubner R, Watkin E. Preliminary Study on Nitrate Injection to Control Souring Problem in Oil Reservoir: Benefits and Side Effects on Steel Material (UNS S31603). Corrosion 2011 Conference and Expo; 13-17 March 2011; Houston (USA): National Association of Corrosion Engineers (NACE), paper no 19153.

Halim A, Gubner R, Watkin E. Preliminary Study on The Benefits and Side Effects of Nitrate Injection on Pitting Corrosion of UNS S31603. 18th International Corrosion Congress (ICC); 20-24 November 2011; Perth (Australia): Australasian Corrosion Association (ACA), paper no 251. (Accepted)

Acknowledgement

I would like to express my sincere gratitude to my supervisors, Professor Rolf Gubner and Dr. Elizabeth Watkin, for their patience, guidance, support, and encouragement. I really appreciate the trust and the golden opportunity they given me to develop my research skills. My special thanks to Australian Development Scholarship (ADS) and Corrosion Centre for Education, Research and Technology (Corr-CERT) for the financial funding throughout my study. I also would like to acknowledge all the staff in the Department of Chemistry, School of Biomedical Sciences, Department of Applied Physics and The Learning Centre (TLC) for their assistance. I would like to extend my gratitude to John Fielder from TLC who has been helping me with my English for the past two years. I also appreciate the assistance and support from Julie Craig and Sarah Treadgold from the International Student Sponsor Unit (ISSU) since the first day I landed in Perth.

I am really grateful for the unforgettable time I spent with all my colleagues in Corr-CERT. Thank you for the encouragement, the great moral support and the friendship. Laura Machuca, for the help and the support in the first hardest few months of my study. I will always remember our first conversation in the library about pitting and crevice corrosion. Mike Oehler and Vedapriya Pandarinathan, for cheering me up every single day of my life and turned all my stress into laughter. I will definitely miss the coffee time, the chat in our cubicle and the note pads. Dr. Devendra Wasnik and Xiang Li, for their company in staying after hours in the last few months. Elaine Jee, for her patience and guidance in teaching me EIS and the time she spent for the meaningful discussion on my EIS circuit models.

Last but not least, I would like to thank God for His blessing and my family for their everlasting love, prayers and support all these years. My special thanks to my mother who always listens to all my problems and for her never-ending support. There are many other people that I cannot mention one by one, especially all my best friends for their encouragement and support. Finally, I would like to dedicate this thesis to all the people who are interested in the petroleum microbiology area.

CHAPTER 1: Introduction

In the petroleum industry, oil recovery is classified into three phases. The first is primary oil recovery; the oil is produced due to the natural drive from the pressure inside the reservoir. However, as the pressure rapidly drops, the primary oil production also decreases.[1, 2] The second phase is secondary oil recovery which is achieved by the injection of another fluid, water or gas, into the reservoir to maintain reservoir pressure and push oil towards the producing well. Therefore, there is an increase in oil production. The third phase is tertiary oil recovery which includes sophisticated techniques aimed at increasing microscopic efficiency or sweep efficiency.[2] The present study focuses on the impact of nitrate injection in the tertiary oil recovery phase. In tertiary oil recovery, nitrate is injected to promote the growth of indigenous microbes that can enhance oil production and control reservoir souring problems. However, it is also reported that nitrate injection may increase the risk of corrosion in the pipelines and metal equipment. This chapter begins with an overview of petroleum microbiology history, followed by an introduction to microbial corrosion and the electrochemical tests used for corrosion monitoring.

1.1 History of Petroleum Microbiology

The remarkable history of petroleum microbiology began as early as 1926 when Beckman found that microbes were able to release trapped oil in porous rock formations[3, 4] and Bastin reported his finding that Sulphate Reducing Bacteria (SRB) resided in samples from 67 wells located in California and Illinois.[5, 6] Beckman's discovery developed into new knowledge of enhancement of oil production using a microbial community, commonly called Microbial Enhanced Oil Recovery (MEOR).[1, 3, 4, 7-9] Bastin's discovery contributed to the knowledge of biodeterioration of materials or corrosion due to the presence and metabolic activities of microorganisms, commonly referred to as Microbiologically Influenced Corrosion (MIC).[10-12]

1.2 History Microbial Enhanced Oil Recovery (MEOR)

After Beckman's discovery, little was known about MEOR until Zobell and his research group carried out a systematic laboratory study in 1947.[3, 4] Thereafter, many other researchers made a contribution to the knowledge of MEOR.[3, 4, 13, 14] The decade of the 1990's is noted as a significant year for MEOR development,[13] as many well documented field trials were reported and also several meetings on MEOR were conducted.[4] By the end of the 1990s, MEOR had become a scientific and interdisciplinary method for enhanced oil recovery.

To date, conventional oil recovery approaches used in the oil industry can only recover approximately one third of the original-oil-in-place (OOIP), leaving behind a large quantity of residual oil which are trapped in the sand grains.[3, 9] The reasons behind this phenomenon are the high viscosity of the trapped oil which result in poor oil mobility,[7, 8] the high interfacial tension between oil-brine water which makes the capillary pressure hold the oil in the reservoir rock,[7, 9] and the strong bond between the oil and the surrounding reservoir rock (surface tension)[8] especially in oil wet formation. MEOR is believed to be one of the advanced technologies able to recover this oil in trapped formation due to the ability of bacteria to produce biosurfactants, biopolymers, bioacids, biomass, biosolvents, gases, and enzymes. This technology is implemented by the addition of nutrients and/or bacteria into oil reservoirs.[3, 4, 7-9, 13, 14]

Further investigation revealed that the addition of nitrate-based media into the reservoir was not only able to increase oil production but also mitigate reservoir souring problems, due to the activity of SRB. This method was known as Bio-Competitive Exclusion (BCX).[15-17] In BCX technology the microbial community is manipulated by introducing nitrate, not only as a microbial nutrient but also as an alternate electron acceptor. With the complementary naturally-occurring volatile fatty acid (VFA) inside the reservoir, it will selectively promote the growth of Nitrate Reducing Bacteria (NRB).[15, 16, 18] NRB will flourish and depress the growth and activity of SRB in using VFA.[15, 16, 19]

1.3 History of Reservoir Souring and Nitrate Injection

The reservoir souring was discovered after seawater was injected into the reservoir during secondary enhanced oil recovery to maintain pressure thus allowing more residual oil production.[18, 20, 21] Seawater is widely used in oil reservoirs, especially in offshore situations because of its proximity and availability.[22, 23] However, the anoxic condition within the reservoir, combined with the high sulphate content of seawater creates a favourable condition for SRB growth.[18, 20, 22, 24] The SRB within the oil reservoir could be either indigenous[5, 17] or introduced with the injection water.[17, 23]

The growth of SRB leads to biogenic hydrogen sulphide (H_2S) production. H_2S is a highly toxic, corrosive and flammable gas with an unpleasant odour.[24, 25] Sulphide contaminates produced oil, gas and water, thus decreasing the oil quality, representing a safety hazard, and causing corrosion of pipelines, tanks, processing and processing equipment.[26, 27]

Strategies for control of souring in oil reservoirs have been widely investigated. To mentioned a few: (1) removal of sulphate from injection water (e.g. by membrane separation)[22, 25, 28]; (2) removal of H_2S from sour water by treatment with physicochemical methods (e.g. with addition of iron salts)[28, 29]; (3) exposure of water to microwave and ultrasonic irradiations; (4) application of biocides such as glutaraldehyde, cocodiamines, and tetrakis hydroxymethyl phosphonium sulphate (THPS)[22, 25, 27, 28, 30]; and (5) microbiological sulphide production control by the use of nitrate and/or molybdite.[15, 17, 20-28, 30-34] The last two methods have been the most widely investigated.

To date, biocide application still has some drawbacks, as it is generally successful in controlling SRB in surface facilities but with limited effectiveness in the reservoir. This happens because chemical components in the reservoir may scavenge biocides through reaction or sorption.[22, 28] Additionally, treatment is often ineffective because biocides fail to kill SRB in protected niches (biofilm)[18, 21, 25] and inactivation of biocides after reaction with biofilm and minerals.[21] Furthermore,

biocides themselves may cause corrosion if applied in high concentrations or even kill the microbial community that may offer protection against corrosion; and the use of biocides targeting SRB may even lead to the emerge of biocide-resistant SRB.[18, 25] Another disadvantage of biocides is some recalcitrant biocides may lead to environmental problems, while biocides that decompose over exposure time may provide additional substrate for SRB growth.[21]

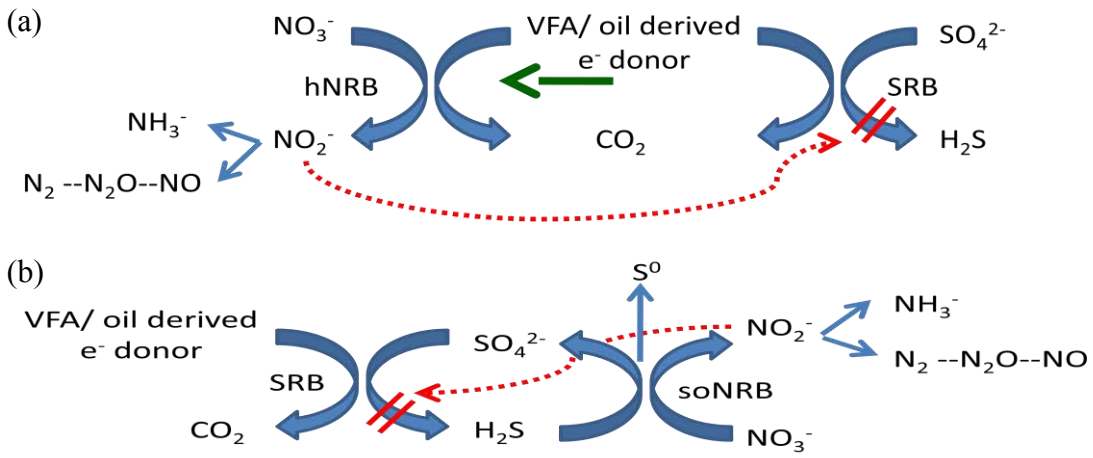

Figure 1.1 Souring control by nitrate injection in oil reservoir can be achieved by (a) biocompetitive exclusion of SRB by hNRB or (b) direct oxidation of sulphide couple with nitrate reduction by soNRB, as described in the text. Nitrite (indicated by red dashed line) is an important feature in both scenarios as it is an inhibitor for enzyme dissimilatory reductase (Dsr) of SRB. Diagrams adapted from Voordouw [23] and Hubert.[17]

The application of nitrate injection has drawn a great deal of attention because it gives synergistic effects, such as increasing oil production and also replacing biocides. Additionally, it is also more efficacious compared to biocides, is low cost and is environmentally friendly.[15, 16, 20, 35] Further investigation reveals that there are two types of NRB: they are heterotrophic nitrate- or nitrite-reducing bacteria (hNRB); and sulphide oxidizing, nitrate- or nitrite-reducing bacteria (soNRB).[17, 18, 23, 36, 37]

Several mechanisms have been proposed for the containment of souring by nitrate or nitrite.[20, 33, 37, 38] A few will be outlined below. First, the competition between SRB and hNRB for VFA may result in the competitive exclusion of SRB (BCX), thus biogenic formation of sulphide can be eliminated (Figure 1.1a).[17, 18, 23, 24, 35]

However, it is also found that some SRB may switch their energy metabolism to reduce nitrate or nitrite instead of sulphate, that is SRB may become hNRB.[18, 24] Second, soNRB couple nitrate or nitrite reduction to the oxidation of the produced sulphide to elemental sulphur or sulphate, creating a sulphur cycle involving soNRB and SRB that results in net removal of sulphide when insufficient organic electron donors are present to reduce all nitrate (Figure 1.1b).[18, 29] And third, nitrite inhibits the reduction of sulphate to sulphide by the enzyme dissimilatory reductase (Dsr), the terminal enzymatic step in the sulphate reduction pathway of SRB. Nevertheless, some SRB may have a nitrite reductase (Nrf) that may prevent this inhibition.[18, 38]

It is undisputed that nitrate application as a substitute for biocides in controlling Sulphate Reducing Bacteria (SRB) and mitigating reservoir souring has been widely used with some successful laboratory and field trials.[18, 20, 32, 36] However, the impact of nitrate treatment and the long-term consequences for MIC are poorly understood. [35] Additionally, it is revealed that the use of nitrate as the nutrient source that can enhance the growth of Nitrate Reducing Bacteria (NRB) still has some drawbacks. Voordouw et al.,[34] mentioned that though nitrate is a lower-potential electron acceptor than oxygen, it is a higher electron acceptor than sulphate; hence its effect on anaerobic MIC should be evaluated. Additionally, their experiments have shown that the presence of the NRB strain CVO increases the corrosion rate of ASTM A366 carbon steel from 0.004 mm/year up to 0.040 mm/year; and in the presence of a mixed culture of NRB strain CVO and SRB, the corrosion rate reached 0.075 mm/year. Hubert et al.[18] indicate that SRB control by nitrate shifted the corrosion risk from the bioreactor outlet to the inlet, and that NRB promoted pitting corrosion on the bioreactor inlet. They concluded that NRB stimulation may not be a practical souring control solution if SRB activity associates with MIC of ferrous metals and their alloys. It is also believed that nitrite, as the intermediate or by-product of the nitrate treatment, may itself induce pitting corrosion in a minority of applications.[11, 39] Therefore, knowledge of SRB and NRB interaction on metal surfaces is essential to help understand the nature of these two bacteria in changing the environment of metal surfaces.

1.4 Microbiologically Influenced Corrosion (MIC) in Steel Materials

Microbiologically influenced corrosion (MIC) is a corrosion process that is triggered, alleviated or accelerated by microbial activities and their metabolites, thus changing the condition at the metal-solution interface.[11, 40-42] Corrosion occurs when materials made of pure metal and/or their mixtures (alloys) undergo a chemical change from a ground state to an ionized species.[42] The main types of bacteria associated with corrosion on iron, mild and stainless steels are sulphate reducing bacteria (SRB), sulphur–oxidizing bacteria,[43] iron oxidizing bacteria (IOB), iron reducing bacteria (IRB), manganese oxidizing bacteria (MOB), bacteria secreting organic acids and exopolymers or slime.[42] Gu[10] stated that microbial involvement in corrosion of metals is a result of adhesion and subsequent metabolic activity on surfaces. To date, MIC and the way it affects corrosion have always been a matter of debate.[41] Javaherdashti,[41] mentioned that acid production by bacteria is presumed to be one of the ways by which corrosion can be enhanced; but other researchers have found contradictory evidence that acid production by aerocbic *Pseudomonas* sp was not a major cause of corrosion. Little et al.[44] also mentioned the conflicting opinions among researchers that exist where the same organism and mechanism to which MIC has been attributed have also reportedly inhibited corrosion. Among these contradictory views, interaction of biofilms with metal surfaces is the most intensively debated topic that has been investigated by a number of researchers.[45-51]

1.5 Microbial Biofilm and Corrosion

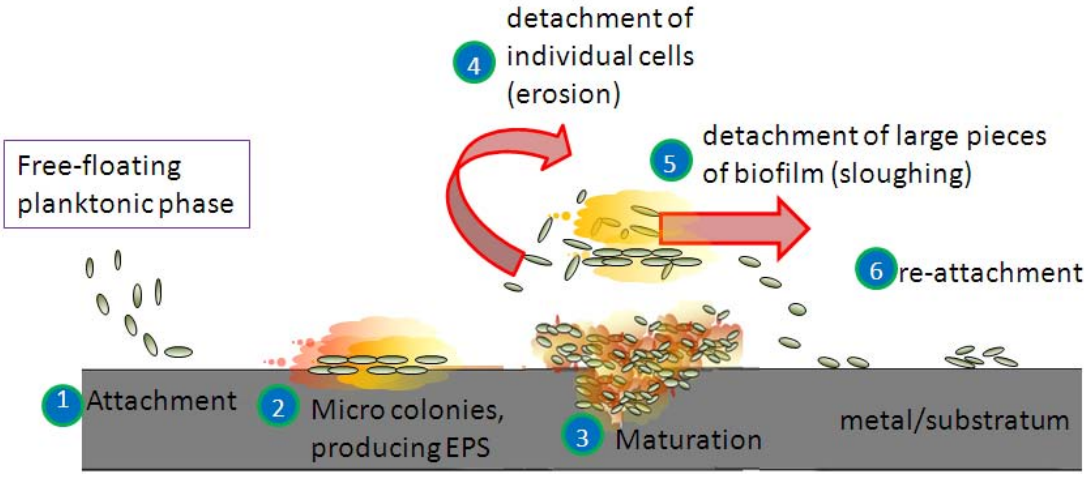

Figure1.2 Progress of bacteria accumulation on steel surface.[52]

Microbes can exist in a free floating state (planktonic state) and attached onto a substrate surface (sessile state).[11, 41] Due to its nature, microbes have the propensity to attach onto surfaces, proliferate and form biofilms - a film layer which consists of microbial populations and is surrounded by extracellular polymeric substances (EPS) (Figure 1.2).[11, 40, 53, 54]

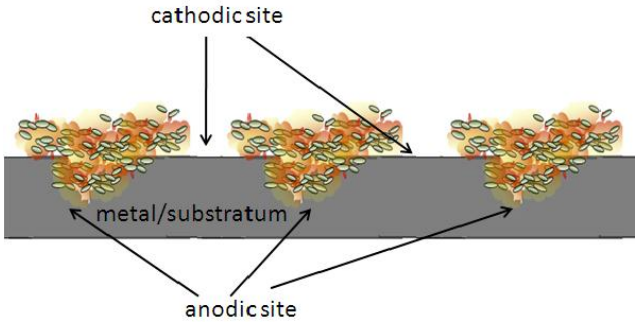

Figure 1.3 A conceptual model for an open, patchy biofilm structure, the areas under the biofilm become anodic sites and outside the biofilm deposit become cathodic sites [41].

The general mechanism of biofilm accumulation is agreed upon by researchers (Figure 1.2): [52, 55] (1) bacteria attachment on metal surface; (2) biofilm initiation and EPS production; (3) biofilm structural development and maturation; (4) biofilm detachment, erosion of individual cell and sloughing of large pieces of biofilm; (5) bacteria cell attachment in another substratum area. Bacteria produce EPS in order to facilitate the adhesion of bacterial cells onto surfaces during their initial development,[10] to trap essential nutrient and buffering fluctuations in pH, toxic metals, biocides, as well as other purposes.[56] The biofilm is formed in order to create a local environment suitable for their growth and to maximize their survival in the surrounding environment.[56] Biofilm accumulation on the metal surface is an autocatalytic process that increases surface irregularity, and consequently influences particle transport and attachment.[54] In such non-uniform structures, establishment of local gradients are highly possible; thus "spots" with high and low concentration of chemicals and gases are formed.[41] The area under bacterial deposit usually has low availability of the cathodic reactant, for example, oxygen and thus is forced to be the anode, while the area outside of the deposit becomes the cathode. This leads to localized corrosion in the form of pitting and crevice corrosion (Figure 1.3).[41, 54]

1.6 Corrosion Inhibition by Biofilm

There are numerous reports[48-51, 57, 58] and reviews demonstrating corrosion inhibition by biofilm.[47, 59, 60] There are several mechanisms which most frequently are proposed for corrosion inhibition by biofilms, for example: (1) oxygen depletion and/or removal at the metal surface by biofilm accumulation and/or respiring cells (Figure 1.4)[44, 47, 57]; (2) a biofilm forms a diffusion barrier hindering the diffusion of corrosion products from the metal surface[44, 60]; (3) microorganisms produce metabolic products that act as corrosion inhibitors, for example siderophores and γ-polyglutamate[44, 47, 58]; and (4) microorganisms produce specific antimicrobial peptides which kill corrosion-causing organisms, for example SRB.[44, 45] Little, et al.[44] conclude that the following critical issues must be addressed before bacteria can be used to predictably inhibit corrosion: (1) the stochastic nature of biofilm, (2) contamination, and (3) natural competition.

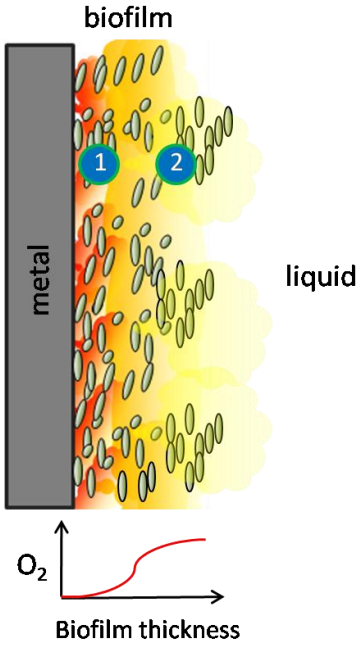

Figure 1.4 Oxygen depletion in the metal-biofilm interphase. There is less oxygen in area 1 compared to area 2.[41]

1.7 Materials Tested in This Study

Two materials are tested in this study. The first is UNS S31603, and the reason for choosing this material is because it is a widely used Corrosion Resistant Alloy (CRA) in the petroleum industry. In general, stainless steel (SS) is commonly used as

a construction material in petroleum industries due to its resistance to localized corrosion in various aggressive environments. According to Moss,[61] SS with a content of more than 12% chrome is corrosion resistant due to its spontaneous development of an extremely stable chromium-oxide layer on the metal's surface. Though SS can develop a passive film that protects the steel from corrosion, in the presence of aggressive anionic species, such as chloride and sulphate ions, localized corrosion may occur.[62-64] Additionally, added alloying elements (in order to improve their corrosion resistance), such as chromium, nickel and molybdenum, may be dissolved during the corrosion process and due to the influence of bacterial adhesion and thus biofilm development.[65] Furthermore, Beech et al.[66] also demonstrated that the profile of the chemical elements within the passive layer of SS 316 and its thickness changed after exposure to *Pseudomonas* sp.

The second chosen material for this study is carbon steel, because it is still widely employed as a construction material for pipe work in the oil and gas industry, despite the advanced innovation of corrosion resistant materials. It is commonly employed in down-hole tubular flow lines and transmission pipelines.[67] However, one of the consequences of using carbon steel is its low corrosion resistance, especially in the presence of water from the external environment.[68]

1.8 Electrochemical Tests

There are many electrochemical tests developed for MIC monitoring.[69-71] The electrochemical tests conducted in this experiment are corrosion potential (E_{corr}), redox potential (E_h), cyclic potentiodynamic polarization scans (CPS), linear polarization resistance (LPR) and electrochemical impedance spectroscopy (EIS).

1.8.1 Open Circuit Potential

E_{corr} or open circuit potential (OCP) can measure the potential difference between the corroding metals and a suitable reference electrode when they are immersed in an aqueous solution.[40] E_{corr} provides information about the passivation layer formed on

the surface and a measure for the thermodynamic risk of the protective layer's integrity.[56]

The application of this technique is simple and can be implemented easily outside laboratory conditions. However, this technique does not provide mechanistic information and is recommended to be used in addition to other electrochemical techniques. In E_{corr} measurement, the contribution from the cathodic and the anodic are monitored together. For this reason, it is important to implement other techniques that can monitor the cathodic and anodic influences of the electrochemical process.[71]

1.8.2 Redox Potential (E_h)

E_h or reduction-oxidation shows the oxidative power of an electrolyte.[70] It is usually measured using an inert electrode such as Pt and a stable reference electrode.[70, 72] If a suitable calibration is provided, it might be used to monitor the changes in the corrosivity of the electrolyte as a result of the bacterial metabolism.[70]

1.8.3 Cyclic Potentiodynamic Polarization Scan (CPS)

The CPS technique offers a qualitatively reasonable and rapid method to predict the propensity of a passivating alloy to suffer from localized corrosion in the form of either pitting or crevice corrosion.[73-75]

In the study of localized corrosion, two critical characteristics of the potential which indicate the susceptibility of different metals and alloys to localized corrosion need to be noted. These potentials are the pitting potential and repassivation potential.[56, 76] Because there has been much research into pitting corrosion, different terminology has been used and is still being used to define pitting potential and repassivation potential. Pitting potential is also known as: Brennert's breakdown potential (E_b), critical pitting potential (E_c), breakthrough potential (E_b), pitting initiation, and pit nucleation (E_n). Repassivation potential (E_r) was also called

protection potential (E_{pp}).[76] In this study, the term critical pitting potential (E_c) and repassivation potential (E_r) will be used.

In the CPS test, a potential is applied to the specimens at a continuous and relatively slow rate versus a reference electrode using a potentiostat. First, the specimen is scanned in the noble (positive) direction on the forward scan until a specific anodic current is reached. Then the direction of the scan is reversed to the active (negative) direction and terminated at the original starting potential or when the direction of the current changes sign, indicating a cathodic current.[73, 77] The result of an ideal CPS curve is depicted on Figure 1.5.

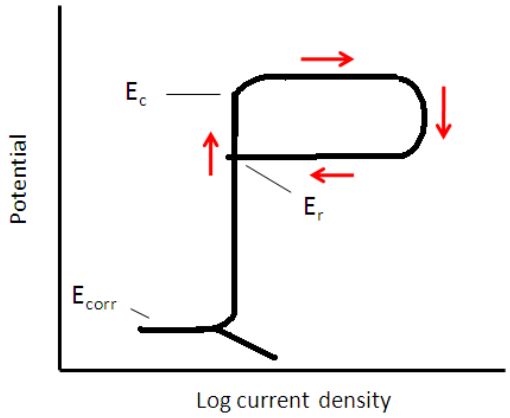

Figure 1.5 Schematic representation of an ideal cyclic potentiodynamic polarization curve for a passivating metal [56, 76]. E_c - critical pitting potential, E_r - repassivation and E_{corr} – corrosion potential. The red arrows show the scan direction.

Some important information from the CPS test which will be discussed in this study will be highlighted below:

1.8.3.1 Hysteresis

The first important parameter is the direction of the curve's hysteresis. According to Silverman,[73] the hysteresis is a result of the disruption of the passivation chemistry of the surface by the increase in the potential (forward scan) and reflects the ease at which that passivation is restored as the potential is decreased back toward the corrosion potential (reverse scan). Additionally, the same author also mentions that from a practical standpoint, a positive hysteresis (when the reserve scan goes in a left

direction on the CPS curve) usually signifies that the alloy will be more resistant to localized corrosion than does a negative hysteresis.[73]

1.8.3.2 Critical Pitting Potential (E_c)

The second important parameter is the E_c. In the early literature, E_c is simply defined as potential below which pits do not nucleate and above which stable pits are growing.[56, 78] In this study, the E_c is best defined as the potential at which passive surface layers are broken,[56] or become unstable and cannot repassivate.[76] This is indicated by the rapid increase in current density in the forward scan of the polarization scan.[56, 77]

1.8.3.3 Metastable Pitting

The third important parameter is the occurrence of metastable pitting. This is indicated by an increase in the current density, followed by a rapid decrease in the current to the original passive current. Metastable pitting can be simply defined as a pit nucleated at the area between E_c and repassivation potential (E_r). This pit is small in size, grows and repassivates in less than a few seconds.[76]

1.8.3.4 Repassivation Potential (E_r)

The fourth important parameter is the E_r. In the early literature, E_r is defined as the potential at which pit growth is arrested or pitting corrosion is prevented.[56, 78] In this study, E_r is best defined as the potential below which no metastable pitting and stable pitting occurs and above which a metastable pit can form and the already nucleated pits can grow.[76] This is indicated by the lowest readable value of current density on the reverse portion of the polarization scan.[73]

1.8.4 Linear Polarization Resistance (LPR)

LPR is an electrochemical method, based on a linear relationship between changes in the applied current, and resulting in current density. It gives a rapid and easily

interpreted result for the corrosion rate, but is not a useful method to observe localized corrosion.[41] LPR can be used to continuously monitor the corrosion rate of a metal or alloy exposed to a corrosive environment.[79] The polarization resistance (R_p) of a material is defined as the slope of a potential-current density ($\Delta E/\Delta i$) curve at free corrosion potential. The R_p value is related to the corrosion current with the help of Equation 1.1.[75, 79]

$$R_p = \frac{B}{i_{corr}} = \frac{(\Delta E)}{(\Delta i)_{\Delta E \to 0}} \qquad (1.1)$$

Where R_p = polarization resistance

i_{corr} = corrosion current

B = empirical polarization resistance constant that can be related to the anodic (b_a) and cathodic (b_c) Tafel slopes with equivalent (2.2)

$$B = \frac{b_a b_c}{2.3(b_a + b_c)} \qquad (1.2)$$

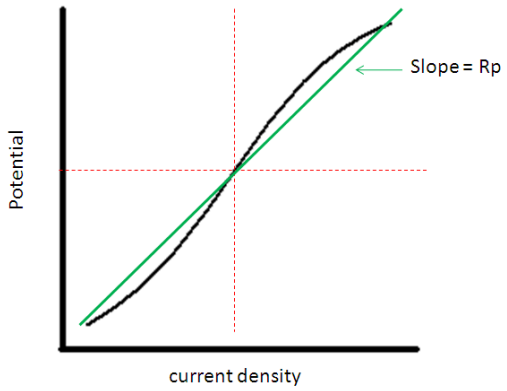

Figure 1. 6 Hypothetical linear polarization plot.[56, 75]

1.8.5 Electrochemical Impedance Spectroscopy (EIS)

The concept of electrical impedance was first introduced by Oliver Heaviside in the 1880s. Impedance is a more general concept than resistance because it takes phase differences into account and has become a fundamental and essential concept in electrical engineering.[80]

EIS is a specific branch of the tree of electrical measurement.[80] It has become a mature technique that has been proven to be extremely effective in the mechanistic study of a wide variety of corrosion phenomena.[79] The complications and sources of error associated with the polarization resistance method were able to be explained and understood after introducing electrical equivalent circuit parameters to represent and simulate the corrosion electrochemical interface in EIS.[81]

In EIS, the impedance is usually measured by applying a small perturbation of alternating current (AC) potential at low amplitude to the working electrodes at a number of discrete frequencies (ω). This is done to allow observation of the system in a pseudo-linear state. It is assumed that a sinusoidal potential excitation is applied and the response to this potential is an AC current signal. In this system, the current response to each one of the discrete frequencies will exhibit a sinusoidal current waveform response at the same frequency but shifted in phase (Figure 1.7) depending upon the circuit parameters of the corroding interface.[81, 82]

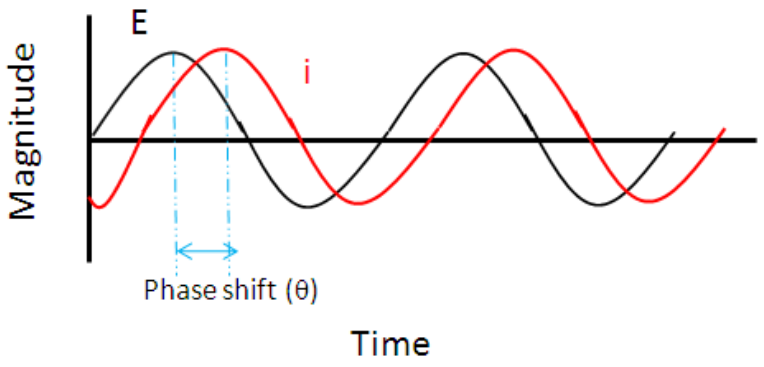

Figure1.7 Sinusoidal current responses to the applied AC potential in a linear system.[71, 82]

A sinusoidal perturbation $E(t)$ of low amplitude (E_0) is imposed over the working electrode, at a given radial frequency (ω)

$$E(t) = E_0 \sin(\omega t) \quad 1.3$$

$$\omega = 2\pi f \quad 1.4$$

The obtained response for each frequency is a sinusoidal current $I(t)$ of phase (θ) and amplitude I_0 in a system that has a linear behaviour:

$$I(t) = I_0 \sin(\omega t + \theta) \quad 1.5$$

The impedance which is equal to resistor can be calculated according to Ohm's Law:

$$Z = \frac{E_t}{I_t} = \frac{E_0 \sin(\omega t)}{I_t \sin(\omega t + \theta)} = Z_0 \frac{\sin(\omega t)}{\sin(\omega t + \theta)} \quad 1.6$$

The impedance is therefore expressed in terms of a magnitude (Z_0) and a phase shift (θ).

In EIS, the impedance data are presented in two curves, the Nyquist plot and the Bode plot.[71, 81, 82] The Nyquist plot gives the typical characteristic behaviour of phenomena occurring on the electrochemical system in the form of semicircles or slopes.[71] On the Nyquist plot (Figure 1.8b), the real impedance value (Z) is plotted on the X-axis and the imaginary value (Z') is plotted on the Y-axis, resulting in the expressed impedance value as a vector of length $|Z|$ or Z modulus (Z_{mod}).[71, 82]

$$|Z| = \sqrt{Z^2 + Z'^2} \quad 1.7$$

$$\tan\theta = \frac{Z'}{Z} \quad 1.8$$

The semicircle is a characteristic of a single "time constant".[82] It is important to mention that in a real situation, the impedance plot may have more than one semicircle, and/or with combination of linear line.[71, 82, 83] Additionally, it is often found that only a portion of a semi circle is observed.[71, 82] The Bode Plot (Figure 1.8c) shows the log frequency value on the X-axis and both the $|Z|$ and the phase angle on the Y-axis.[71, 82]

AC circuit theory in terms of circuit analogues is used to model the electrochemical corrosion process. This model facilitates understanding and leads to better predictions of corrosion rates and overall corrosion behaviour. The electrochemical process is modelled by linear circuit elements such as resistors, capacitors and inductors. An example of a simple corroding system is the Randles circuit as depicted on Figure 1.8. This equivalent circuit (Figure 1.8a) consist of a solution

resistance, a double layer capacitor (C_{dl}), and a charge transfer/polarization resistance (R_{ct}). The C_{dl} is in parallel with the R_{ct}. The solution resistance (R_s) can be observed at the intercept of the real axis value at high frequency (Figure 1.8b).[71, 82-84] Once the physical model has been built, computer software is available to allow fitting of impedance data to an appropriate equivalent circuit.[79]

EIS has generated much interest in MIC studies[69, 79] because when a reasonably small magnitude of sinusoidal potential around E_{corr} (usually 5 to 10 mV rms) is applied, it does not markedly affect bacterial growth and activity.[58, 79]

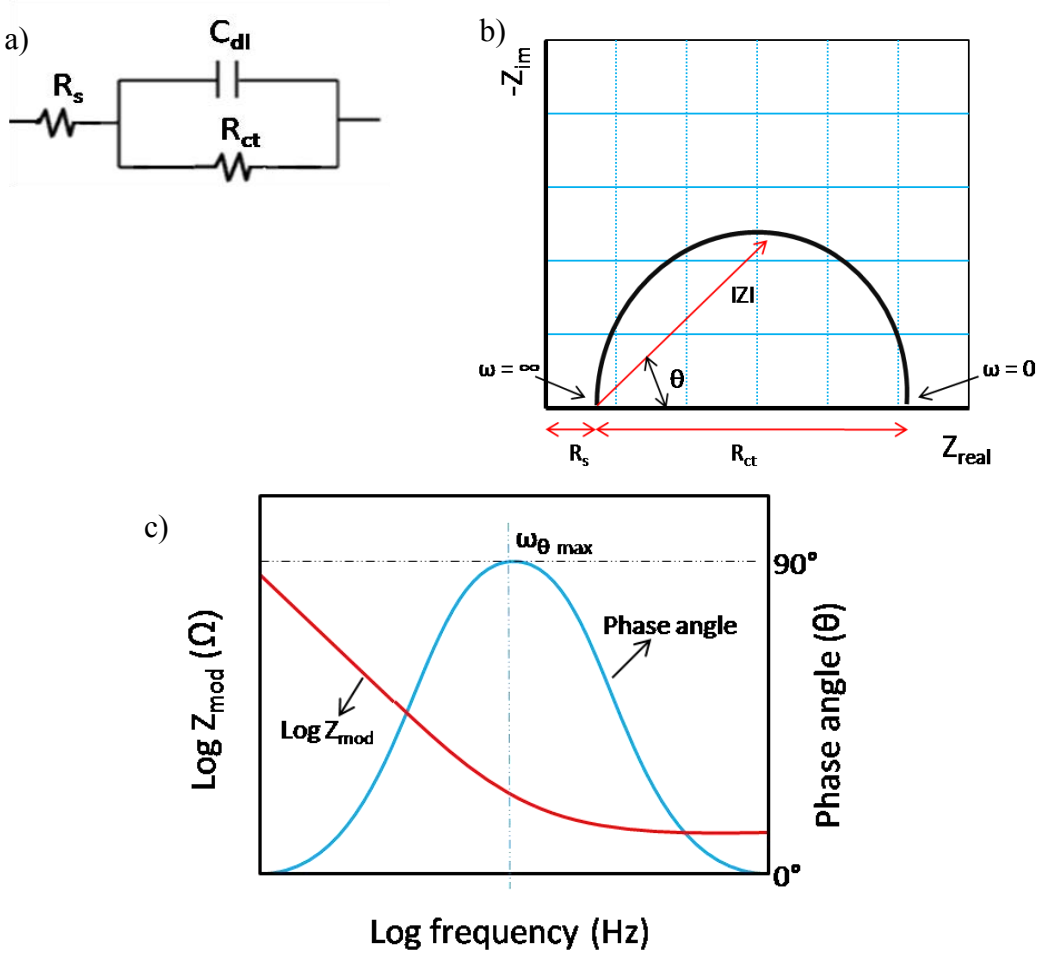

Figure 1.8 (a) Electrical circuit model of a Randles circuit, (b) Nyquist plot of a Randles circuit, (c) Bode plot of a Randles circuit.[71, 82-84]

1.9 Research Focus in This Study: MIC Study in a Stagnant Control System

There is much research on the impact of nitrate treatment using a bioreactor to mimic reservoir conditions[18, 26] or sand packed columns[21, 22, 85] in a laboratory, but only a few studies have been conducted to understand the impact of nitrate treatment on the corrosion of steel.[18, 27] In addition, some debate continues since the field conditions are somewhat different from what is created in laboratory conditions, such as scale formation[86, 87]; also, in the field it is most likely that oil-in-water emulsion forms in the post production stage.[87]

This study will discuss electrochemical experimentation of SRB and NRB using a mixture of fresh sample brine and crude oil from the field with a controlled system. To the best of the author's knowledge, this is the first electrochemical experiment with a production water and crude oil mixture. Other researchers sharing the same interest have used synthetic media[33, 36] and/or a field brine sample[86, 88] without mixing it with a crude oil sample. For brevity, this study has limited its scope to a batch culture experiment on the impact of SRB and NRB using electrochemical techniques, weight loss measurement and steel surface analysis without any material renewal during immersion time.

1.10 Research Objectives

1. Bacteria isolation and mechanistic study of oil reservoir souring control by sodium nitrate application;
2. Electrochemical study of nitrate injection impact on UNS S31603 material in corrosive production water-oil mixture samples from an oil field;
3. Electrochemical study of nitrate injection impact on carbon steel material in corrosive production water-oil mixture samples from an oil field in pre-sour condition.

CHAPTER 2: Methodology

2.1 Material Preparation

The working electrode specimen was made from a UNS S31603 sheet and a carbon steel ASTM A572-50 carbon steel sheet, with the nominal elemental composition shown in Tables 2.1 and 2.2. The sample was cut into 1 cm x 1 cm x 0.5 cm coupons, connected to a wire, mounted in CaldoFix-2 Resin (Struers) and mechanically polished using silicon carbide papers (Struers) in a sequence of 120, 320 and 600. They were degreased in ethanol and dried under nitrogen gas flow. Prior to electrochemical testing, samples were sterilized by immersion in Decon 90® overnight and then immersed in 70% ethanol for one hour.

Table 2.1 Chemical composition of UNS S31603 working electrode (wt%)

C	Cr	Mn	Mo	N	Ni	P	S	Si	Fe
0.022	17.4	1.76	2.03	0.046	10.00	0.030	0.001	0.37	balance

Table 2.2 Chemical composition of ASTM A572-50 carbon steel working electrode (wt%)

Al	As	C	Cr	Mn	Mo	N	Nb	Ni	P	S	Si	Sn	Fe
0.027	0.002	0.14	0.023	0.64	0.004	0.008	0.001	0.028	0.018	0.014	0.151	0.005	balance

2.2 Sample Site Description

Production water and crude oil samples were obtained from an offshore oil field off the northwest of Western Australia. This oil field, with a reservoir temperature of 50ºC, and depth of 800 m, has been flooded with seawater to enhance oil production. Some wells have had break through which was shown by the high sulphate and chloride values. The formation water contains barium, therefore by mixing it with seawater, barium sulphate precipitation was formed, causing scale on steel surfaces. As a result, a scale inhibitor has been injected to prevent precipitation. The chemical composition of the production water sample is provided in Table 2.3. Due to the high content of sulphate in the formation water sample, sodium nitrate is chosen instead of calcium nitrate to avoid a calcium sulphate scaling problem.

Table 2.3 Chemical composition of production water sample

Component*	Unit (mg/L)
Barium (Ba^{2+})	<0.1
Calcium (Ca^{2+})	770
Iron (as Fe)	< 0.1
Magnesium (Mg^{2+})	480
Potassium (K^{+})	200
Sodium (Na^{+})	13000
Strontium (Sr^{2+})	28
Bicarbonate (HCO_3^{-})	150
Chloride (Cl^{-})	22000
Nitrate (NO_3^{-})	<0.1
Sulphate (SO_4^{2-})	600
Volatile Fatty Acid (VFA)	Not detected
pH @20.7ºC	6.9
Electrical conductivity @25ºC	48000 µS/cm
Resistivity @25ºC	0.21M.Ohm

*All amounts are in (mg/L) except where stated otherwise

2.3 Bacteria Isolation, Bacterial Counting and Inoculums

2.3.1. Media Preparation

The media used in this experiment were Starkey broth,[89] Postgate B broth,[89] nitrate broth (Fluka®), and Thioglycollate medium (Oxoid). All liquid media were made anaerobically by flushing the serum bottles with nitrogen to generate an anaerobic condition and then sealed with a butyl rubber stopper and aluminium crimp cap (Grace, Australia). The media pH were adjusted to between 7 and 7.5 by adding 5 M KOH (Sigma-Aldrich). The media were then autoclaved at 121°C for 15 minutes and stored at room temperature until use.

2.3. 2. Bacteria Isolation

The consortium used in this study was isolated from both production water and the crude oil sample. SRB was isolated using Starkey broth,[89] while NRB was isolated using nitrate broth (Fluka®) supplemented with 5 mM sodium nitrate ($NaNO_3$, Chem-Supply, 99%). Approximately 10% (v/v) production water sample and crude oil sample were aseptically inoculated into nitrate broth and Starkey broth in 50mL serum bottles containing 40 mL media in duplicate. The serum bottle cultures were

then incubated at 50°C for one month. Every week, 1 mL of the samples was taken with a sterile syringe, and was grown in Thioglycollate agar in a Petri dish. The agar was supplemented with 5 mM $NaNO_3$ (Chem-Supply, 99%) for NRB isolation and 0.5 g/L $FeSO_4.7H_2O$ + 0.5% lactic acid solution ($C_3H_5NaO_3$, Fluka®) for SRB isolation. The Petri dishes were then incubated inside an anaerobic jar for three to seven days at 50°C. Gas Pack™ EZ Anaerobe Container System (BD Scientific) was put inside the jar to remove all the oxygen and kept the system anaerobic.

2.3.3 Bacterial Counting

Both SRB and NRB were enumerated by a three-tube most probable number (MPN) procedure using 10-fold serial dilutions in selective media.[31, 90] SRB were enumerated in Postgate B media,[89] and NRB were enumerated in nitrate broth as described above. Both of the SRB and NRB cultures tubes were incubated for four weeks at 50°C. The SRB were scored positive when blackening occurred. The NRB were scored positive when the media colour change into red after the addition of five drops of sulfanilic acid solution and five drops of α-naphthylamine, as per manufacturer instructions.

In addition to the MPN method, bacterial direct counting was performed using a Helber Counting Chamber Z30000 (Hawksley, UK). The bacteria in the counting chamber were observed under an Olympus Phase Contrast Microscope, at 400x magnification. The bacteria were counted in eight small squares from three randomly chosen big squares of the counting chamber (Figure 2.1).

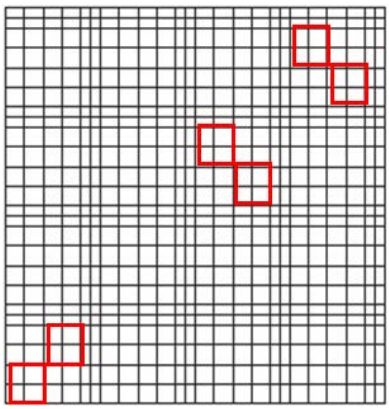

Figure 2.1 Helber counting chamber Z30000, red squares indicate randomly chosen areas for bacterial counting.

Each small square of the Helber counting chamber Z30000 has an area of 1/400 mm^2 and depth of 0.02 mm. This means each single square has the volume of:

$$V = {}^{1}\!/_{400}\, mm^2 \times 0.02mm = 5.10^{-5}\, mm^3 = 5.10^{-8}\, cm^3 = 5.10^{-8}\, mL \qquad 2.1$$

The bacteria cell density can be calculated as follow:

$$\text{Bacteria cell/mL} = \frac{x}{N \times 5.10^{-8}} \qquad 2.2$$

Where x = number of bacteria counted in N square, N = number of squares observed. The standard deviation, S_x, was calculated to evaluate the precision of the counting. (90)

Due to the fact that the MPN method is based on a Poisson distribution, the standard deviation is not defined. Instead, the confidence limits (95%) were calculated using Equation 2.3 based on a 10-fold dilution series.(90)

$$S_{conf} = e^{\ln(MPN) \pm 2\frac{0.58}{\sqrt{n}}} \qquad 2.3$$

Where n is the number of replicates. For the three tubes MPN, n = 3.(90)

2.3.4 Inoculum Preparation

The inoculums were prepared in the same media as the test solution, 10% (v/v) crude oil in production water. This was conducted in order to minimize the lag phase of the bacteria. The NRB inoculums media was supplemented with 5 mM $NaNO_3$ and the SRB inoculums media was supplemented with 0.5% lactic acid.

2.4 MIC Experiment in Electrochemical Cell

2.4.1 General Test Condition for Both UNS S31603 and ASTM A572-50 Carbon Steel

All glass equipment, production water and crude oil were sterilized using an autoclave at 121ºC, 15 psi for 15 minutes. All tests were conducted using 700 mL production water +10% (v/v) crude oil as the electrolyte. These electrochemical experiments were conducted in a closed batch culture system without any water/nutrient renewal at 50ºC using 1 L electrochemical cells. There were four test condition evaluated in this study: (1) Control cell (no bacteria), (2) SRB inoculated cell, (3) NRB inoculated cell, and (4) Mixed bacteria (NRB+SRB) inoculated cell. The Control and the mixed bacteria (NRB+SRB) inoculated cells were supplemented with 5 mM $NaNO_3$ and 0.5% lactic acid solution. The NRB inoculated cell was supplemented with 5 mM $NaNO_3$, and the SRB inoculated cell was supplemented with 0.5% lactic acid solution. All experiments were performed in a three-electrode system: An Ag/AgCl reference electrode (RE), a platinum coated titanium mesh counter electrode (CE) and working electrodes (WE). Triplicate samples of WE mounted in resin were put in each cell to compare their electrochemical behaviour in exactly the same biochemical conditions. The cells were purged with filtered sterilized nitrogen to displace the oxygen and keep the oxygen level as low as possible. A condenser was fitted in the cell to prevent evaporation and maintain a constant level of the test solution throughout the immersion time. All connecting parts in the cells were covered with Parafilm^{TM} to ensure the system was closed and as little oxygen as possible from the air could enter the cell.

2.4.2 Long Term Immersion Test of UNS S31603

An Ag/AgCl Reference Electrode (RE) was fitted in the cell using a Luggin capillary, which was filled with 1.2% agar/agar. The upper part of the Luggin was filled by 3 M KCl. The experiment was run over 28 days.

2.4.3 Long Term Immersion Test of ASTM A572-50 Carbon Steel

Two additional steel samples were hung using a nylon string for weight loss measurements. An Ag/AgCl RE was fitted in the cell using a Luggin capillary. The Luggin capillary was filled with production water. An O-ring was used to hold the RE in the Luggin capillary. The experiment was run over 21 days.

2.4.4 General Test Monitoring for Both UNS S31603 and ASTM A572-50 Carbon Steel during Immersion Time

Periodic microbiological and electrochemical analyses were conducted during the immersion time. At each sample time the pH and oxygen level inside the cells were measured. Measurement of the pH was conducted using a Cole Palmer autoclavable pH electrode (John Morris Scientific Pty Ltd, Australia) which was connected to an Orion 5 Star pH meter (Thermo Fisher Scientific Pty Ltd, Australia). The oxygen level inside the cell was measured using an oxygen meter (Orbisphere, UK).

2.5. Electrochemical Analysis

2.5.1 Electrochemical Test for UNS S31603

E_{Corr} was measured every four hours with a Potentiostat 20 (ACM Instruments, UK) for 28 days. At the end of the experiment, two of the triplicate samples were polarized to measure the general corrosion rate and critical pitting potential (E_c) value. The general corrosion rate was estimated by LPR and the E_c was measured by CPS. Due to the fact that CPS is a destructive test, one of the samples was not polarized for biofilm and pit observation purposes. Both LPR and CPS were conducted using a Gamry DC105 (Gamry Instruments, USA). LPR was conducted according to *ASTM Standard G 59-97, Standard Test Method for conducting potentiodinamic polarization resistance measurement*.[91] CPS was conducted according to *ASTM Standard G-61, Standard test method for conducting cyclic potentiodynamic polarization measurement for localized corrosion susceptibility of iron-, nickel- or cobalt based alloys*.[92] The potential was swept at a constant rate of

0.5 mV/sec and reversed upon attaining a potential apex of 1.5 V or a current density of 1.5 mA-cm^{-2}. The scan was terminated at 0.1 mV with respect to the original E_{corr}. LPR was conducted by applying ±0.5 mV overpotential in respect to E_{Corr}, with a scan rate of 0.125 mV/s.

Redox Potential (E_h) was measured at each bacterial sampling time using a platinum wire electrode against an Ag/AgCl reference electrode. The test was conducted according to the *US Geological Survey Reduction-Oxidation Potential, version 1.2 (9/2005)*.[72] Prior to use, the platinum electrode was cleaned with aqua regia solution (1 concentrated nitric acid : 3 concentrated hydrochloric acid) at 70ºC for one minutes and calibrated using Zobell's solution.[72]

2.5.2 Electrochemical Test for ASTM A572-50 Carbon Steel

E_{Corr} was measured every four hours with a Potentiostat 20 (ACM Instruments, UK) for 21 days. LPR and EIS were conducted to estimate corrosion rate every five days. LPR was conducted using a Gamry DC105 and EIS was conducted using a Gamry EIS300 (Gamry Instruments, USA). LPR was conducted by applying ±0.5 mV overpotential in respect to E_{Corr}, with a scan rate of 0.125 mV/s. EIS was conducted by applying a sinusoidal voltage signal of 10 mV in a frequency range of (10^{-2}-10^{4}) Hz. LPR data was analysed using Echem Analyst computer software (Gamry Instruments, USA) and EIS data was analysed by ZSimWin computer software, version 2.0 (Princeton Applied Research, USA). The EIS results were fitted to the suitable circuit model and the charge transfer resistant (R_{ct}) value obtained from the simulation results were used to calculate the corrosion rate according to ASTM standard G102-89.[93] Redox Potential (E_h) was measured at each bacterial sampling time as explained in Section 2.4.1

2.5.3 Weight Loss Measurement (ASTM A572-50 Carbon Steel).

At the end of the experiment, the weight loss coupons were immersed in Milli-Q water in a separate glass beaker, and sonicated for 2 minutes to remove all attached debris. The coupons were dried at 70ºC for 15 minutes, cooled in desiccators for 15

minutes, and weighed. The coupons were then cleaned using Clarke's solution for 10 seconds, rinsed in Milli-Q water, dried and cooled as described above. This was repeated three times until a stable value was observed. The weight loss was then used to estimate the corrosion rate using *ASTM Standard G1-03, Standard practise for preparing, cleaning and evaluating corrosion test specimens*.[94]

2.6 Production Water Analytical Analysis

All analytical measurements were conducted based on APHA standard. Sulphate was analysed using a Thermo Scientific Aquakem 250 discrete analyser; sulphide in water was analysis by methylene blue colourimetric using Shimadzu UV Mini 1240 spectrometer ; nitrate and nitrite expressed as nitrogen by FIA (APHA 4500NO3-I) [95] using Lachat QuikChem 8000 flow injection analyser. All measurement replications were conducted according to NATA accreditation no 8 as follows: the analytical analysis was run over 20 replications and duplicate readings taken for every tenth sample. Statistical analysis was conducted and resulted in approximately 5% of Regression Point Displacement.

2.7 Examination of Surface Film

Corrosion products, NRB and SRB biofilm analysis on the steel surfaces was conducted using Scanning Electron Microscopy (SEM). Prior to observation, the biofilm was fixed by immersing the coupons overnight in 4% glutaraldehyde in phosphate buffer solution (PBS) at 4°C. The coupons were then soaked in a PBS for 10 minutes, and dehydrated using serial dilution of ethanol (10%, 30%, 50%, 70%, 90% and 100%), each for 10 minutes; the final step was repeated. The same procedure was also applied to the control corrosion coupons in order to check whether contamination had occurred. Afterwards the coupons were dried using nitrogen, coated with gold approximately 2 nm and placed in desiccators. Different accelerating voltages were used to examine different surface morphologies. It was demonstrated that when low accelerating voltage is used, greater surface morphology is revealed. Electron Disperse Spectroscopy (EDS) was conducted to observe the elemental analysis of the steel surface. The data obtained from the EDS were then

analysed using Inca computer software version 4.11 (Oxford Instrument Analytical Ltd).

2.8 Steel Surface Analysis

The changes in the steel surface were observed using a light microscope-Infinite Focus Microscope (IFM) (Alicona Instruments, Germany). The 2D surface profile, 3D surface roughness, pit depth, and pit volume were analysed using the Alicona IFM computer software.

Prior to the analysis, the steel was cleaned according to the *ASTM standard G1-03, Standard practice for preparation, cleaning and evaluating corrosion test specimens*, [94] to remove all corrosion product attached to the steel surface. In brief, the procedure was as follows. The UNS S31603 coupons were scrubbed using a sterile cotton bud and then soaked in Milli-Q water and sonicated for 5 minutes using an ultrasonic water bath. Then, the coupons were soaked in 50 mL nitric acid (sp gr 1.42) for 20 minutes at 60°C. Later, the coupons were rinsed with Milli-Q water, soaked in Milli-Q water again, and sonicated for 5 minutes. Last, the coupons were degreased with ethanol and kept in desiccators until microscopic analysis was done. If the result of the microscopic analysis shows that there are still some corrosion products attached to the surface this cleaning process is repeated. The carbon steel coupons were cleaned with Clarke's solution as described in Section 2.5.3.

CHAPTER 3: General Microbiology Results and Test Conditions

3.1 Introduction

This chapter will briefly discuss the microbiological results and also provide an introduction to the test conditions in Chapter 4 and Chapter 5.

3.2 Bacteria Isolation and Characterization

The bacteria isolation was conducted using selective media. Starkey broth was used for the isolation of lactate utilizing bacteria (Desulfotomaculum and Desulfovibrio).[89] The nitrate broth was used for the isolation of nitrate reducing bacteria.[89] The samples from both the inoculated broth media were then grown in agar media to isolate the bacteria as a single colony. Two NRB bacteria colony morphologies were observed in Thioglycollate agar supplemented with 5 mM $NaNO_3$ after the samples were incubated in the nitrate broth for one month. One type has a flat round shape with an entire margin (NRB1); the second one has a flat irregular surface with lobate margin (NRB2) (Figure 3.1). Further testing was conducted to ensure that these bacteria were nitrate reducers. Each colony was taken by a sterile scalpel and regrown in nitrate broth inside serum bottle vials and flushed with nitrogen to keep the vials anaerobic. After three days of incubation, five drops of sulfanilic acid solution and five drops of α-naphthylamine solution were added to the broth, as per manufacturer instructions. It was revealed that only NRB1 were capable of reducing nitrate to nitrite, indicated by the changes of the media colour to pink after addition of sulfanilic acid and α-naphthylamine. These bacteria were observed to be gram variable, rod shape bacteria (Figure 3.3a). Additionally, further investigation revealed that the NRB were able to oxidize sulphide (Appendix 2).

The SRB were unable to grow in Thioglycollate agar. In order to further investigate these bacteria characteristics, a sample was taken from the liquid media and gram staining was performed. It was revealed that the SRB obtained were gram negative, rod shape bacteria (Figure 3.3b). A further molecular method or biochemical tests was not employed to prove whether the NRB and SRB were pure culture or not.

Therefore, in this experiment, both bacteria are considered as consortia. Both of the NRB and SRB consortia are motile, as their movement was observed inside the counting chamber under a phase contrast microscope.

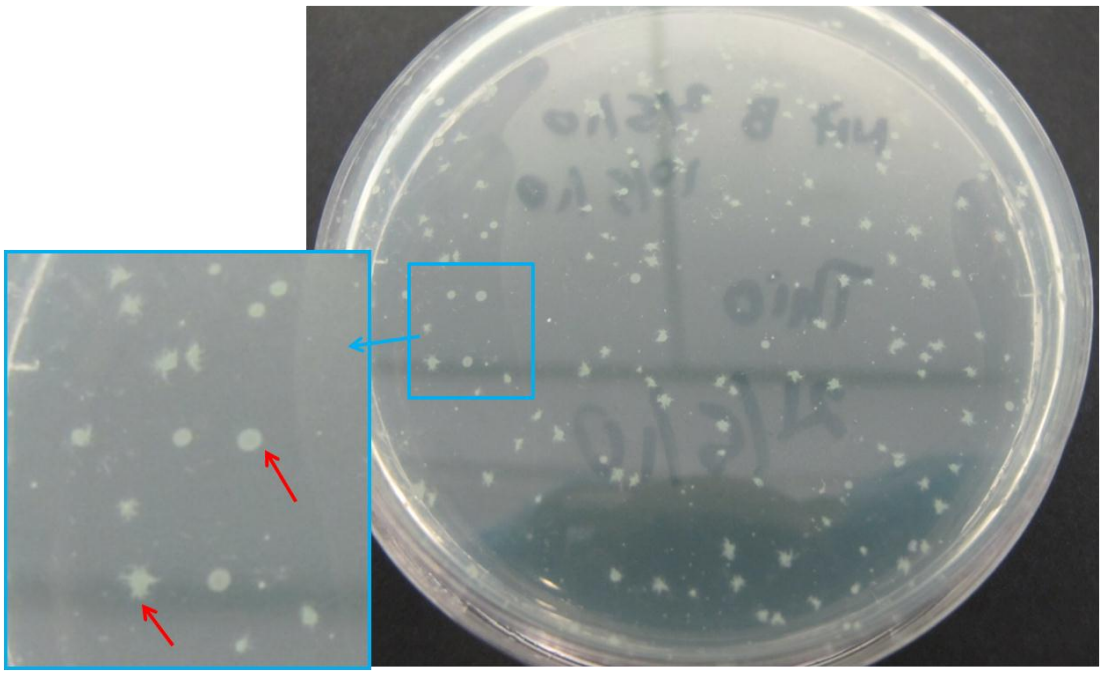

Figure 3.1 Two different NRB colonies (red arrows) were observed on Thioglycollate agar supplemented with 5 mM $NaNO_3$

As mentioned earlier, in this study crude oil was used as the organic carbon needed for a microbe's metabolism and it may also become a limiting factor due to toxic water-soluble hydrocarbon.[11] No other carbon source was added for the bacteria nutrient. It is evident that the bacteria (both NRB and SRB) were able to utilize the crude oil as oil droplets formed in between the crude oil phase and the water phase (Figure 3.4). Further investigation into hydrocarbon catabolism by bacteria were not conducted. However, the mechanistic stages of hydrocarbon catabolism by bacteria according to Ward et al.[96] will occur in the following order: sensing and taxis, substrate accession and uptake, and, if toxicity is an issue, efflux to maintain tolerable levels within cells. Additionally, it has been proven in numerous publications that some NRB and SRB are able to degrade different compounds of hydrocarbon.[96-100]

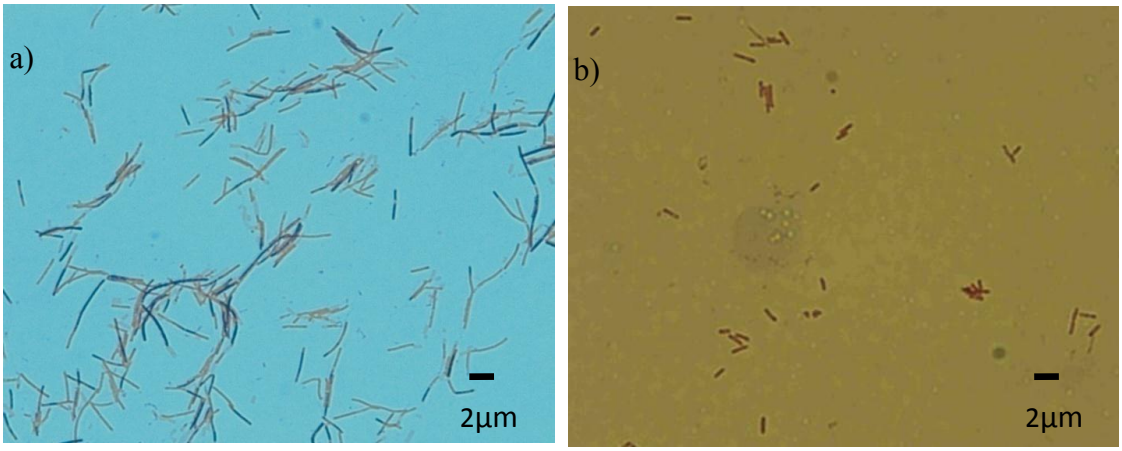

Figure 3.2 Light microscopy of gram stained (a) NRB, (b) SRB

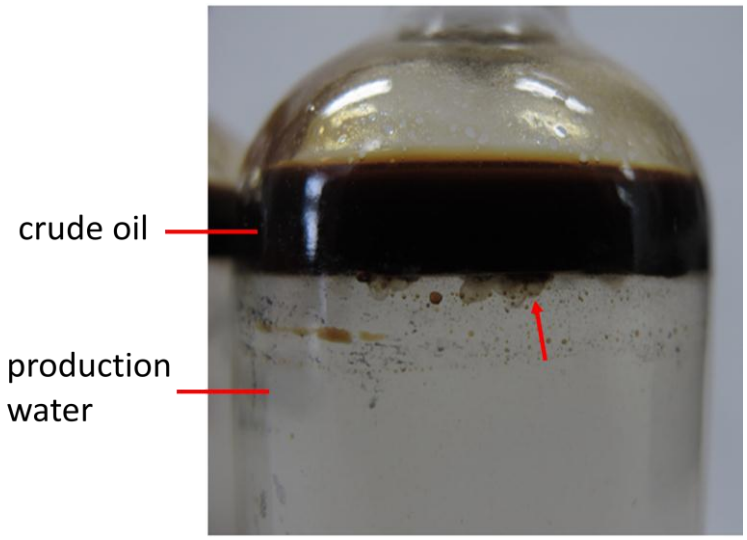

Figure 3.3 Oil droplets (red arrow) were observed in between the crude oil phase and production water phase after bacteria inoculation.

3.3 General Test Condition

This study is divided into two major sets of experiments. The first is an evaluation of nitrate injection impact on UNS S31603. The second is an evaluation of nitrate injection impact on carbon steel in pre-sour conditions. As mentioned earlier, crude oil was used in this experiment as the carbon source for bacteria. Furthermore, several authors[101-104] mention that the presence of crude oil will affect the corrosion behaviour of the steel. The oily phase may form a protective layer on the steel and inhibit corrosion. This happen because crude oil has a very low

conductivity and a very low solubility of corrosion products[104] and hence inhibits the anodic partial reaction (iron dissolution).[101] The absorbed oil phase is also considered to facilitate the cathodic partial reaction as oxygen is more soluble in the oil phase.[101, 104]

In order to achieve the prerequisite minimum level of oxygen inside the cells, all cells were purged with filter sterilized nitrogen for 3 hours before bacteria inoculation. A complete anaerobic condition was not able to be achieved because traces of oxygen were still observed throughout the test. However, the upper limit of the dissolved oxygen inside the cell will not exceed the value detected in the gas phase (Figure 3.4a and 3.4b). Therefore, it is postulated that the NRB and SRB isolated in this study are not strict anaerobic bacteria. Both bacteria could be either microaerophilic that are able to tolerate 2-10% oxygen exposure[105] or aerotolerant anaerobic bacteria.[105, 106]

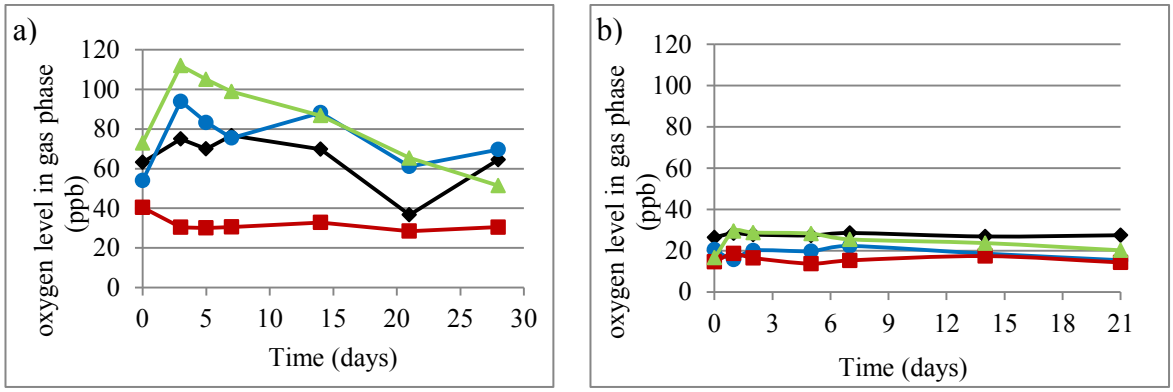

Figure 3.4 Oxygen level inside the electrochemical cell throughout immersion time for (a) UNS S31603 at 50°C for 28 days, (b) carbon steel, at 50°C for 21 days. (◆) control, (■) inoculated with SRB, (▲) inoculated with NRB, (●) inoculated with mixed bacterial (NRB+SRB).

The schematic figure of the electrochemical test design is shown in Figure 3.5. The temperature is maintained at 50±2°C by placing the electrochemical cells inside a water bath.

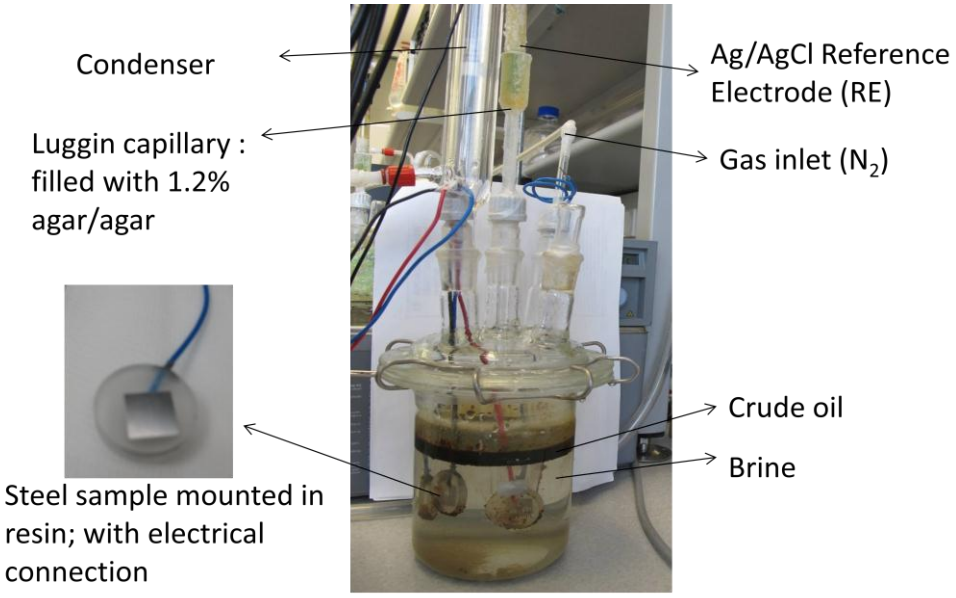

Figure 3.5 Electrochemical test design used to evaluate the impact of nitrate injection on UNS S31603 and carbon steel.

3.4 Concluding Remarks

Two different colonies of NRB bacteria were isolated from the crude oil and injection water samples, but only one was able to reduce nitrate. The SRB was only able to grow in liquid media but not in agar, therefore the bacteria colony morphology could not be observed. However, any further molecular methods or biochemical test was not employed because it is beyond the scope of this study. Therefore, no conclusion on the purity of the cultures obtained and also identification of the bacteria species could be drawn. Herein both bacteria are considered as consortia. Crude oil is taken into account in this experiment as it is an important carbon source for the bacteria in petroleum reservoirs and also because it may affect the corrosion behaviour of the steel. A complete anaerobic condition could not be achieved because traces of oxygen were still found.

CHAPTER 4: The Impact of Nitrate Injection on UNS S31603

4.1 Introduction

This chapter will discuss the impact of NRB, SRB and mixed bacteria (NRB+SRB) on UNS S31603 for long term exposure (28 days) in a corrosive biochemical mixture of production water and crude oil from field samples. Some short-term experiments (7 days) were also conducted to provide additional data.

4.2 The Effect of Immersion Time on Sulphate, Nitrate, Nitrite and Levels

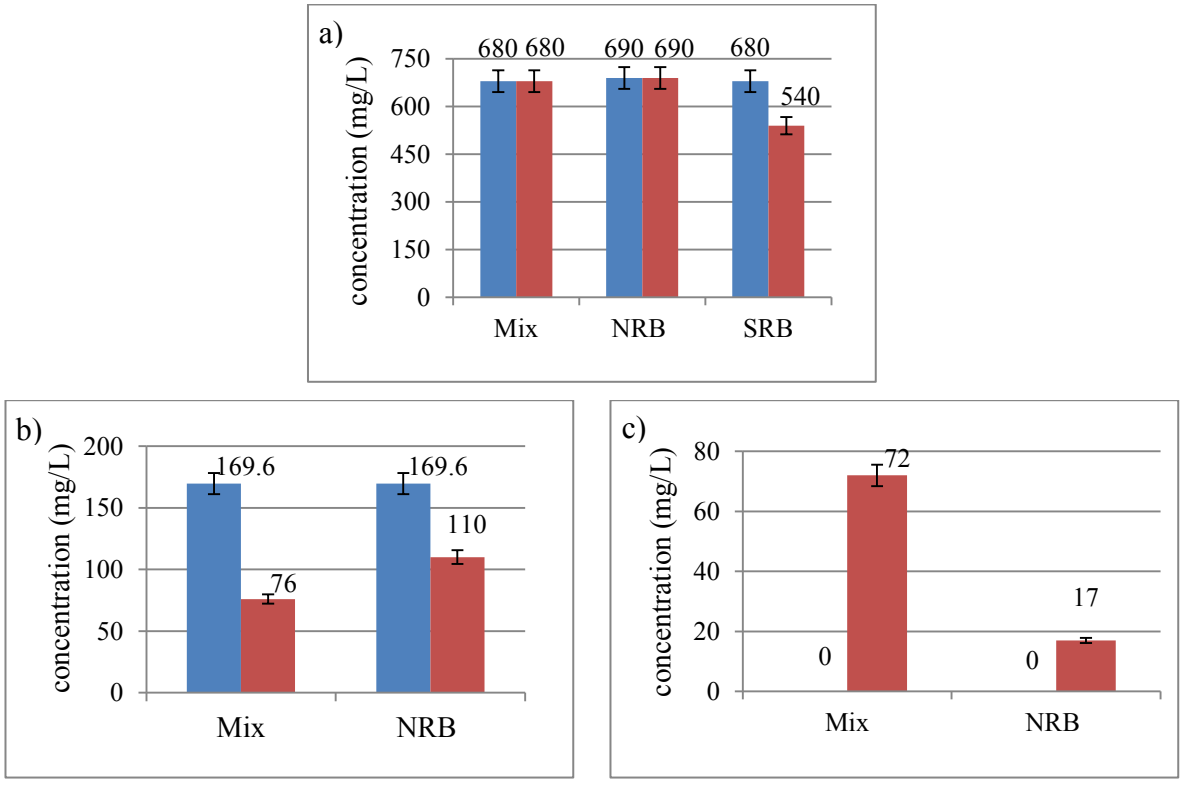

Figure 4.1 Concentration of (a) sulphate, (b) nitrate, and (c) nitrite before and after immersion time. (▬) before immersion time, (▬) after immersion time. Bars represent 5% RPD

The introduction of 5 mM sodium nitrate (equal to approximately 170 mg/L active nitrate) can promote the growth of NRB. The sulphate in SRB inoculated cells decreased over the period of the experiment (Figure 4.1a), indicating sulphate reduction activity. In addition, after the first week of the experiment, H_2S gas odour was detected from the SRB inoculated cell, and after two weeks, the brine water started to blacken (Appendix 1). The sulphate value did not change in the NRB

inoculated cell and the mixed bacteria (NRB+SRB) inoculated cell (Figure 4.1a), indicating inhibition of sulphate reduction. Furthermore, the mixed bacteria inoculated cell did not suffer from blackening until the end of the experiment (Appendix 1). These observations are in agreement with SRB cell numbers in Figure 4.2c that shows SRB growth is suppressed to below the detection limits. This confirms that with NRB present, sulphate reduction by SRB is inhibited. The nitrate level (figure 4.1b) in the NRB inoculated cell and mix bacteria inoculated cell shows a decrease, which indicates that the nitrate is consumed by the NRB. Nitrite production in the mix bacteria inoculated cell is higher than in the NRB inoculated cell (figure 4.1c). Nitrite, which is produced as an intermediate substance from nitrate reduction[107] is an inhibitor for sulphate reduction to sulphide which is catalysed by dissimilatory sulphite reductase (Dsr) of the SRB[18, 38]. It is predicted that, in the presence of SRB, NRB will maintain nitrite as an intermediate substance rather than reducing it further to nitrogen gas.

4.3 Bacteria Enumeration, pH and Redox Potential (E_h)

Bacteria growth (Figure 4.2 a,b,c) was observed by the MPN method and also by direct counting. MPN may lead to an under estimation of the total numbers as non-viable bacteria will not grow in the media, therefore bacterial direct counting was conducted as confirmation. The numbers of NRB in the NRB inoculated cell (Figure 4.2a) increased slightly from test-initiation day until day three and then slightly decreased until day seven. From day seven, the NRB population was increasing until day 21 and decreased from this point forward. The SRB growth in the SRB inoculated cell (Figure 4.2b) was relatively stable in the first week, and then the numbers started to increase until day 10, after which the numbers declined rapidly. In the cell inoculated with the mixture of NRB and SRB, it was demonstrated that, the SRB population was suppressed below the detection limit (<0.03) by the NRB, show in Figure 4.2c. This is confirmed by the fact that when the NRB population started to decline, the SRB started to re-grow (Figure 4.2c).

The pH of the crude oil/brine solution (Figure 4.3a) in the control cell slightly decreased from test initiation until day 15 and then remained stable until day 28. This

could be due to the lactate added to the cell. The pH in the NRB inoculated cell fluctuated in near neutral conditions (pH about 7.5) from test initiation until day 15. The pH then decreased and reached the lowest value of 6.5 on day 21, followed by an increase. For the mixed bacteria inoculated cell, the pH increased from test initiation and reached the highest value of eight on day five, then decreased. The pH in SRB inoculated cells was slightly increased on test initiation until day three, followed by a decrease until day five and an increase afterwards.

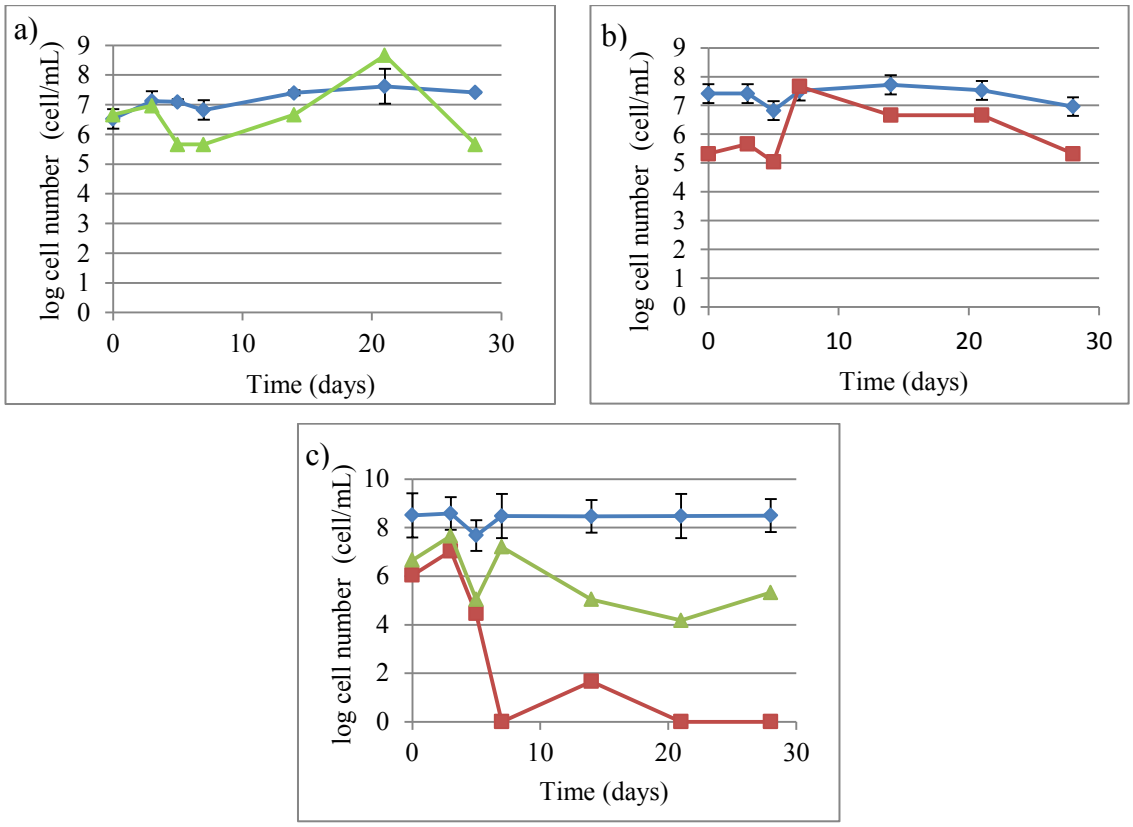

Figure 4.2 Bacterial populations throughout immersion time at 50°C for 28 days: (a) NRB inoculated cell, (b) SRB inoculated cell, (c) mixed bacteria (NRB+SRB) inoculated cell. (◆) total bacterial direct counting, (■) MPN for SRB, (▲) MPN for NRB

E_h shows the oxidative power of a solution. At the beginning of the experiment, all cells showed decreasing values of E_h (Figure 4.3b) because of the decrease in oxygen concentration as the cell was purged with nitrogen. All test cells showed positive values of E_h throughout the test with the SRB inoculated cell being an exception.

The E_h for the control cell and the NRB inoculated cell fluctuated in a range between 150 to 270 mV. This might be due to traces of oxygen in the cells (Figure 3.4a and 3.4b) and the nitrogen gas tubing was blocked by some salt on a few occasions,

allowing traces of oxygen to enter the cell. Therefore, the tubing was changed. After the first week, the E_h in the mixed bacteria inoculated cell was quite stable in the range between 100 and 140 mV. It is postulated that this is due to the fact that NRB prevented sulphate reduction and maintained nitrite at high levels, thus maintaining E_h at a positive value.[28] The E_h in the SRB inoculated cell decreased rapidly after the second week, and showed a negative value until the end of the immersion time. This could be due to the activity of SRB and further production of biogenic sulphide.[22] E_h is an important parameter to observe SRB growth because of the SRB prerequisite of -100 mV to start its growth.[18, 28, 31]

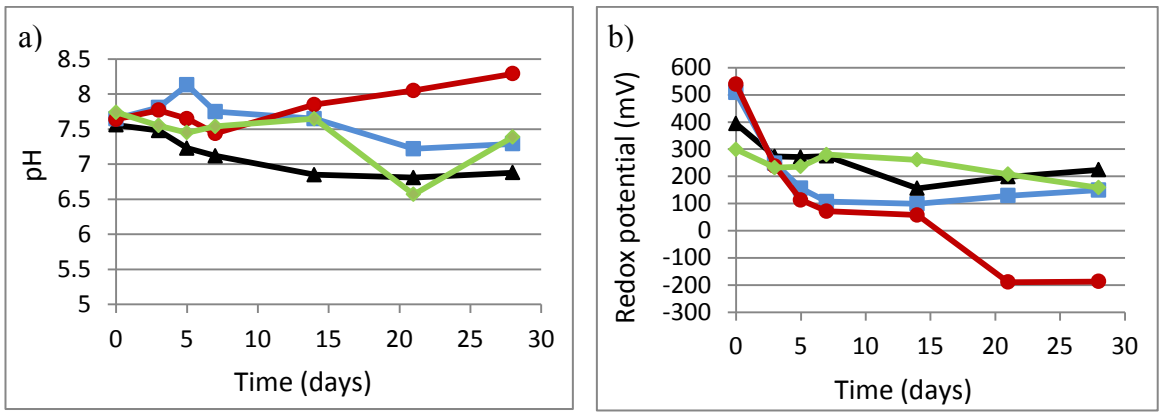

Figure 4.3 (a) pH and (b) redox potential changes during immersion time at 50°C for 30 days. (◆) control, (■) SRB inoculated, (▲) NRB inoculated, (●) mixed bacteria (NRB+SRB) inoculated.

4.4 The Effect of Immersion Time on Corrosion Potential (E_{corr}) of UNS S31603

The behaviour of E_{corr} transient of UNS S31603 during the corrosion test in corrosive production water +10% (v/v) crude oil for 28 days is shown in Figure 4.4. The E_{corr} started at different values for all the coupons in the four cells. The initial E_{corr} value from the lowest to the highest in sequence was: -323±1 mV (SRB), -313±50 mV (NRB), -247±9 mV (mixed bacteria), -222±17 mV (control). The final E_{corr} value from the lowest to the highest in sequence was: -436±48 mV (SRB), -331±51 mV (NRB), -228±23 mV (mixed bacteria), -172±43 mV (control).

Figure 4.4 shows the variation of E_{Corr} as a function of time for all the samples under four different conditions. Data presented are average data from a triplicate sample

and the bar shows the standard deviation. An Increase E_{corr} or ennoblement, increases the corrosion risk of stainless steel by elevating E_{corr} towards the steel pitting potential.[108]

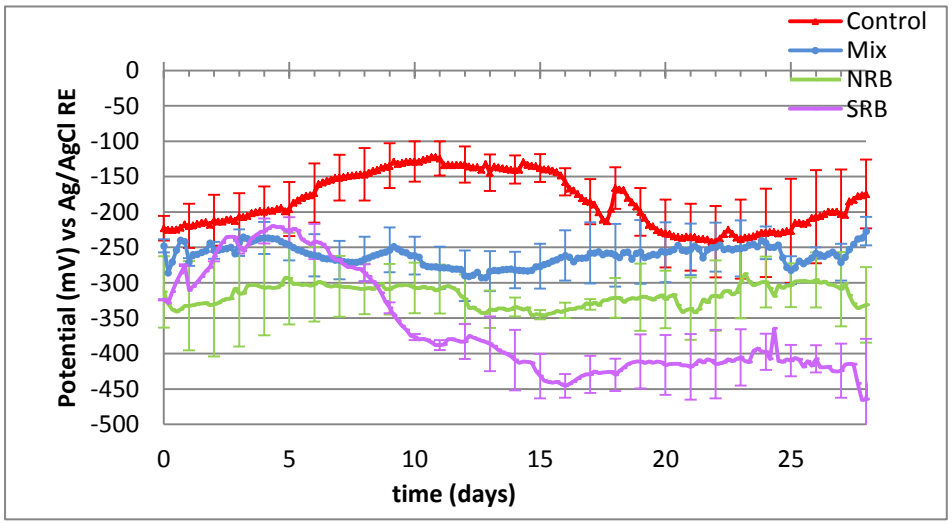

Figure 4.4 Open circuit potential (E_{corr}) as a function of time for UNS S31603 during immersion in production water +10 (v/v) crude oil at 50°C for 28 days. Data is based on the average of three samples with a standard deviation bar.

The E_{corr} for corrosion coupons in the control cell increased rapidly. The ennoblement for corrosion coupons in the control cell lasted for 11 days, and then the E_{corr} remained stable for four days; this may be attributed to the formation of a stable passive layer.[109, 110] A noticeable E_{corr} decrease of approximately 81 mV was noted from day 15 to day 17. This may indicate a weakening of steel passivity or surface activation,[109] which led to pit growth on the surface. This was proven by a distinguishable pit which was observed on the non-polarized sample after the termination of the test (Figure 4.14a). From this point forward, the E_{corr} shifted again towards a positive potential, reached a peak on day 18 and decreased again until day 22. Thereafter, the E_{corr} rapidly increased again until day 28.

Ennoblement happened on the corrosion coupons in the SRB inoculated cell from test initiation until day five of exposure, with two spikes noted at 19 hours and 60 hours of exposure. Thereafter, E_{corr} decreased until day 16, followed by an increase of 50 mV and remained relatively stable until day 27. However, some spikes were noted as the potential increased for a short time on days 23 and 24. On days 27 and 28 a decrease in the E_{corr} of approximately 50 mV was noted. It is postulated that the

spikes found were attributed to the formation of small pits and this was confirmed by the surface analysis on the non-polarized sample after the termination of the test (figure 4.14c).

Fluctuations in the E_{corr} of the corrosion coupons in the NRB inoculated cell and in the mixed bacteria inoculated cell were observed. However, these fluctuations are not significant as they are still within the range of 50 mV. Additionally, no pits were found in both non-polarized corrosion coupons of the inoculated cell as well as in the mixed bacteria inoculated after the termination of the test (Figure 4.14b and 4.14d)

Ennoblement of corrosion coupons in the SRB inoculated cell may take place because of bacteria colonization on the steel surface.[111, 112] This is demonstrated by the SEM observation at the end of the experiment (Figure 4.12a-c). Other possibilities that may cause steel ennoblement are: (1) enzymes production by bacteria[112-114]; (2) the changes of the cathodic properties of the stainless steel as a result of microbial activity on the surface,[112]; (3) the decrease of passive current density due to biofilm formation on the surface,[112, 114]; (4) production of inhibitors by bacteria that are retained in the biofilm matrix,[112]; (5) reduction of the chloride concentration at the surface that is covered by the biofilm.[112]

Ennoblement of the corrosion coupon in the control cell, might have taken place because of: (1) incongruent dissolution of the alloy, or as the result of corrosion progress. A simple explanation of the corrosion progress is that the formation of a corrosion product deposit may polarize, that is increase the overpotential, for the anodic reaction[115]; (2) the difference in the semi-conductive properties of the passive film[114]; (3) the changes of the production water composition after autoclave sterilization. As mentioned earlier in Section 2.2, reservoir breakthrough was observed in the field as indicated by high level of sulphate and chloride. Therefore, the production water is almost similar to seawater. Some authors mentioned that autoclaving drives CO_2 out of the seawater, causing a shift in the carbonate buffer system[116] and may cause precipitation.[117, 118] However, autoclave is still the most reliable method for killing bacteria, bacteriophages and bdellovibrios.[118]

It was demonstrated that the E_{corr} varied for each cell. Interestingly, the E_{corr} of corrosion coupons in the control cell showed a more positive value compared to the corrosion coupons in the bacteria inoculated cell throughout the experiment. The graphs for all experiments are not smooth as some small fluctuations were noted. This could be attributed to oxygen penetration as shown by the traces of oxygen found inside the cells (Table 3.4). Oxygen may have diffused inside the cells when the samples were taken for bacterial counting. As mentioned earlier, it was observed that there was some salt plugged into the nitrogen tubing a few days after the experiment began. This may also have contributed to the disruption of nitrogen circulation in the cells.

4.5 Cyclic Polarization Scan (CPS)

At the end of the experiment, CPS was conducted on two of the triplicate samples. CPS curves for the coupons immersed for four weeks were compared with the CPS curves obtained from the non-exposed coupons (standard). These corrosion coupons were allowed to stabilize in the E_{corr} for one hour before the CPS was conducted.

As explained above (Section 1.8), CPS offers a qualitatively reasonable prediction of the propensity of a passivating alloy to suffer from localized corrosion.[73-75] However, in reality, the curve obtained will normally be far from the ideal curve in Figure 1.5. The CPS curves obtained from the corrosion coupons after long-term immersion in four different conditions and the standard coupon are shown in Figures 4.5 and 4.6. The key values of the curves are shown in Tables 4.1 and 4.2

4.5.1 Features Useful in the Interpretation of CPS Curve

4.5.1.1 Hysteresis

It can be seen that all the reverse scans of all the corrosion coupons in the four different conditions, and also the standard coupons, show negative hysteresis as the reverse scans go to the right of the CPS curve (Figure 4.5 and Figure 4.6). This means localized corrosion may occur. The size of the loop itself is often related to

the amount of pitting: the larger the loop, the higher the surface damage when pitting occurs.[73] The order of the size of the hysteresis loop after four weeks of immersion time (Figure 4.5 and Figure 4.6) can be summarized in the following order: SRB> control > mixed bacteria> standard> NRB.

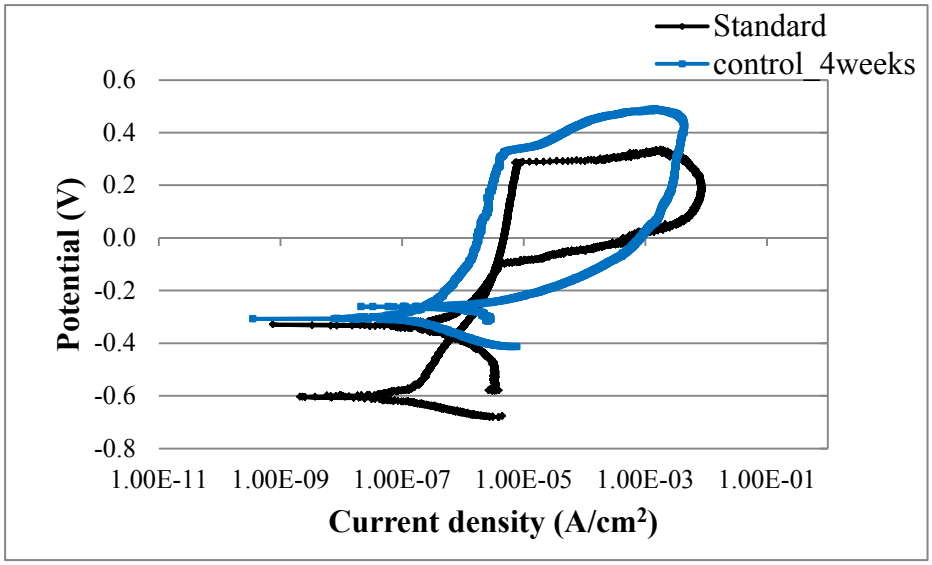

Figure 4.5 Cyclic polarization scan (CPS) results of standard corrosion coupon and corrosion coupons in control cell after four weeks of immersion time in production water +10% crude oil at 50°C. All hysteresis loops are negative which indicates localised corrosion may occur.

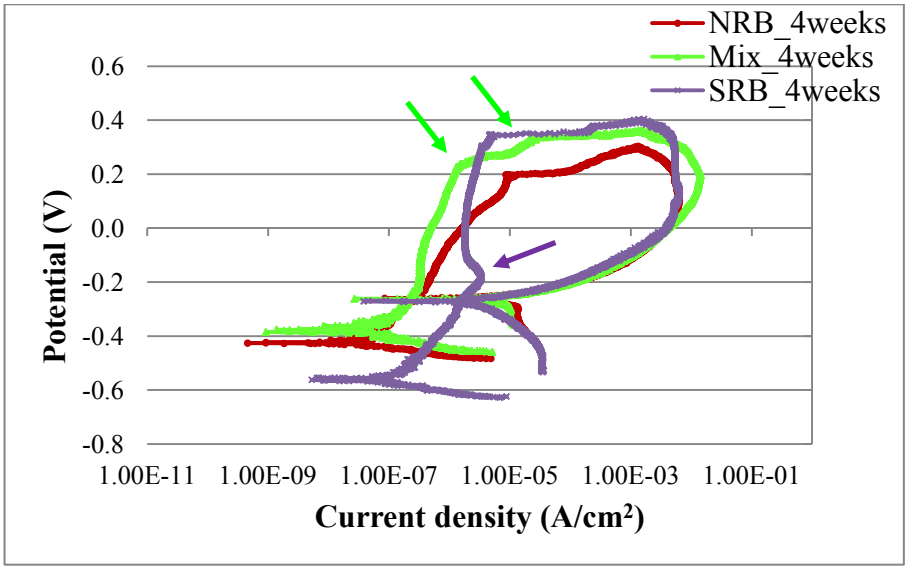

Figure 4.6 Cyclic polarization scan (CPS) results of corrosion coupons in bacteria inoculated cells after four weeks of immersion time in production water +10% crude oil at 50°C. The purple arrow shows metastable pitting on corrosion coupons in SRB inoculated cell. The green arrow shows an example of typical two E_c value obtained in the CPS curves. All hysteresis are negative, which indicates localised corrosion may occur.

4.5.1.2 Critical Pitting Potential (E_c)

The order of the E_c values after four weeks of immersion time (Table 4.1 & Table 4.2) can be summarized in the following order: SRB > control > standard > mixed bacteria > NRB. One important highlight from these results is the NRB decrease the in E_c value to a greater extent compared with other conditions. Additional experiments were conducted in the same manner for the NRB inoculated cell, the mixed bacteria (NRB+SRB) inoculated cell and the control cell for one week of immersion time. Surprisingly, the E_c results (figure 4.6) change in the following order: mixed bacteria> standard > NRB > control. It is necessary to stress that the aim of this study is to evaluate the NRB impact on corrosion of UNS S31603. Therefore, evaluation of SRB impact on corrosion of UNS S31603 is not the main focus and is not put under scrutiny.

Table 4.1 Key summary value used to interpret cyclic polarization scan results (Figure 4.5). Results were obtained from duplicate samples. Scan rate used for both forward and reverse scans was 0.5 mV/s against the Ag/AgCl Reference Electrode

Coupons ID	Standard	Control	
time / parameter		1 week	4 weeks
E_c (mV)	305 ± 16	266 ± 35	360 ± 37
E_r (mV)	-180 ± 64	> -196	-273 ± 8

Table 4.2 Key summary value used to interpret cyclic polarization results (Figure 4.6). Results were obtained from duplicate samples. Scan rate used for both forward and reverse scans was 0.5 mV/s against the Ag/AgCl Reference Electrode

Coupons ID	NRB		Mixed		SRB	
time / parameter	1 week	4 weeks	1 week	4 weeks	1 week	4 weeks
E_c (mV)	297 ± 43	117± 12	398 ± 49	281 ± 9	-	367± 68
E_r (mV)	-259 ± 10	-257 ± 4	-134 ± 35	-224 ± 39	-	-282± 20

The conclusions that can be drawn from these E_c results, as illustrated in Figure 4.8 are: (1) the UNS S31603 steel passivity increased with longer exposure time, as shown by the increasing E_c value; (2) the UNS S31603 steel passivity decreased with

longer exposure time in both the NRB inoculated cell and the mixed bacteria (NRB+SRB) inoculated cell, as shown by the decreasing E_c value; (3) it is postulated that in this particular corrosive environment, bacteria, in this case the NRB and the mixed bacteria (NRB+SRB), may offer a beneficial protection for a short period of time, but with longer exposure time it may have detrimental effects. To test this prediction, a steel surface analysis was conducted by SEM, and thus revealed that, after four weeks, the biofilm grew into a mature biofilm and formed patchy colonies on the steel surfaces (Figure 4.11a and Figure 4.13a).

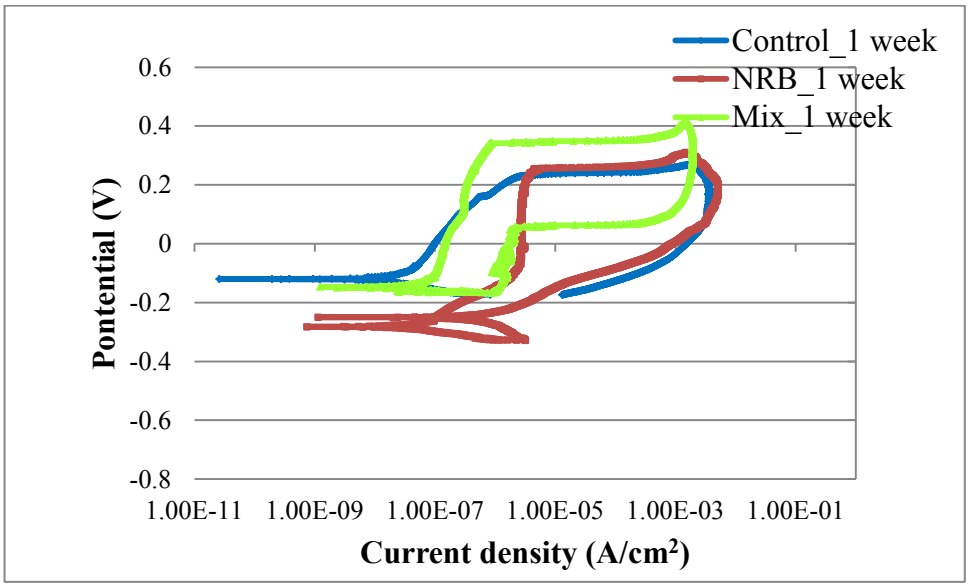

Figure 4.7 Cyclic polarization results of corrosion coupons in bacteria inoculated cells and control cell after one week of immersion time in production water +10% crude oil at 50°C. All hysteresis are negative which indicates localised corrosion may occur.

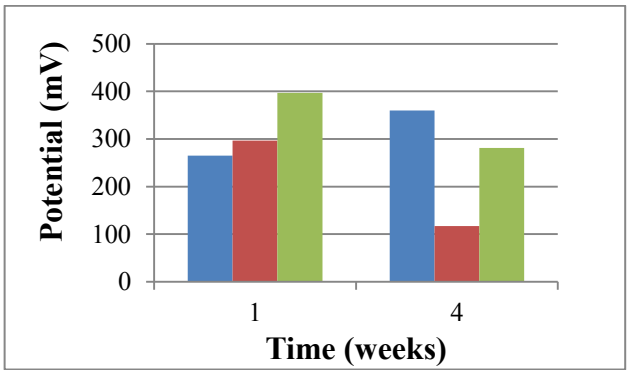

Figure 4.8 Summary of the critical pitting potential changes after corrosion coupons were immersed for one week and four weeks in production water and 10% (v/v) crude oil at 50°C. ( ) control, ( ) NRB inoculated, ( ) mixed bacteria (NRB+SRB) inoculated

One crucial point to mention is that the changes in E_c may be influenced by the presence of biofilm on the steel surface or bacterial metabolite in the water chemistry environment. As mentioned above (Section 1.5), microbes, in this particular case bacteria, have the propensity to attach to surfaces. Once they attach to steel surfaces they will proliferate, produce EPS and grow into mature biofilm (Figure 4.11a-c, Figure 4.12c and Figure 4.13a-c). The bacteria metabolite scrutinized in this study is nitrite, as it has been known as both an oxidizing agent and corrosion inhibitor.[18, 39] Insufficient amounts of nitrite promote corrosion, but nitrite serve as a corrosion inhibitor at sufficient concentrations.[18] Generally, the effect of nitrite on corrosion is a function of its availability and lower concentrations of nitrite have been found to increase the corrosion rate.[39] It can be inferred from Figure 4.1c that the nitrite level when the CPS test was conducted was 72 mg/L for the four week mixed bacteria culture and 17 mg/L for the four week NRB culture. Additional measurements were also conducted to check the nitrite levels of the one week samples. The nitrite level was 83 mg/L for the one week mixed bacteria culture and was 1.8 mg/L for the one week NRB culture. The fact that the nitrite level for the NRB inoculated cell was always lower than the mixed bacteria inoculated cell is in agreement with the E_c values obtained; the E_c value for the corrosion coupon in the NRB inoculated cell was always lower than the mixed bacteria inoculated cell for the same exposure time. However, it is also noticeable that in the one week NRB inoculated cell where the nitrite value is as low as 1.8 mg/L, the E_c is higher than the four week mixed bacteria inoculated cell (Table 4.2) that contains 72 mg/L nitrite. Therefore, it is deduced that the E_c was not influenced by the nitrite concentration alone, but also influenced by the biofilm that was attached to the steel surface. This confirms the earlier prediction that the biofilm may have detrimental effects in longer exposure times.

Another important point to mention is that some materials show two pitting potentials, which can be distinguished from the curves. Figure 4.6 shows an example of this phenomenon (the two pitting potentials shown by green arrows). Raetzer-Scheibe et al.,[78] who also observed this phenomena, proposed that this may happen when pitting occurs at the grain boundary regions of the alloy.

4.5.1.3 Metastable Pitting

In the CPS curve of the corrosion coupon in the SRB inoculated cell after four weeks of immersion time, metastable pitting was observed at a potential of aprroximately -190 mV. Starosvetsky et al.[119] suggest that metastable pitting passivation in a solution containing sulphide is due to ferrous sulphide precipitation, and thus the rate of current increase is restrained. This was evident in the microscopic observation results on the sample that was not polarized, where some micro pits are observed (Figure 4.16a, 4.16b). Additionally, sulphide presence is also evident by the blackening of the brine solution (Appendix 1).

4.5.1.4 Repassivation Potential (E_r)

As seen in Tables 1 and 2, the E_r of the standard corrosion coupon is higher than the E_r of the corrosion coupons in the control cell and in the bacteria inoculated cells, except for the one week mixed bacteria inoculated cell. However, the E_r of the mixed bacteria corrosion coupons after four weeks of immersion show a lower value compared to the standard corrosion coupons. It is also noted that with longer immersion time, the E_r show a decreasing value, except for corrosion coupons in the NRB inoculated cell which show a relatively stable value after one week and four weeks of immersion time. From these results it can be concluded that E_r decreases (becomes more active) after exposure in a corrosive environment or the ability of the steel to repassivate after pit forms has been reduced with longer exposure time in a corrosive environment. Other researchers noted that E_r measurements for stainless steel were related only to the conditions necessary to repassivate a growing pit after a specific period of pit propagation (dependent on the extent of pit growth).[64, 76, 120] This also means that the E_r was dependent of the change in E_c value. Another important point that has to be kept in mind is that the lower potential of the E_r means a poorer repassivation ability and its crevice susceptibility may be high.[76]

4.5.2 Additional Information from CPS Results

It is important to mention, that in this experiment, the determination of the E_c and E_r resulted in quite highly scattered results. However, other researchers also found similar phenomena with highly scatter results from several samples of the same materials.[76, 77] Some authors mention that this dispersion is not due to measurement error but to the mechanism of localized corrosion. This high level of dispersion value is attributed either to random probabilistic phenomena or to instability and deterministic chaos.[76] Additionally, the crude oil may not have formed a uniform layer on the steel surfaces.

4.6. Linear Polarization Resistance (LPR)

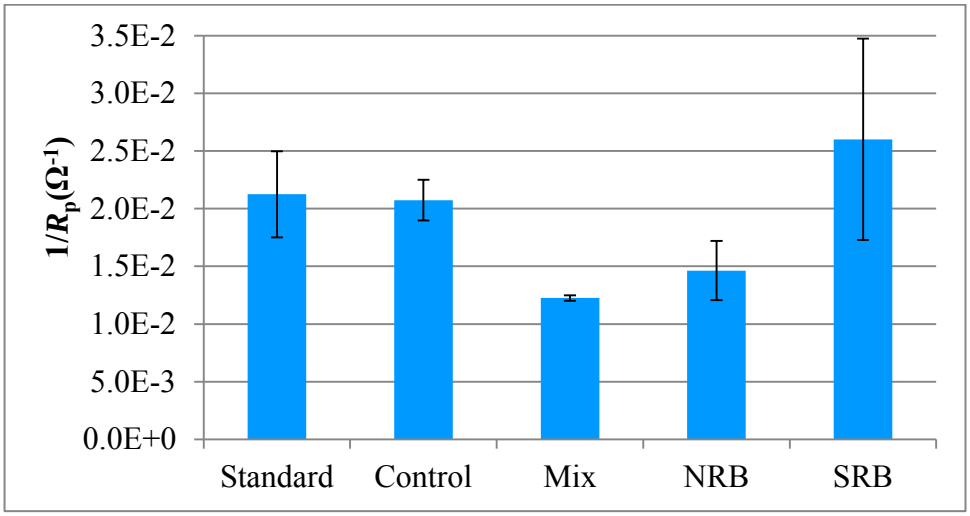

Figure 4.9 Time dependence of R_p obtained from Linear Polarization Resistance. Scan rate used was 0.125mV/s against Ag/AgCl reference electrode. Data presented are average from duplicate samples and the bar represents actual value

To confirm general corrosion rates, LPR was conducted with a low overpotential (5 mV) in order not to destroy the material. The R_p is inversely proportional to corrosion rate, the decrease in R_p reflects the increase in corrosion rate as described in Equation 1.1.[93, 121] It can be deduced from Figure 4.9, that there is not much change in corrosion rate of standard and control corrosion coupons. There is a slight decrease of corrosion rate in mixed bacteria (NRB+SRB) and NRB inoculated cells. The high corrosion rate in the standard and control samples could be induced by the high chloride content of the brine (approximately 21000 mg/L). Little et al.[114]

mention that chloride must be present in a concentration at least comparable to that of all other anions otherwise corrosion is inhibited. The lower corrosion rate value of the corrosion coupons in the bacteria inoculated cells may be related to balance of the anion presence in the brine due to bacteria metabolism such as formation of nitrite, organic acid (e.g. acetate); or by biofilm formation. Additionally, Mansfeld[112] also mentions that corrosion inhibition by biofilm formation has been observed for different materials exposed to corrosive environments. An important point to be considered is how long the bacteria biofilm can eventually inhibit corrosion before it starts inducing localized corrosion.

The corrosion rate for corrosion coupons in the SRB inoculated cell is higher than the corrosion coupons in the NRB inoculated cell, the corrosion coupons in the mixed bacteria (NRB+SRB) inoculated cell and also the corrosion coupons in the control cell. This may be due to the presence of the metastable pits on the surface. Therefore, based on CPS and LPR results, it can be concluded that, in terms of localized corrosion, the presence of NRB is worse than SRB, but not in terms of the general corrosion rate.

4.7 Film Surface Analysis on UNS S31603 Coupons by SEM and EDS

4.7.1 Representative Corrosion Coupons in the Control Cell

SEM was carried out to validate the corrosion products formation and the adhesion of bacteria on the steel surface. EDS was also conducted to verify the corrosion product and the bacterial biofilm on the steel surface. Figure 4.10 shows the representative SEM images and EDS spectra of the corrosion coupons from the control cell after 28 days of immersion in corrosive production water +10% (v/v) crude oil. Figure 4.10a shows tiny, round crystals of corrosion products covering the steel surface (red arrows) while Figure 4.10b shows a solid spongy film formed on the steel surface. EDS analysis shows that this spongy film consists mainly of iron (Fe), carbon (C), nickel (Ni) and oxygen (O), and weak signals of silica (Si) and sulphur (S). The area inside this layer shows the same results, but with a higher Fe and Cr peak and extra weak signals of phosphate (P) and chloride (Cl). However, further study on the type of films formed on the surfaces was not conducted. The

existence of S and Cl peaks strengthen our earlier prediction (Section 4.6) that corrosion attack took place in this particular corrosive brine. Nevertheless, no distinguishable pit could be found when the samples were observed under SEM.

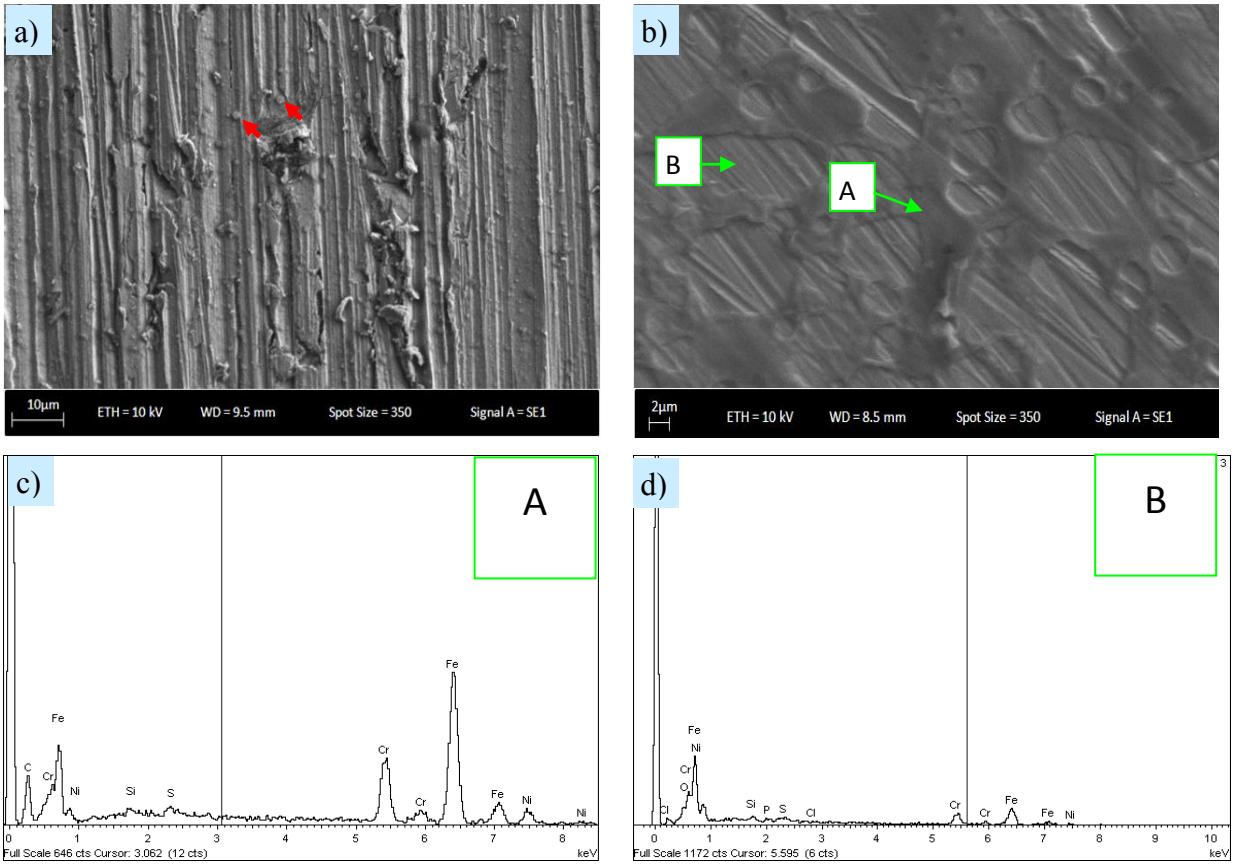

Figure 4.10 Representative SEM images of a corrosion coupon in the control cell after 28 days of immersion time in production water +10% (v/v) crude oil. (a) steel surface morphology, some small particles of corrosion products were found on the surface, no distinguishable pit can be observed (b) a film was observed on steel surface (c,d) EDS spectra from representative corrosion products layer in two different spots

4.7.2 Representative Corrosion Coupons in the NRB Inoculated Cell

Figure 4.11a shows patchy colonies of bacteria forming biofilm on a steel surface (red arrows) and some bacteria were also found to start proliferating and forming a colony on the steel surface (yellow arrow). Additionally, a bacteria colony forming a biofilm and embedded with corrosion products can also be seen (blue arrow). Figure 4.11a and figure 4.11b were taken using 5 kV accelerating voltage, so that small round crystals of corrosion products can be seen uniformly covering the steel surface.

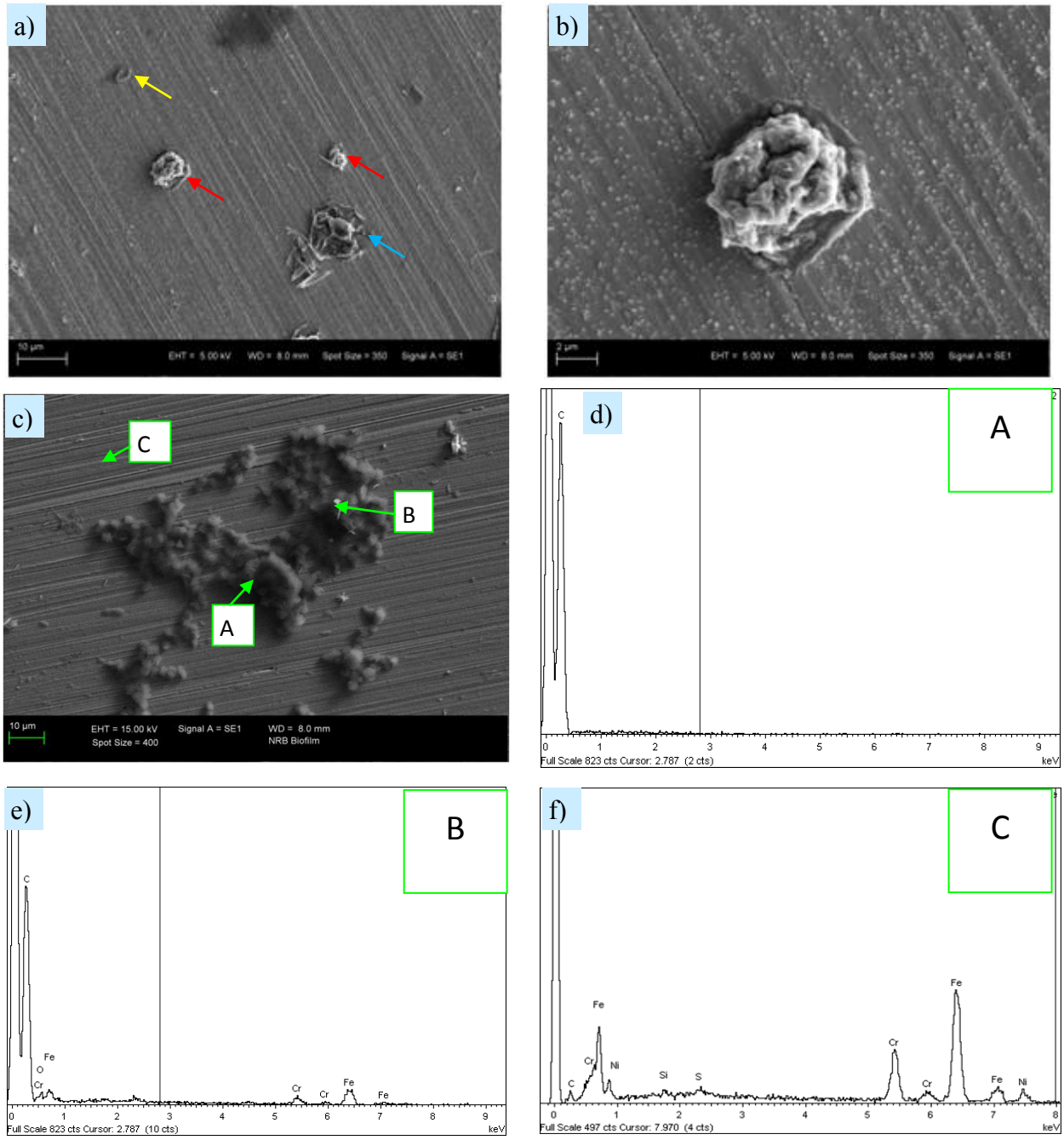

Figure 4.11 Representative SEM images of a corrosion coupon in the NRB inoculated cell after 28 days of immersion time in production water +10% (v/v) crude oil. (a) most of the bacteria formed patchy bacterial colonies on steel surfaces (red arrow), bacteria colonies embedded with corrosion product (blue arrow) and bacteria started proliferate and form a colony (yellow arrow); (b) bacteria colony and small particles of corrosion products can be observed on the steel surface, picture was taken with 5 kV to get more surface morphology; (c) bacteria colony on steel surface, picture was taken with 15 kV to get EDS spectra from three different spots; (d,e) EDS spectra from bacteria biofilm; (f) EDS spectra from steel surface.

Figure 4.11c shows mature bacteria biofilm, which was taken using 15kV accelerating voltage, and EDS spectra were taken in three different spots (as shown by the green arrow). The EDS spectra A that was taken on the biofilm shows only a C peak (Figure 4.11d). The EDS spectrum B that was also taken on the biofilm shows Fe, Cr and O peaks in addition to the C peak. This means that some corrosion products were embedded in the biofilm. The EDS spectra C that was taken in the steel area near the biofilm, does not show any O peak. This means no oxide layer formed on the area near the biofilm, or that the oxide layer may have been broken by the biofilm.

4.7.3 Representative Corrosion Coupons in the SRB Inoculated Cell

Figure 4.12a shows that, in a SRB inoculated cell, most of the bacteria attached and spreading as a single cell on the steel surface; however, some bacteria biofilm also found (Figure 4.12c). Figure 4.12b shows bacterium starting to produce EPS. The EDS spectrum A reveals that some corrosion products embedded in the biofilm. In the EDS spectrum B, there is a weak peak of sulphur (S) in addition to other typical stainless steel components (Fe, Cr, Mn, Ni, Si). This indicates a very thin ferrous sulphide film formed on the surface. EDS spectrum C shows a strong peak of S, and also there are barium (Ba), calcium (Ca), phosphorous (P) and O peaks in addition to other typical stainless steel components. This may indicate some corrosion products and also some inorganic precipitation (e.g. $BaSO_4$)

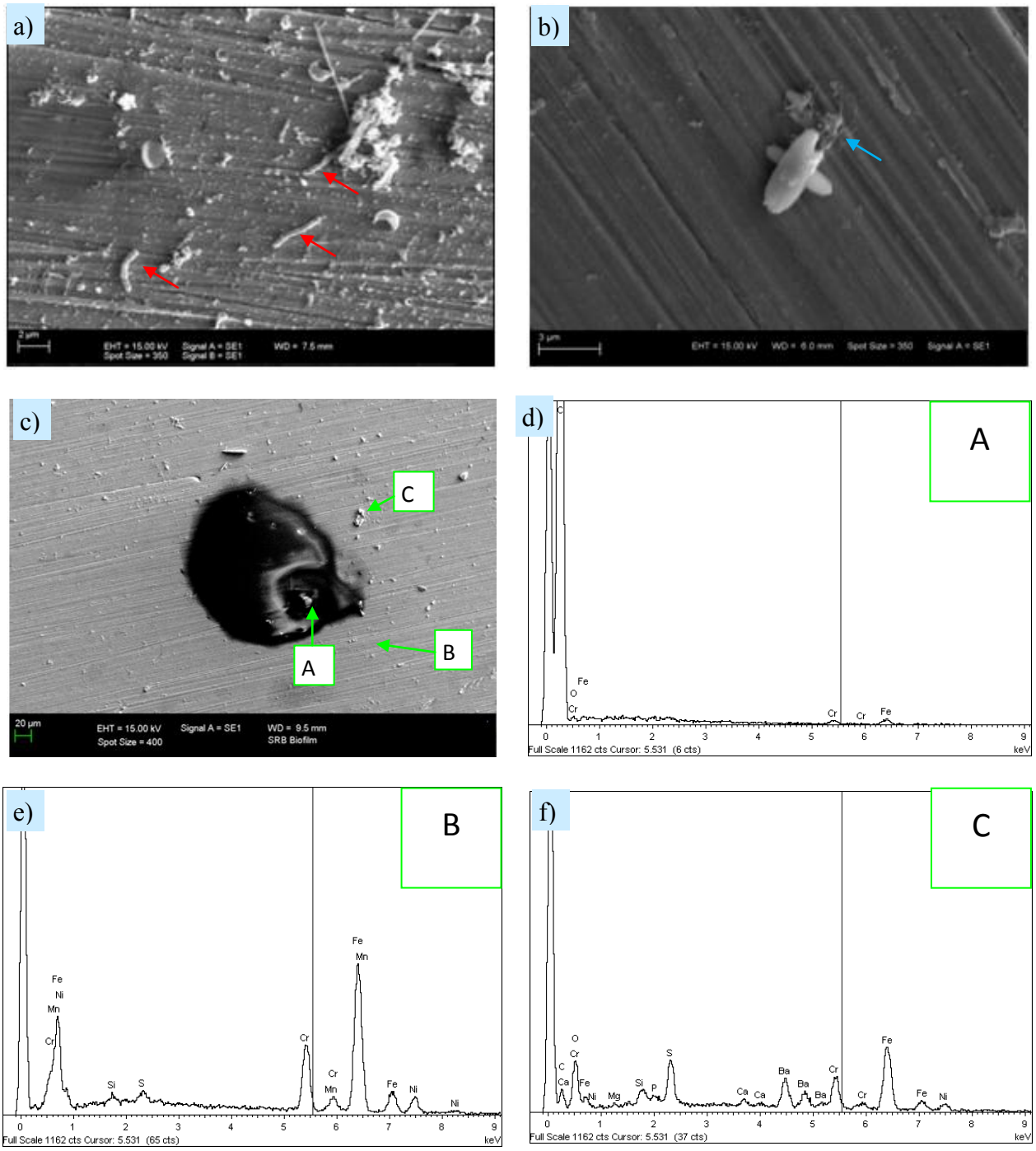

Figure 4.12 Representative SEM images of a corrosion coupon in the SRB inoculated cell after 28 days of immersion time in production water +10% (v/v) crude oil. (a) most of the bacteria were found as a single cell spreading on the steel surface on steel surfaces (red arrow); (b) bacteria start producing EPS (blue arrow); (c) mature bacteria biofilm on steel surface; (d) EDS spectra from bacteria biofilm; (e) EDS spectra from steel surface; (f) EDS spectra from corrosion products

4.7.4 Representative Corrosion Coupon in Mixed Bacteria (NRB+SRB) Inoculated Cell

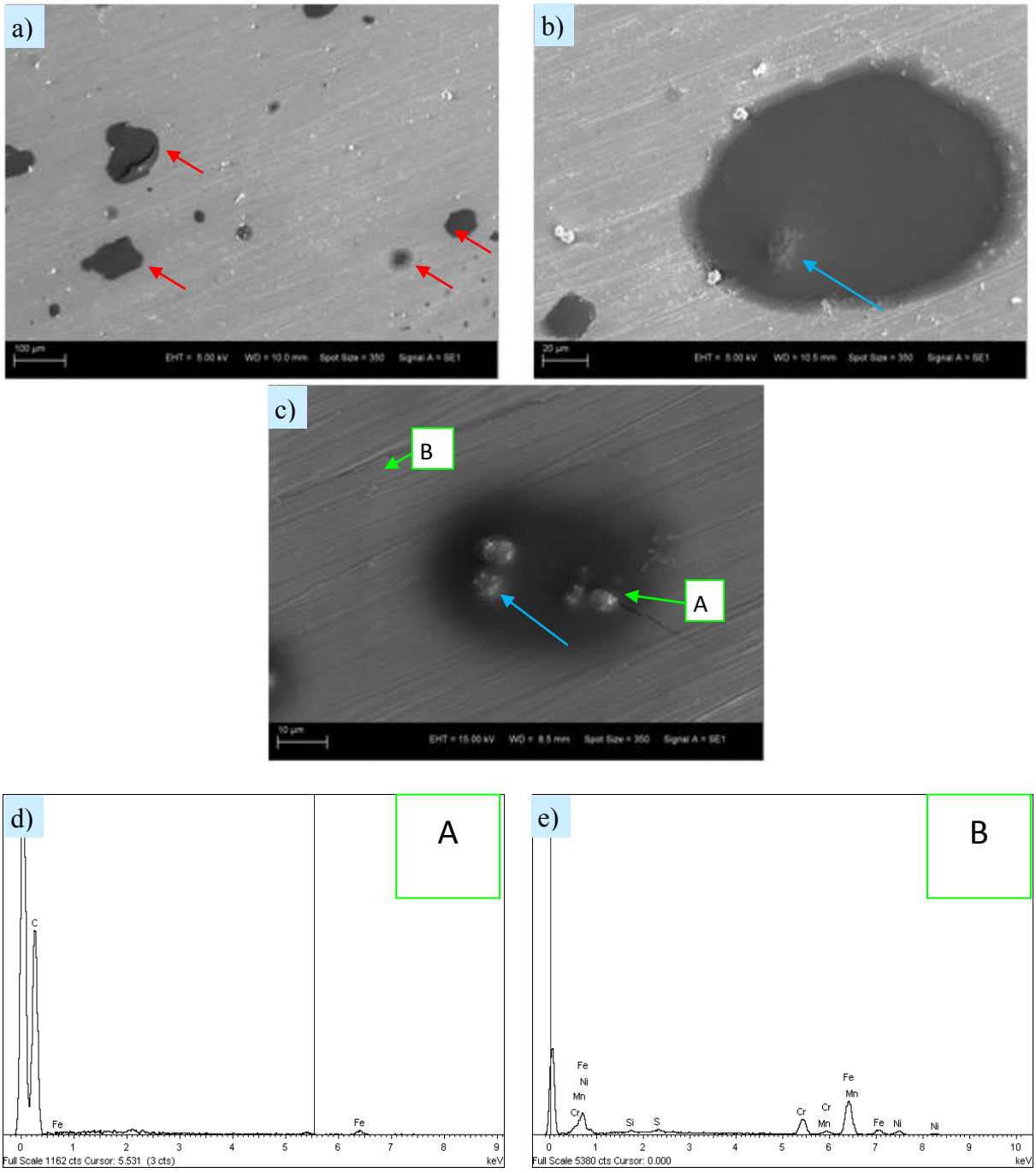

Figure 4.13 Representative SEM images of a corrosion coupon in the mixed bacteria (NRB+SRB) inoculated cell after 28 days of immersion time in production water +10% (v/v) crude oil. (a) patchy bacteria colonies on the steel surface (red arrow); (b) bacteria cell entrapped inside EPS (blue arrow); (c) bacteria biofilm on steel surface; (d) EDS spectra from bacteria biofilm; (e) EDS spectra from steel surface

The SEM reveals that the bacteria formed patchy colonies on a steel surface (Figure 4.13a). When low accelerating voltage was used (5 kV), the corrosion products can be seen on the surface (Figures 4.13a and 4.13b). It can be seen that the bacteria cells are hidden underneath the EPS (Figures 4.13 b and 4. 13c) as indicated by the blue arrow. EDS spectra was taken at two different spots. Spectrum A, which was taken on the biofilm, shows a strong C peak and weak Fe peak. This indicated some corrosion products embedded inside the biofilm. Spectrum B, which was taken on the steel surface, shows typical stainless steel components and an extra weak S peak. This may indicate a very thin ferrous sulphide film.

4.8 Steel Surface Analysis by Light Microscopy

4.8.1 Steel Surface Analysis of Non-polarized Corrosion Coupons after Corrosion Products Removal

Steel surface morphology was performed on corrosion coupons that were not polarized (Figure 4.14a-d) to observe pit formation after immersion in the corrosive biochemical solution. One distinguishable pit (Figure 14.4a) was found on the control corrosion coupon. This pit was easily observed, even when low magnification was used (5x). This is not surprising as based on E_{corr} observation in Section 4.4, there is a fairly large potential decease from day 15 until day 17. The 3D observation was performed on the pit to characterize it (Figure 4.15a-c). It was revealed that the pit has a volume of 25,541 μm^3 (Figure 4.15a) and a pit depth of 43.51 μm (Figure 4.15b,c). When higher magnification is used (50x) some micro pits are observed on the corrosion coupons from the SRB inoculated cell. The 3D observation was performed to characterize these micro pits. Some representative micro pits are shown in figure 4.16a-b. The smallest pit found has a pit volume of 94.78 μm^3 and a pit depth of 1.47 μm; and the biggest pit found has a pit volume of 381.73 μm^3 and depth of 3.58 μm.

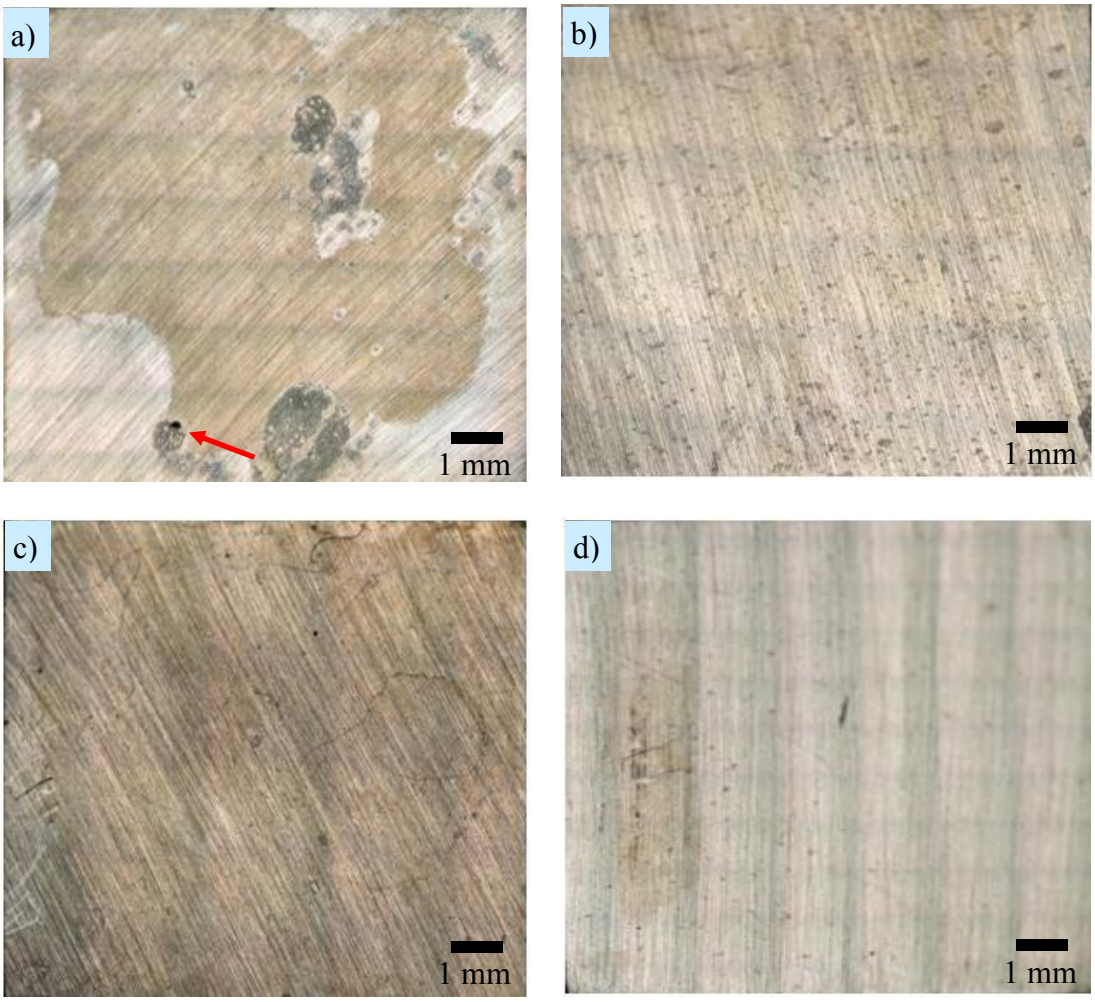

Figure 4.14 2D images of non-polarized corrosion coupons surface morphology after 28 days immersion (a) control, (b) NRB inoculated, (c) SRB inoculated, (d) mixed bacteria inoculated. Red arrow shows a pit which formed on the steel.

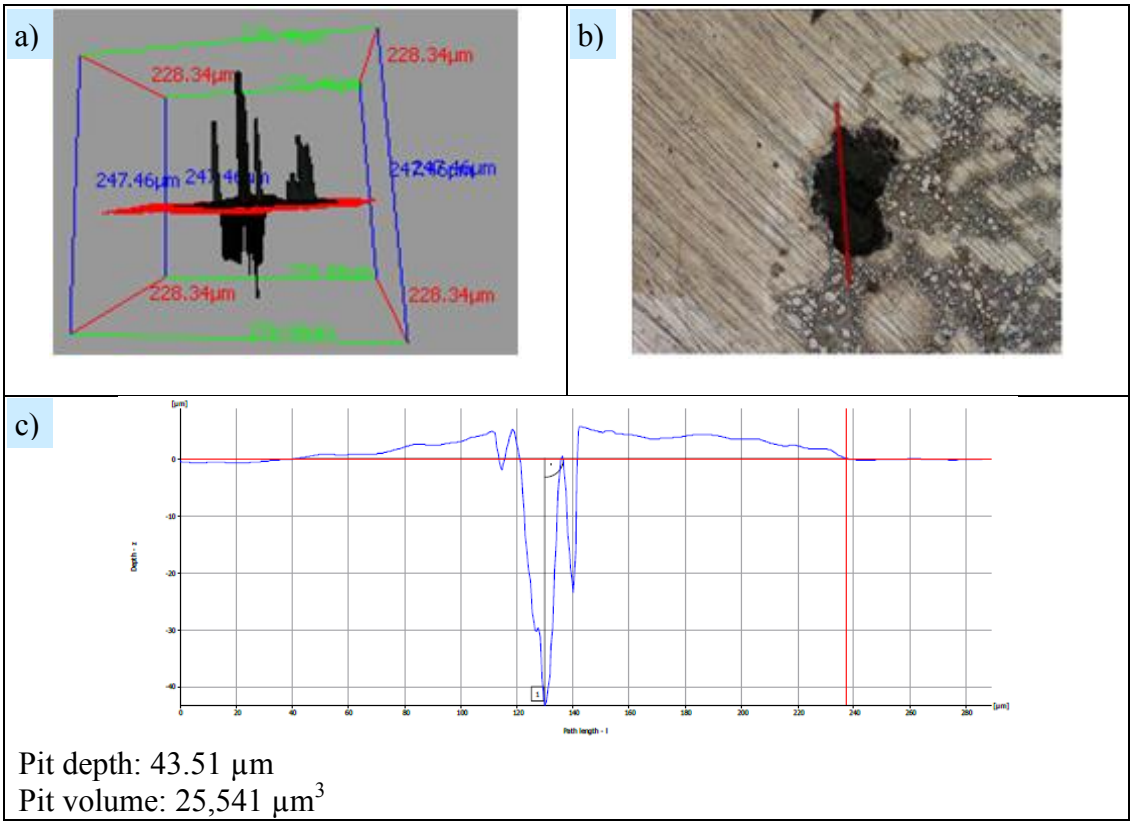

Figure 4.15 Pit morphology of a corrosion coupon in control cell (a) 3D picture of pit volume, (b) pit surface morphology, (c) 3D pit depth measurement

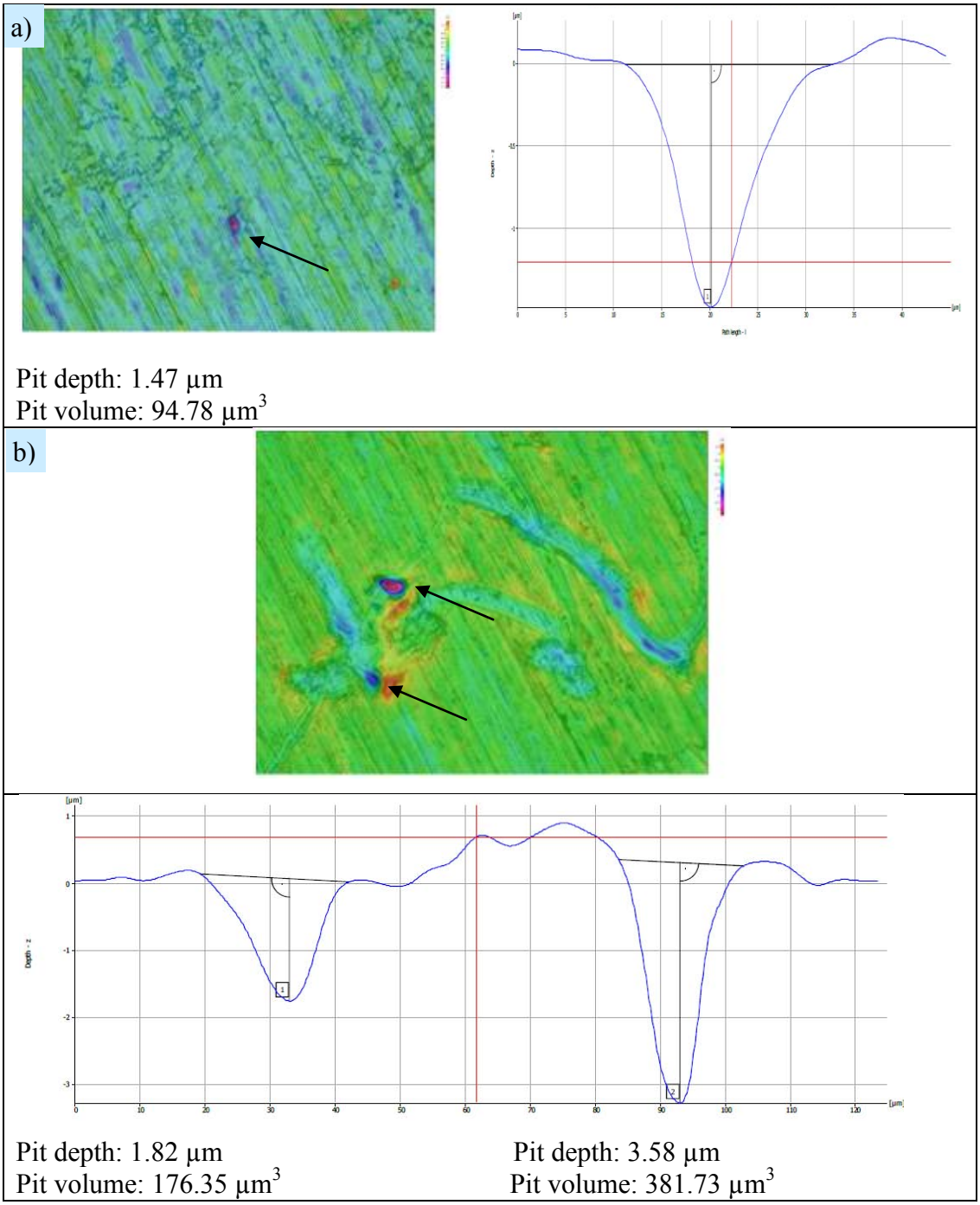

Figure 4.16 (a,b) Representative micro pits from a corrosion coupon in the SRB inoculated cell

4.8.2 Steel Surface Analysis of the Polarized Corrosion Coupons after Corrosion Products Removal

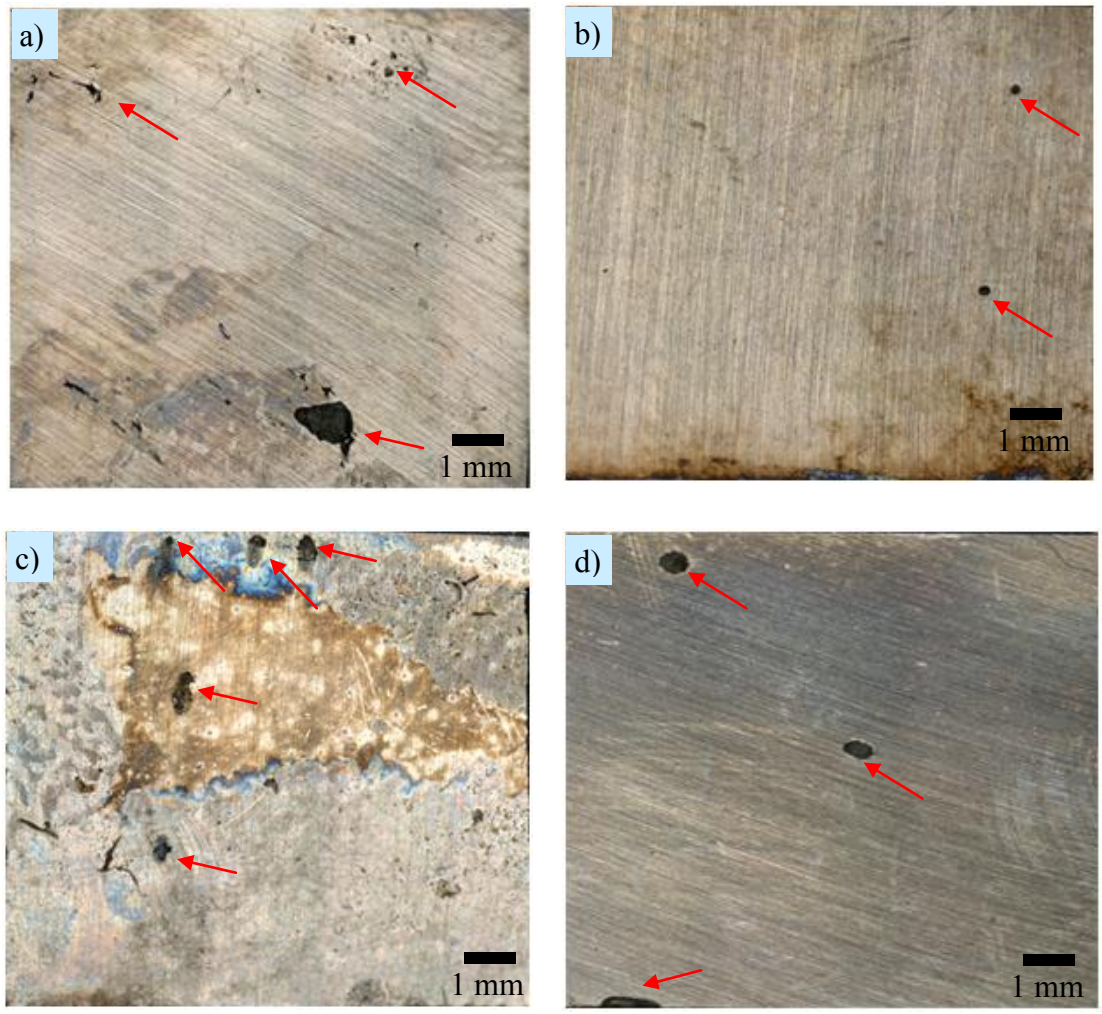

Figure 4.17 2D images of corrosion coupons surface morphology after cyclic polarization (CPS) was conducted: (a) control; (b) NRB inoculated; (c) SRB inoculated; (d) mixed bacteria (NRB+SRB) inoculated. Red arrows show pits which formed on the steel.

In order to observe surface damage after the sample was polarized during the CPS test, 2D observation was performed on the steel surface using a light microscope (Figure 4.17). It can be seen that the most severe surface damage happened on the SRB corrosion coupon, followed by the control corrosion coupon, mixed bacteria (NRB+SRB) corrosion coupon and NRB corrosion coupon. This result is in agreement with the CPS hysteresis results in Section 4.5.1.1.

4.9 Concluding Remarks

The following conclusions can be made based on the results found:

- Addition of nitrate can stimulate the growth of NRB and impose a strong inhibition effect on the activity of SRB, thus eliminating biogenic sulphide formation or H_2S gas production.
- Bacteria metabolites and biofilm influences the passivity behaviour of UNS S31603, as they change both the critical pitting potential and repassivation potential of the steel.
- NRB decreases the critical pitting potential to a greater extent than SRB; hence, increasing the risk of localised corrosion. This may be due to the formation of patchy bacterial biofilm on the steel surface, thus weakening the formation of a homogenous passive film on the steel surface. Additionally, NRB consumption of nitrate may also increase the risk of localised corrosion as nitrate is generally known as a corrosion inhibitor.
- It is revealed from the mixed bacteria culture cell that, in the presence of SRB, NRB does not grow aggressively; hence, the critical pitting potential can still be maintained at a "safe" level.
- It is also noted that the general corrosion rate of the coupon in the SRB inoculated cell is higher than the general corrosion rate of the coupon in the NRB inoculated cell.
- In this particular corrosive biochemical environment (high chloride and sulphate levels), NRB, SRB and mixed bacteria (NRB+ SRB), give beneficial protection to UNS S31603 for a short time.
- The underlying principle of nitrate injection cannot be predicted easily, and has to be studied on a case by case basis. Further work is required to understand the biological materials that were produced by NRB, especially in the presence of other bacteria, which in reality may not only be SRB.

CHAPTER 5: The Impact of Nitrate Injection on ASTM A572-50 Carbon Steel

5.1 Introduction

This chapter will discuss the impact of NRB, SRB and mixed bacteria (NRB+SRB) on carbon steel material after a long term exposure (21 days) in a corrosive biochemical mixture of production water and crude oil from field samples. The mixed bacteria cell was pre-soured by biogenic sulphide from the SRB inoculated solution. This pre-soured condition was chosen as carbon steel is, in reality, widely used as a construction material for pipeline. Therefore, it is most likely that sulphides are present in the reservoir with souring problems.

5.2 The Effect of Immersion Time on Sulphate, Sulphide Nitrate, and Nitrite Levels

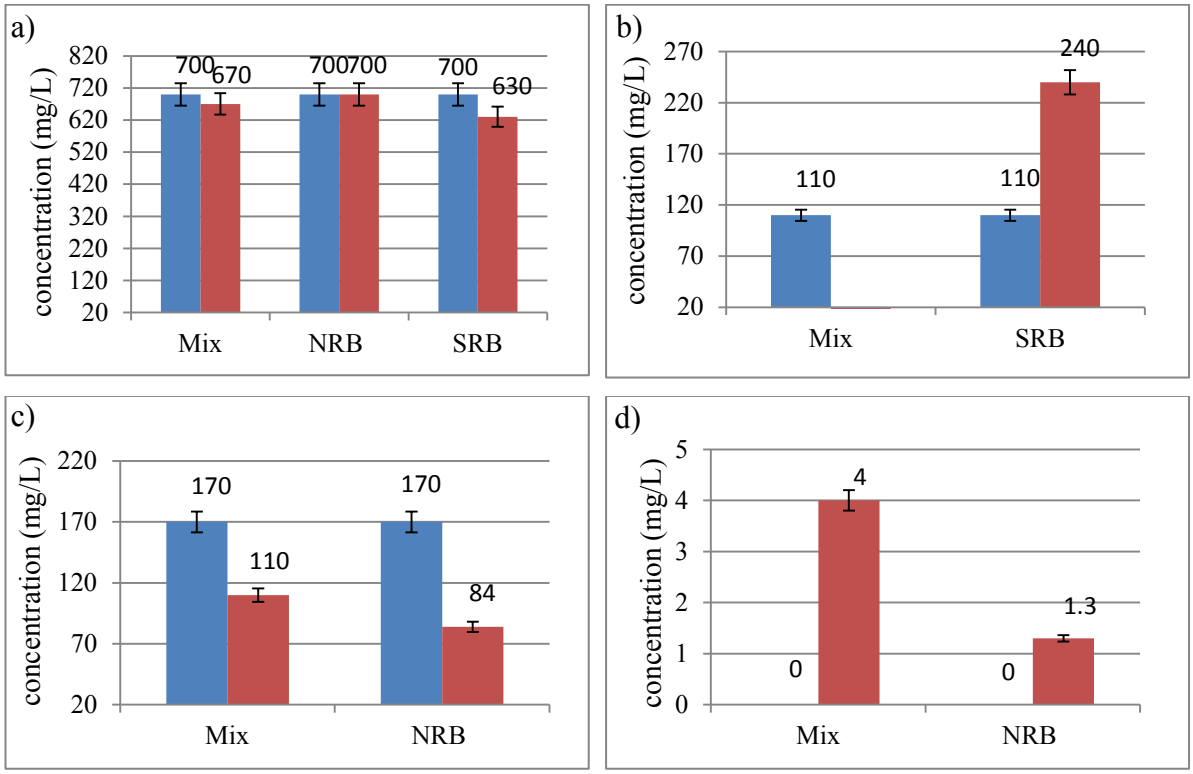

Figure 5.1 Concentration of (a) sulphate, (b) sulphide, (c) nitrate and (d) nitrite before and after immersion. (■) before immersion, (■) after immersion time. Bars represent 5% RPD.

A significant decrease of the sulphate level was observed inside the SRB inoculated cell, but no significant decrease was observed in the mixed bacteria inoculated cell

(Figure 5.1a). In this study, it is demonstrated that the NRB is able to oxidize the pre-existing sulphide (Figure 5.1b). The nitrate level (Figure 5.1c) in the NRB inoculated cell and mixed bacteria inoculated cell show a decreasing level, which indicates that the nitrate is consumed by the NRB. Nitrite production in the mixed bacteria inoculated cell is higher than in the NRB inoculated cell (Figure 5.1d). This result is in agreement with the previous experiment (Section 4.1), which shows that in the presence of SRB, NRB maintains nitrate as an intermediate substance rather than being completely reduced into nitrogen gas.

5.2 Bacterial Enumeration, Redox Potential (E_h) and pH

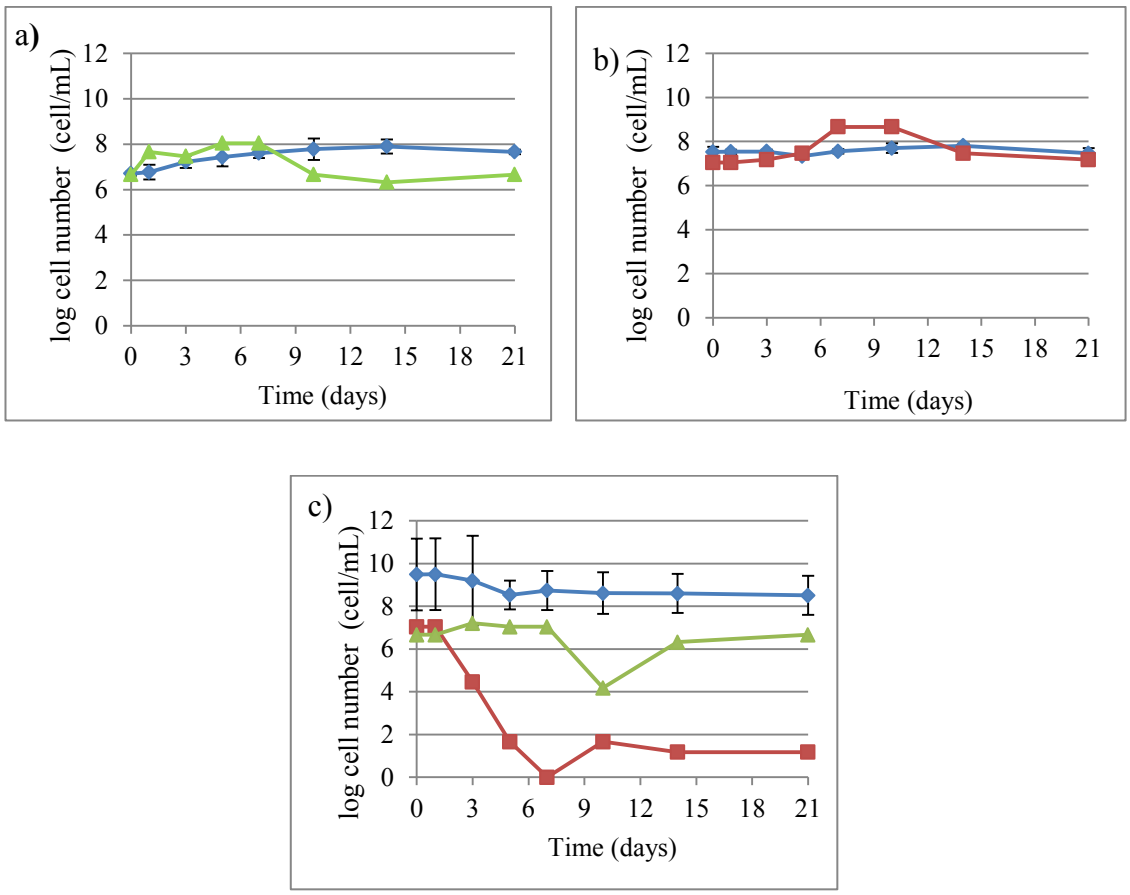

Figure 5.2 Bacterial population throughout immersion time at 50°C for 28 days: (a) NRB inoculated cell, (b) SRB inoculated cell, (c) mixed bacteria (NRB+SRB) inoculated cell. (◆) – total bacterial direct counting, (■) – MPN for SRB, (▲) – MPN for NRB

Bacterial growth was measured using the MPN and also by direct counting. As mentioned above (Section 4.2) MPN may lead to an under estimate of the numbers, therefore, bacterial direct counting was conducted as confirmation. There isn't much

variation of the bacteria growth and pH results obtained from both materials studied, the ASTM-A572-50 carbon steel compared to UNS S31603 (see Section 4.2 for details).

The growth of NRB in the NRB inoculated cell (Figure 5.2a) increased during the first week and then started to decline. The growth of SRB in the SRB inoculated cell (Figure 5.2b) was stable in the first week, increased at day seven and declined after day 10. In the mixed bacteria inoculated cells, it could be seen that, in the presence of NRB, the SRB population was suppressed. Although SRB was still detected in at a low level (in the order of one magnitude), the desired effect, removal of sulphide was achieved (Figure 5.1b). Additionally, when the NRB population declined it could be seen that SRB started to re-grow (Figure 5.2c).

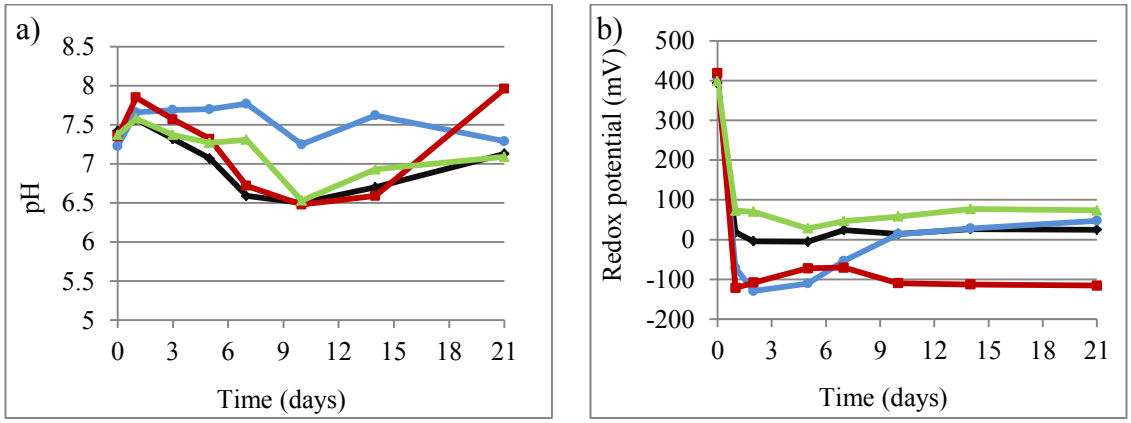

Figure 5.3 (a) pH and (b) redox potential during immersion at 50°C for 21 days. (◆) – control, (■) – inoculated with SRB, (▲) – inoculated with NRB, (●) - inoculated with mixed bacteria (NRB+SRB).

The pH of the production water/crude oil for all cells increased during the first day of immersion (Figure 5.3a). For the control cell, the pH decreased in the 1st week and increased rapidly thereafter. The pH in the NRB inoculated cell and in the mixed bacteria inoculated cell showed a similar pattern for the first two weeks of immersion time, although the pH in the NRB inoculated cell was slightly higher. The pH in both cells decreased slightly on days one to three, remained stable until day seven, decreased again until day 10 and increased until day 14. After that, the pH for the NRB inoculated cell increased slightly while the pH for the mixed bacteria

inoculated cell decreased slightly. The pH for the SRB inoculated cell decreased after day one until day 10, and increased rapidly afterwards.

Similar to the UNS S31603 results, at the beginning of the experiment, all cells showed a rapid decrease in the value of E_h (Figure 5.3b) because of the decrease in oxygen concentration as the cell was purged with nitrogen. Both the control and the NRB inoculated cells showed positive E_h values throughout the test. The E_h in the control cell was stable within 20 mV while the E_h in the NRB inoculated cell fluctuated in the range of 20 mV to 70 mV. The E_h in the SRB inoculated cell showed a negative value throughout the test. The E_h in the mixed bacteria inoculated cell initially showed a negative value below -100 mV. This could be due to the sulphide, which was present in the solutions. However, the E_h gradually increased, accompanied by a decrease of the SRB population in the cell. After one week, the E_h reached a value above -100 mV. This indicated that the NRB inhibited the SRB growth, oxidised sulphide and increased the E_h.

5.3 The Effect of Immersion Time on Corrosion Potential (E_{corr}) of ASTM A572-50 Carbon Steel

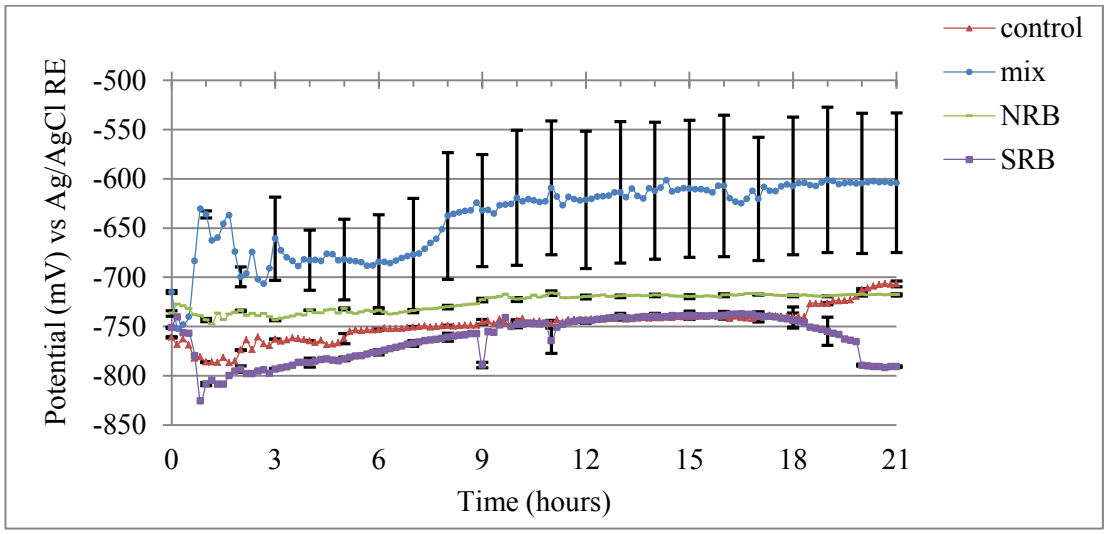

Figure 5.4 E_{corr} as a function of time for carbon steel during immersion at 50°C in production water +10% (v/v) crude oil for 21 days. Data is based on the average of three samples with a standard deviation bar.

Figure 5.4 shows the variation of E_{corr} as a function of time for all the samples under four different conditions. Data presented are average data from triplicate samples and

the bar shows the standard deviation value. E_{corr} initiation values varied for all the coupons in the four cells. The initial E_{corr} values from the lowest to the highest in the sequence were: -760±1mV (control), -751±1 mV (SRB), -735±1 mV (NRB), and -715±1 mV (mixed bacteria). The final E_{corr} values from the lowest to the highest in sequence were: -790±1 mV (SRB), 717±1 mV (NRB), -707±3 mV (control), and -604±70 mV (mixed bacteria). The E_{corr} value for all steel samples under four different conditions decreased immediately after the test began. This was due to oxygen decrease as the cells were purged with nitrogen.

Corrosion coupons in control cell showed an increasing E_{corr} value, approximately 42 mV with respect to the initial value from day two until day 12, and remained stable until day 18. After that, the E_{corr} increased again approximately 38 mV. As mentioned earlier in Section 4.4, the shift towards the positive value of the corrosion coupons in control cell could be attributed to incongruent dissolution of the alloy, or as the result of corrosion progress.[115]

E_{corr} for the corrosion coupons in the NRB inoculated cells increased rapidly after the first day. The E_{corr} increased approximately 20 mV from day two until day 10 and remained stable at -716 ± 2 mV until the end of the exposure time. E_{corr} increase could be attributed to biofilm and/or corrosion products formation on the steel surface. Additionally bacterial enzyme may also contribute to the shift of E_{corr} value in a positive direction.[113]

E_{corr} for the corrosion coupons in the SRB inoculated cell decreased rapidly by approximately 87 mV on the first day of immersion then increased rapidly onwards. However, spikes of potential decrease were noted on days 9 and 11. As mentioned earlier (Section 4.4), this could indicate the surface activation, which led to pit growth on the surface.[109] The E_{corr} changes in the SRB inoculated cell could be attributed to sulphide ion (S^{2-}) produced by SRB metabolism. The sulphide precipitation with the Fe^{2+} ion will form an ion sulphide (FeS) film, which is a good electric conductor.[122] It has a low over voltage for hydrogen evolution,[122] and consequently tends to change the E_{corr} of the metal where it deposits.[71, 122] However, iron sulphide films formed in the absence of oxygen are usually unstable,[71] and

have a porous structure.[122] These films relate to unstable protection of the steel as they may protect the material initially, but with changes in environmental conditions (most importantly iron concentrations) may suffer from breakdown and structural transformation, and thus lead to an increase in corrosion rate.[71, 122] The latter relates to inhomogeneous film formation on the surface as some parts of the metal surface may remain uncovered (become anodic) and some parts may be covered by the iron sulphides (become cathodic), and thus result in localized corrosion,[71, 122] if the anode to cathode ratio is small.

In the mixed bacteria inoculated cell, a slight decrease in the E_{corr} followed by a significant increase was noted on day one. The E_{corr} fluctuated until day three; this could be attributed to dynamic bacterial population changes of the NRB and SRB (Figure 3c). The E_{corr} then increased until the termination of the test. Additionally, in the mixed bacteria inoculated cell, after the third day of immersion the standard deviation of the E_{corr} was quite high. It is postulated that this could be attributed to the different bacterial biofilms which form on the steel surfaces.

The E_{corr} results show the behaviour of the corrosion coupons in four different conditions as a function of time. This provides information about pit formation as indicated by the potential decrease and also the film formation on the steel surfaces, as indicated by the increase in potential.

5.4 Corrosion Behaviour of Carbon Steel in a Corrosive, High Chloride and Sulphate Production Water.

LPR and EIS were employed to evaluate the corrosion coupons in four different conditions. Both techniques are chosen because they are non-destructive electrochemical techniques.[41, 75, 79] The R_{ct} value obtained from both LPR and EIS equals to R_p value, which can be used to calculate corrosion rate if the Tafel constant is known. LPR is used to monitor the instantaneous corrosion rate of the corrosion coupons. EIS is used to characterize the changes of electrochemical reaction at the metal surface, as well as to study of the formation of corrosion products and biofilms.[123] Figure 5.5 and 5.6 show the Nyquist and the Bode plots, respectively, of

the carbon steel corrosion coupons in production water +10% (v/v) crude oil for different immersion times in the four different conditions.

5.4.1 EIS Spectra

A few important things will be highlighted in this section in order to understand the interpretation of the EIS spectra in further discussion. The magnitude of the impedance loop in the Nyquist curve corresponds to the capacitive behaviour of the electrode. A depressed semi-circle with the centre below the real impedance axis shows a typical behaviour of solid metal electrodes that have a frequency dispersion of the capacitive properties.[123, 124] The diameter of the semi-circle of the impedance loop corresponds to the charge transfer resistance in relation to the formation of the films and/or corrosion product layers.[125] The frequency vs. phase angle plot of the Bode curve can be used to confirm the time constant related to film formation on the electrode. Additionally, the changes in the curve's peak indicate the transformation of the film. The peak in the high and mid frequency region is most probably related to the film (e.g. oxide film, biofilm) and/or corrosion products layer, while the peak in the low frequency region is most probably related to the charge transfer resistance or the electrical double layer of the electrode. The frequency vs. log $|Z|$ mod plot of the Bode curve shows the stability of the film formed on the surface; the narrower the changes in the slope, the more stable is the film on the surface.[123] Additionally, the steeper slope denotes a higher resistance value.

5.4.1.1 Control Cell

The Nyquist plot of the corrosion coupon in the control cell (Figure 5.5a) shows a depressed semi circle with the centre below the real impedance axis. A marked increase in both the impedance magnitude and the impedance diameter of the loop observed from 12 hours to 120 hours of exposure time, is indicative of the formation of a protective layer on the surface. The diameter of the impedance loop then increases slightly from 120 hours to 240 hours of exposure and decreases slightly in the 360th hour of exposure. An abrupt decrease of the impedance loop is clearly seen in the 480th hour of exposure, which indicates a decrease in the film's resistance. In

the frequency vs. phase angle plot of the Bode curve (Figure 5.6a), a shift in the frequency peak from the high frequency region (10^2 to10^4) Hz at 12th hour to the mid frequency region (1-10^2) Hz between 120th hour and 360th hour is noted. After 480 hours of exposure the peak splits into two peaks, one in the mid frequency region (1 to 10^2) Hz and the other in the low frequency region (10^{-2} to 1) Hz. This indicates changes in the film formation on the steel surface. The frequency vs. log |Z| mod plot of the Bode curve (Figures 5.6b) shows that the impedance spectra oscillate in a narrow range (from the logarithmic values of about 3.6 to 3.8) between 12 hours and 360 hours of exposure and decreases with a longer exposure time (480 hours). This indicates that during the initial exposure time a stable film formed on the surface and after a longer exposure time there was a sudden change in the film formation. The results obtained from the EIS spectra are in agreement with the E_{corr} result (Figure 5.4) which shows a potential shift in a positive direction after 360 hours of exposure time. This confirms that the marked change of the impedance spectra is not an artefact of the instrument noise but likely a response of a phase transformation.

5.4.1.2 NRB Inoculated Cell

The Nyquist plot of the corrosion coupon in the NRB inoculated cell (Figure 5.5b) shows depressed and incomplete semicircles. The impedance loop increases with time from 12 hours until 120 hours of exposure and a rapid decrease in the impedance loop is noted after longer exposure time (from 120 hours onwards). In the frequency vs. phase angle plot of the Bode curve (Figure 5.6c), on the initial exposure of 12 hours, two distinguishable peaks can be seen, one in the high frequency region (10^2 to 10^4) Hz and the other in the low frequency region (10^{-2} to1) Hz. However, the peak in the low frequency region vanished over time after 12 hours and the curve remains relatively stable until 480 hours of exposure. The frequency vs. log |Z| mod plot of the Bode curve (Figures 5.6d) shows that the impedance spectra increases after 12 hours of exposure time and oscillate in a narrow range (from the logarithmic values of about 3.6 to 3.8) between the 120th hour and the 480th hour of exposure time. As mentioned earlier, this may indicate a stable film formation on the steel surface. This result is also in accordance with the E_{corr} result which shows a stable value over time (Figure 5.4).

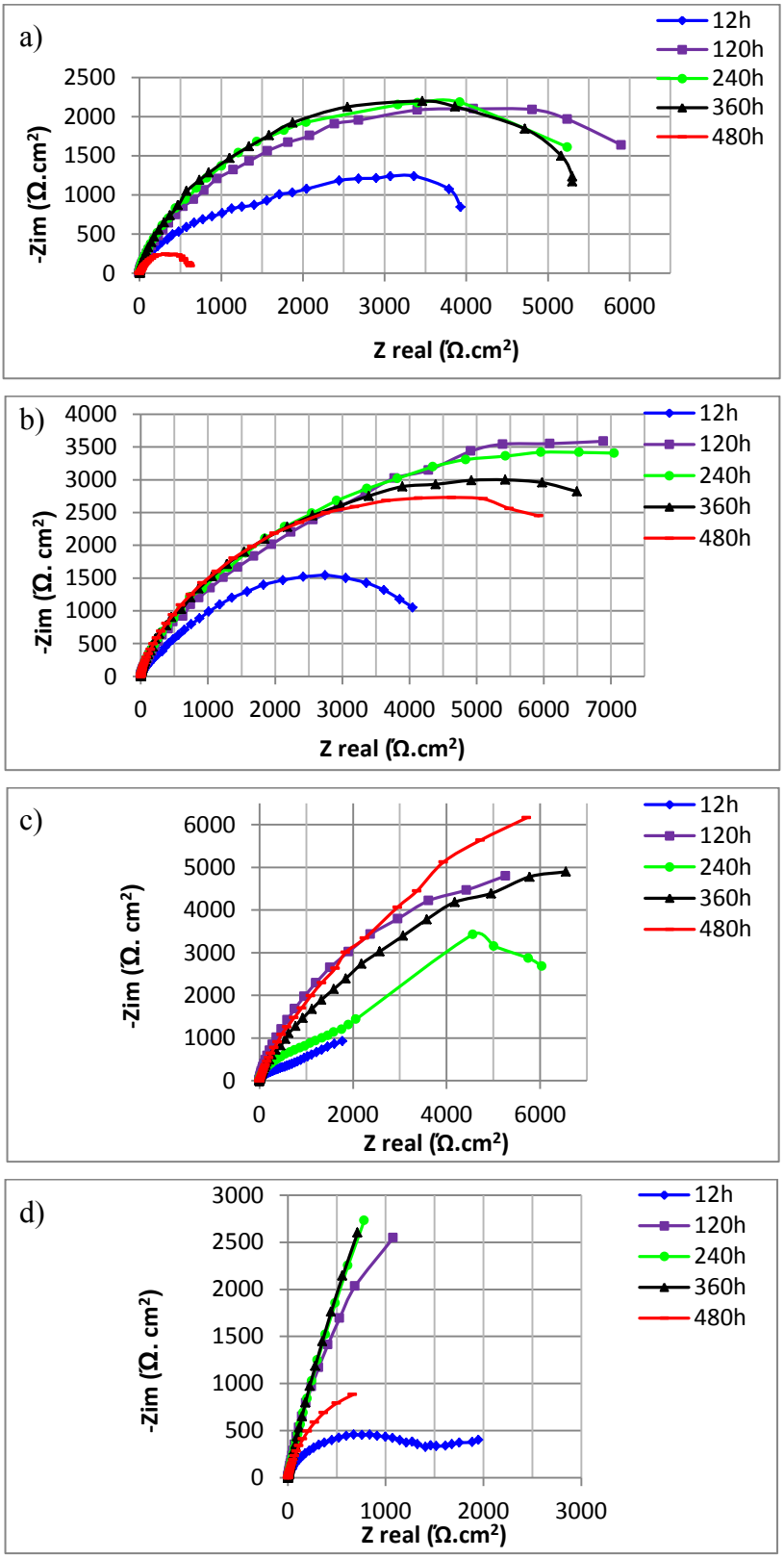

Figure 5.5 Representative Nyquist curves of (a) coupon in control cell (b) coupon in NRB inoculated cell (c) coupon in SRB inoculated cell (d) coupon in mixed bacteria (NRB+SRB) inoculated cell at 50°C in production water +10% (v/v) crude oil mixture.

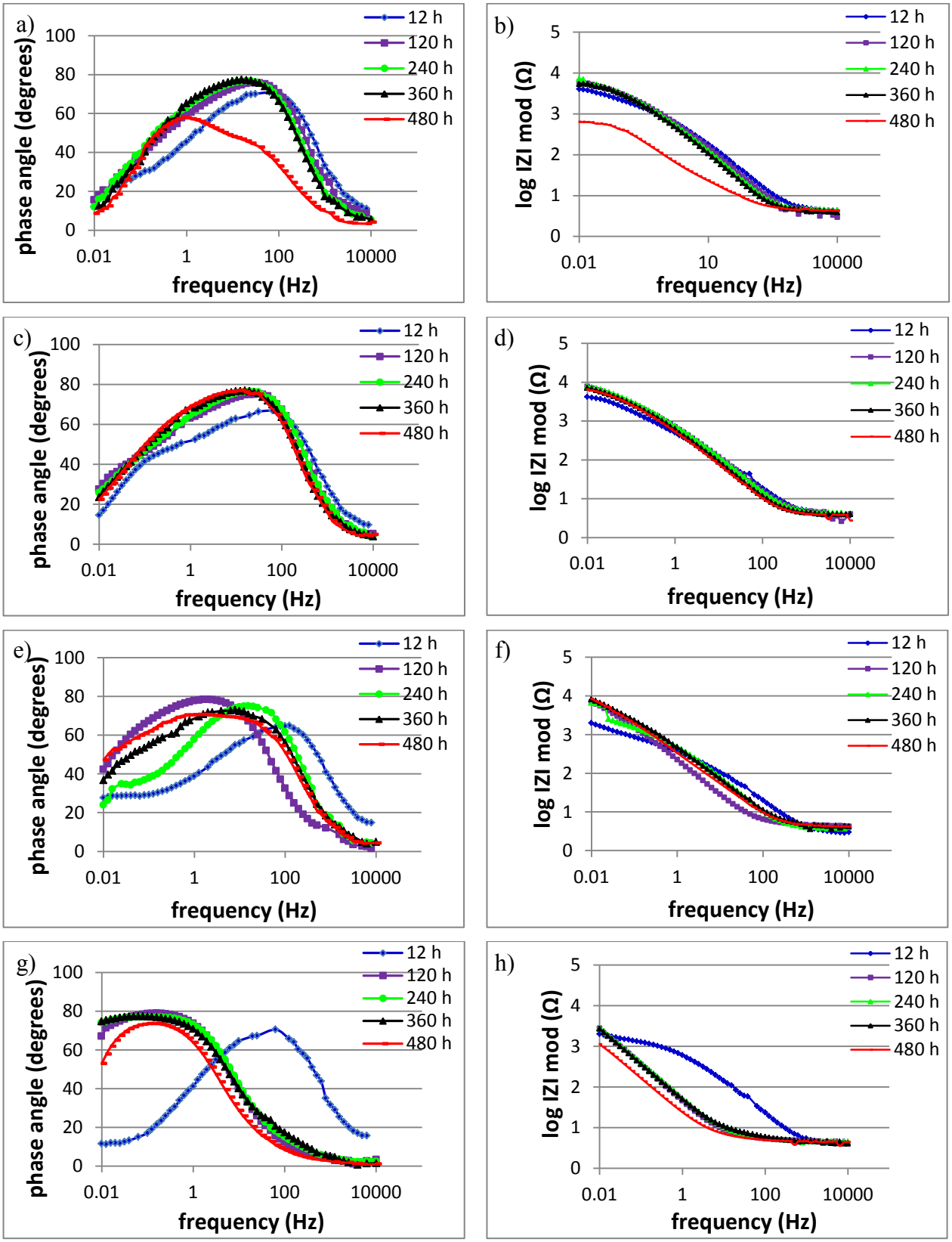

Figure 5.6 Representative Bode curves of (a, b) coupon in control cell; (c, d) coupon in NRB inoculated cell; (e, f) coupon in SRB inoculated cell; (g, h) coupon in mixed bacteria (NRB+SRB) inoculated cell at 50ºC in production water +10% (v/v) crude oil mixture.

5.4.1.3 SRB Inoculated Cell

The Nyquist plot of the corrosion coupon in the SRB inoculated cell (Figure 5.5c) also shows depressed and incomplete semicircles. The impedance loop is not stable and changes over time for the first 240 hours, and then increases. This may be ascribed to the porous corrosion-products layer on the steel surface in the first 240 hours and a build-up of a stable layer afterwards. Additionally, a straight line, corresponding to a second time constant is observed in the high frequency. In the frequency vs. phase angle plot of the Bode curve (Figure 5.6e), it is observed that from the 12^{th} hour of exposure to the 120^{th} hour of exposure, the curve's peak shifts from the high frequency region (10^2 -10^4) Hz to the mid frequency region (1 -10^2) Hz. In the 240^{th} hour of exposure time, the peak splits into two peaks, one in the low (10^{-2} -1) Hz frequency region and the other on the mid frequency region. The peak in the low frequency exhibits a weak signal and vanishes overtime. However, the peak in the 360^{th} hour and the 480^{th} hour of exposure time are flatter compared to the previous peaks; this could indicate two overlay peaks. Therefore, it is predicted that the peak in the low frequency region that appears in the 240^{th} hour measurement increases and overlays the peak on the mid frequency region on the 360^{th} hour and 480^{th} hour of exposure plots. This dynamic change in the curve's peak denotes the dynamic change in the biofilm and/or corrosion products layers on the surface. The frequency vs. log |*Z*| mod plot of the Bode curve (Figure 5.6f) shows an increasing value after 12 hours, and oscillates in a narrow range until 480 hours (from the logarithmic values of about 3.8 to 3.9). This denotes that though there is a dynamic change in the biofilm and/or corrosion products, the total resistance of the film remains stable. The dynamic change in the surface film and/or corrosion products layer is in accordance with the E_{corr} result as few potential shifts are noted throughout immersion time (Figure 5.4).

5.4.1.4 Mixed Bacteria (NRB+SRB) Inoculated Cell

The Nyquist plot of the corrosion coupon in the mixed bacteria (NRB+SRB) inoculated cell (Figure 5.5d) also shows depressed and incomplete semicircles. The impedance loop increases from 12 hours until 360 hours of exposure, and decreases

at the 480 hours of exposure. Additionally, a straight line, corresponding to a second time constant is observed. The frequency vs. phase angle of the Bode magnitude plot (Figure 5.6g), shows that the curve's peak shifts from high frequency (12 hours) to low frequency (between 120 hours and 480 hours). This indicates that the second time constant takes the overall response of the electrochemistry process on the electrodes. The frequency vs. log |Z| mod plot of the Bode curve (Figure 5.6h) exhibits an increasing value from 12 hours (logarithmic value of about 3.2) to the 120 hours (logarithmic value of about 3.4), remains stable on the logarithmic value of approximately 3.4 on the 120 hours until 360 hours and decreases by 480 hours (logarithmic value of about 3.0).

5.4.2 Equivalent Circuit Models

The design of the equivalent circuit model has to take into account each phenomenon that may contribute to the electrochemical reaction that may take place on the metal interface; for example, an electrical double layer formation, a biofilm formation, and corrosion products formations.[123, 126] However, as many other electrochemical techniques, EIS records only a general surface response, thus an idealized model is unlikely to be able to capture all the essential details of corrosion deposits yielded at a specific area.[115] The impedance results are fitted to different circuit models (Figure 5.7a-d) and the simulation results are depicted in Table 5.1. The determination of the quality of fitting to the equivalent circuit model was first evaluated by the chi-square value and second by error distribution vs. frequency, comparing experimental with simulated data.[127] A constant phase element (CPE) was used in all the equivalent circuits instead of a capacitor to represent the deviation from true capacitive behaviour, as it is clearly observed that the impedance loop in all of the Nyquist curves for the four different cells exhibit a depressed semi circle. This behaviour is possibly due to the presence of the dispersing effects of the corrosion products and/or biofilm. The CPE is defined in the following equation[123, 127].

$$Z = \frac{(j\omega)^{-n}}{Y^{o}} \qquad 5.1$$

Where, Z = impedance of CPE

j = imaginary number ($j^2 = -1$)

ω = angular frequency (rad/s)

n = the CPE power, adjustable between 0 and 1

$Y°$ = constant of CPE

The rest of the circuit elements represent:

R_s = solution resistance

R_{cp} = the resistance of corrosion product

R_{cp+bf} = the resistance of corrosion product and biofilm

R_{ct} = the charge transfer resistance

Q_{cp} = the CPE of corrosion product

Q_{cp+bf} = the CPE of corrosion product and biofilm

Q_{ct} = the CPE of the R_{ct}

O = the finite diffusion

W = the Warburg or the semi-infinite diffusion

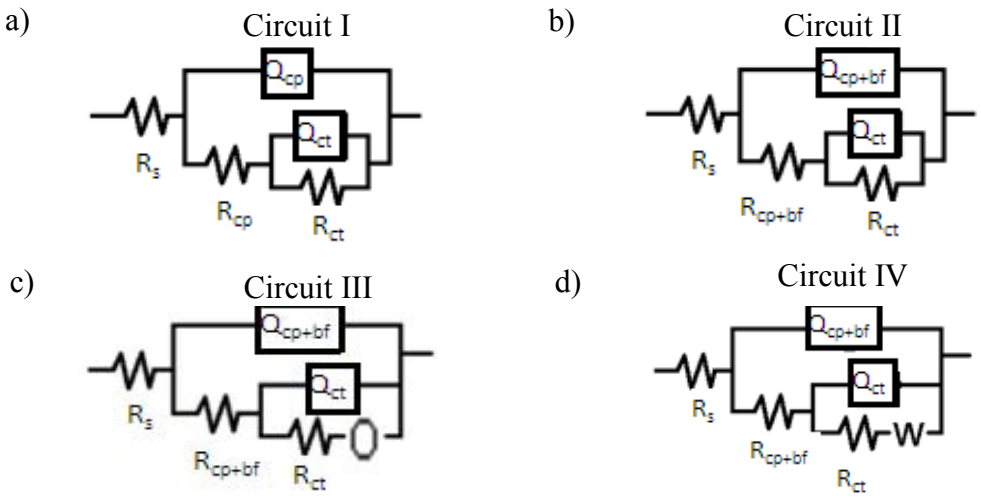

Figure 5.7 The equivalent circuit used for the analysis of impedance spectra of carbon steel immersed in different conditions: (a) control, (b) NRB inoculated cell, (c) SRB inoculated cell, (d) mixed bacteria (NRB+SRB) inoculated cell

5.4.2.1 Control Cell

The spectra of the corrosion coupons in the control cell can be well fitted to circuit model I. The contribution from the corrosion product layer is taken into account as the light microscopy result shows a black corrosion layer covering almost all the surface area (Figure 5.15). Additionally, SEM results show distinguishable corrosion

product layers on the surface (Figure 5.11a). The R_{cp} increases from 12 hours to 240 hours, and decreases afterwards with an abrupt decrease at the 480th hour (Table 5.1). This result is in accordance with the early prediction that there is a decrease in the film resistance after 240 hour of exposure (Section 5.4.1.1). The R_{ct} initially shows a high value and increases with exposure time until 120 hours and then starts decreasing, with an abrupt decrease after 360 hours (Table 5.1). The increase in the R_{ct} can be ascribed to the build up of an inhibiting layer that slows down and/or inhibits the corrosion process while its decrease can be ascribed to the acceleration and/or changes in the corrosion phenomena on the steel surface.

5.4.2.2 NRB Inoculated Cell

Circuit model II was designed to fit the impedance spectra obtained from corrosion coupons in the NRB inoculated cell. The biofilm contribution was taken into account since it could clearly be seen in the SEM results that the bacteria formed biofilm on the surface (Figure 5.12a). As most of the bacteria cells were mixed with the corrosion products (Figure 5.12b), the resistance of the corrosion products and bacteria were considered as a single value (R_{cp+bf}). The R_{cp+bf} increases with time until 360 hours of immersion and decreases afterwards. The starting value of the R_{ct} is similar to results obtained from the control cell. This may indicate that the electrochemical reaction (or corrosion reaction) that occurs on the steel samples in the initial stage of the experiment is similar for both control cell and NRB inoculated cell. The R_{ct} value increased significantly from 12 hours to 120 hours and increased slightly on 240 hours of exposure. A rapid decrease took place afterwards (360 hours and 480 hours). The R_{ct} increment was comparatively much higher than the corrosion coupons in the control cell. This may indicate protective effects from the bacteria, which will be explained in Section 5.7.

5.4.2.3 SRB Inoculated Cell

The observed straight line in the high frequency of the Nyquist curve (Figure 5.5c) indicates that a diffusion process takes place. Therefore, it was necessary to take into consideration the diffusion effect when circuit model III was built. The diffusion

effect was considered to be a finite diffusion process (*O*) as the phase angle of diffusion is less than 45º. It is worth mentioning that at high frequency, the *O* impedance element may become indistinguishable from Warburg impedance (*W*). The *O* diffusion happens when the concentration of the diffusing species in the bulk solution is homogenous.[71] In this particular system, it may be influenced by the ferrous sulphide and/or the SRB cell and/or biofilm on the steel surface. The O diffusion is defined by the following equation [71, 123]:

$$Z_0 = \left(\frac{1}{Y_0 \sqrt{j\omega}} \right) \tanh\left[B\sqrt{j\omega} \right] \qquad 5.2$$

Where,

$$B = \frac{\delta}{\sqrt{D}} \qquad 5.3$$

$$Y_0 = \frac{1}{\sigma\sqrt{2}} \qquad 5.4$$

And,

δ = the Nernst diffusion layer thickness,

D = the average value of the diffusion coefficient species

σ = the Warburg coefficient

The ratio of B divided by Y_0 is accepted as a description of the diffusion resistance of a protective film of finite length.[123]

The R_{cp+bf} increases with time from test initiation until test termination. However, a marked decrease is noted after 120 hours of exposure. This marked decrease may indicate local breakdown of the FeS film. As explained earlier (Section 5.3) the FeS film is unstable and may easily break down due to the changes in the environment. The initial R_{ct} value is quite low compared to the control cell and the NRB inoculated cell; this indicates more corrosive effects of the surrounding environment. This is most likely due to the any SRB metabolite which is introduced from the inoculums solution. The R_{ct} increases rapidly from test initiation and reaches its maximum value at the 360th hour of exposure and then decreases. However, a slight decrease is noted after 240 hours of exposure.

5.4.2.4 Mixed Bacteria (NRB+SRB) Inoculated Cell

In circuit model IV, the diffusion effect is also taken into consideration when the circuit model is built as a distinguishable straight line can be seen in the Nyquist curve. However, *W* is used instead of *O*, as the phase angle of diffusion is 45º (Figure 5.5d). The magnitude of the Warburg impedance $|Z_w|$ is inversely proportional to the square root of the frequency ($1/(\omega)^{0.5}$), with a slope value of -0.5, according to the so-called "semi-infinite" Warburg impedance equation [71, 125]:

$$|Z_w| = \frac{\sigma}{\omega^{0.5}} - j\frac{\sigma}{\omega^{0.5}} \qquad 5.5$$

Where, σ is the Warburg coefficient. This impedance can be observed when the region available for diffusion is not a limiting one or unrestricted to a large planar electrode.[125] This is in accordance with the SEM observation (Figure 5.14c) which shows a round, flat biofilm on the steel surface.

The R_{cp+bf} decreases with time from test initiation until test termination. The R_{cp+bf} values are also lower compared to the other bacteria inoculated cells (NRB inoculated cell and SRB inoculated cell). This may denote that the biofilm and/or corrosion products in this particular condition provide less protection. The initial R_{ct} value is as low as the R_{ct} in the SRB inoculated cell. This confirms the prediction that the corrosive effect is caused by any SRB metabolite which is introduced from the inoculums solution. The R_{ct} value then increases significantly from the 12th hour and reaches its peak in the 360th hour of exposure. However, the R_{ct} value decreases sharply afterwards. This may indicate that during the initial stage, the biofilm and/or corrosion products are protective, but with longer exposure time they may increase corrosion risk.

Interestingly, the diffusion process on the corrosion coupons only happens in the cells with SRB. It is predicted that this diffusion process occurs because of the porous FeS_x structure which is formed by sulphide precipitation on the steel surfaces. While the type of the diffusion, *O* or *W*, is attributed to the biofilm.

Table 5.1 Comparative analysis of the magnitude of equivalent circuit parameters obtained from simulation for four different conditions: (a) control, (b) NRB inoculated cell, (c) SRB inoculated cell, (d) mixed bacteria (NRB+SRB) inoculated cell. The equivalent circuit model is indicated in Figure 5.7.

a)

Time (hours)	12	120	240	360	480
R_s (Ω)	4.20	4.17	4.46	4.42	4.51
CPE (S/s^n)	1.19E-04	1.42E-04	1.70E-04	1.83E-04	1.47E-03
n	0.8822	0.9172	0.9198	0.9291	0.7560
R_{cp} (Ω)	611.43	1003.73	1134.03	449.00	82.46
CPE (S/s^n)	4.46E-04	2.63E-04	2.53E-04	3.87E-04	4.47E-03
n	0.4984	0.5735	0.6518	0.6305	0.8661
R_{ct} (Ω)	4913.33	7041.33	6513.33	5573.33	788.80

b)

Time (hours)	12	120	240	360	480
R_s (Ω)	3.78	4.31	4.46	4.40	4.08
CPE (S/s^n)	1.81E-04	1.83E-04	1.57E-04	2.12E-04	2.34E-04
n	0.8702	0.9247	0.9378	0.9310	0.9349
R_{cp+bf} (Ω)	280.57	513.80	556.23	946.83	315.47
CPE (S/s^n)	4.81E-04	3.95E-04	2.52E-04	2.54E-04	2.26E-04
n	0.6521	0.5297	0.5198	0.5526	0.5413
R_{ct} (Ω)	4715	1.10E+04	1.56E+04	1.32E+04	1.24E+04

c)

Time (hours)	12	120	240	360	480
R_s (Ω)	2.79	3.07	2.94	3.91	3.47
CPE (S/s^n)	2.00E-04	2.22E-04	3.02E-04	3.82E-04	8.34E-04
n	0.8692	0.5923	0.7256	0.7455	0.7599
R_{cp+bf} (Ω)	184.43	1.52	226.43	1195.20	1350.94
CPE (S/s^n)	3.68E-03	8.86E-04	3.56E-04	5.94E-04	1.58E-03
n	0.4933	0.9486	0.8175	0.6682	0.9430
R_{ct} (Ω)	1537.33	2669	2461.33	7.32E+04	1.01E+04
Y	2.38E-03	3.67E-03	1.01E-03	1.07E-02	3.77E+13
B	4.96	5.04	27.79	3.97	1.30E+4

d)

Time (hours)	12	120	240	360	480
R_s (Ω)	3.84	4.30	4.37	4.23	4.19
CPE (S/s^n)	1.65E+04	2.22E+03	1.74E-03	2.00E-03	3.19E-03
n	0.8829	0.8639	0.8840	0.8523	0.8355
R_{cp+bf}(Ω)	576.33	10.32	4.07	4.23	2.34
CPE (S/s^n)	4.72E+04	2.35E+03	3.36E-03	3.57E-03	4.46E-03
n	0.6192	0.9116	0.8907	0.8656	0.8488
R_{ct} (Ω)	1280	8282.67	1.28E+04	2.02E+05	4128.3
W	9.48E-03	8.58E+13	2.25E+11	4.55E+12	6.20E+14

*S= Siemens; s= second

5.5 Corrosion Rate Measurement

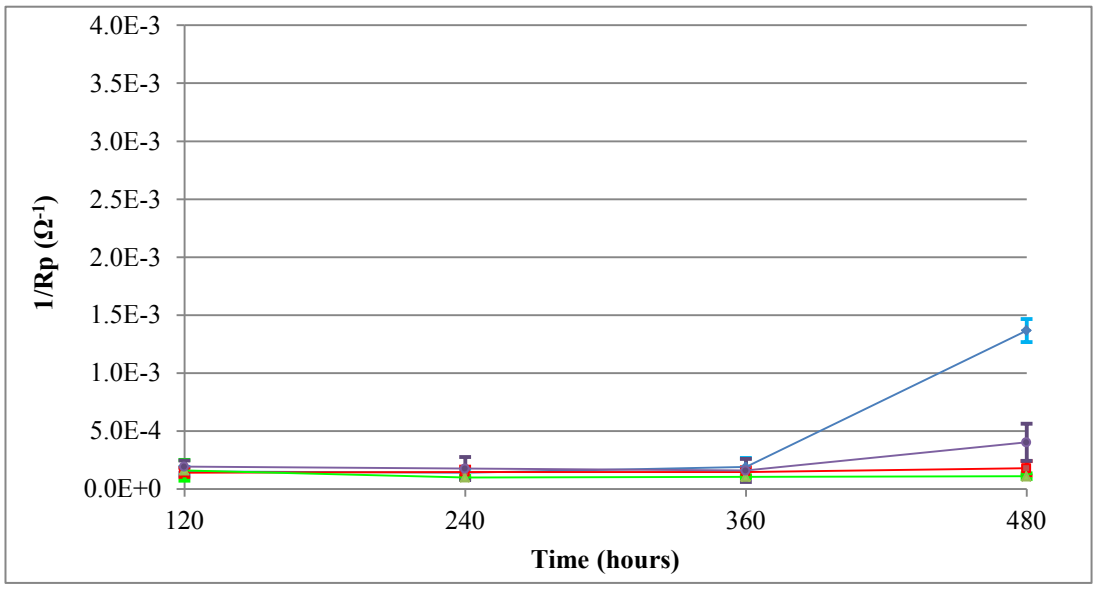

Figure 5.8 Time dependence of R_p obtained from Linear Polarization Resistant (LPR) measurement. Data presented is an average of the three samples and bar represent standard deviation. (◆) – control, (▲) – corrosion coupons in NRB inoculated cell, (■) – corrosion coupons in SRB inoculated cell, (●) – corrosion coupons in mixed bacteria (NRB+SRB) inoculated cell.

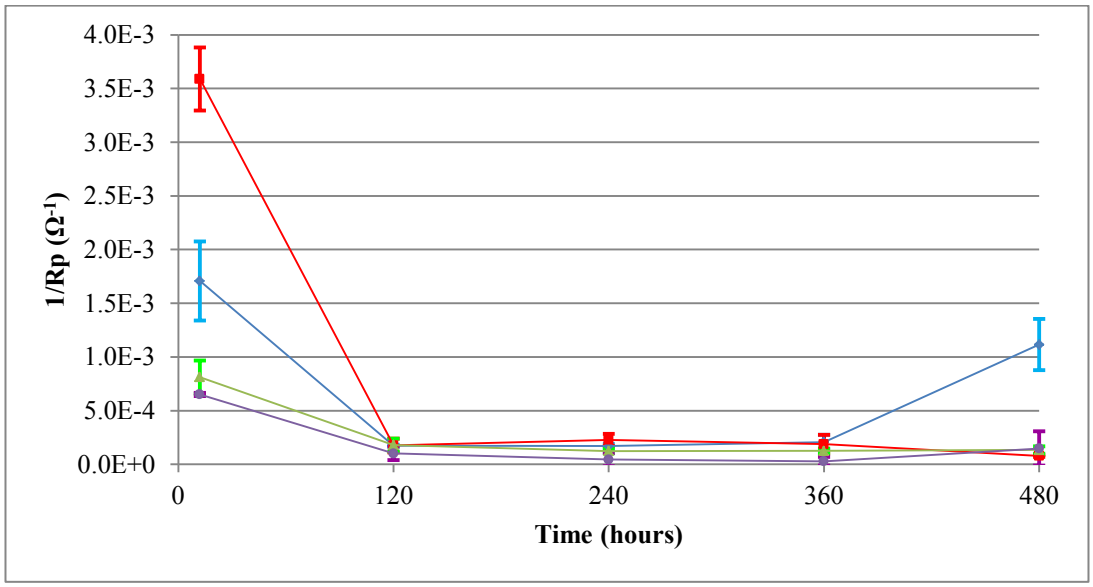

Figure 5.9 Time dependence of R_p obtained from Electrochemical Impedance Spectroscopy (EIS) measurement. Data presented is an average of the three samples and bar represent standard deviation. (◆) – control, (▲) – corrosion coupons in NRB inoculated cell, (■) – corrosion coupons in SRB inoculated cell, (●) – corrosion coupons in mixed bacteria (NRB+SRB) inoculated cell.

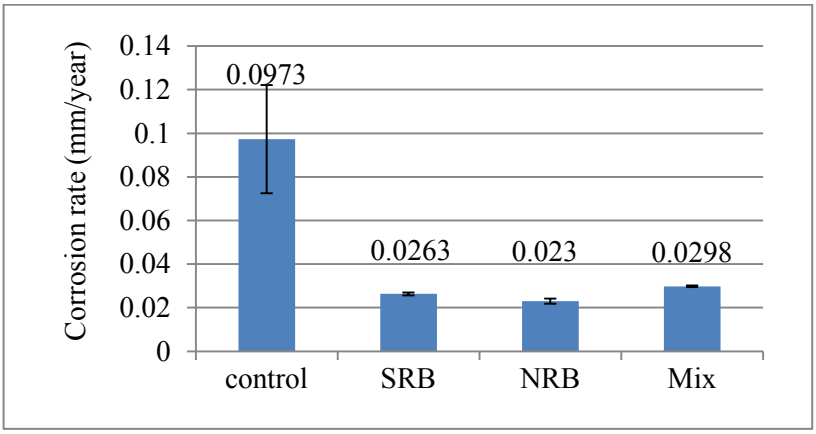

Figure 5.10 Corrosion rate results obtained from weight loss measurement after 21 days of immersion time. Data presented are average from duplicate samples and the bar represents actual value

As mentioned earlier, the R_{ct} obtained from both LPR and EIS equals to R_p. The R_p is inversely proportional to corrosion rate, the decrease in R_p reflects the increase in corrosion rate as described in Equation 1.1. [93, 121] Therefore, the $1/R_p$ values in Figure 5.8 and 5.9 equal to the changes of corrosion rate throughout the immersion.

LPR was only conducted after 120 hours of exposure. As seen on Figure 5.8, the $1/R_p$ value of the corrosion coupons in the control cell fluctuates in the range of (1.41E-4 to 1.89E-4) Ω^{-1} from 120 hours until 360 hours of exposure and an abrupt increase up to 1.37E-3 Ω^{-1} is noted at the 480th hour of exposure. The $1/R_p$ value of the corrosion coupons in the NRB inoculated cell initially decreases from 1.60E-4 Ω^{-1} (120 hours) to 9.87E-5 Ω^{-1} (240 hours) and thereafter, remains stable in the range of (1.05E-5 to 1.09E-4) Ω^{-1} until 480 hours of exposure. The corrosion rate of the corrosion coupons in the SRB inoculated cell shows a relatively stable value in the range of (1.41E-4 to 1.45E-4) Ω^{-1} from 120 hours until 360 hours of the exposure time and an increase up to 1.78E-4 Ω^{-1} is noted at the 480th hour of exposure. The $1/R_p$ value of the corrosion coupon in the mixed bacteria inoculated cell was slightly higher than single cultures of NRB or SRB. The initial value is 1.92E-4 Ω^{-1} then decreases to 1.59E-4 Ω^{-1} at the 360th hour of exposure and increases to 4.02E-4 Ω^{-1} at test termination (480 hours).

The $1/R_p$ value obtained from EIS will be discussed below. The $1/R_p$ value of the corrosion coupons in control cell is initially 1.71E-3 Ω^{-1} then decreases and remains

stable in the range of (1.70E-4 to 2.06E-4) Ω^{-1} from 120 hours until 360 hours of exposure. An abrupt increase is noted after 360 hours and reaches 1.11E-3 Ω^{-1} at the 480th hour. The $1/R_p$ value of the corrosion coupons in the NRB inoculated cell is initially 8.12E-4 Ω^{-1} (12 hours) then decreases and remains stable in the range of (1.24E-4 to 1.80E-4) Ω^{-1} from 120 hours until 480 hours. The $1/R_p$ value of the corrosion coupons in the SRB inoculated cell is initially 3.59E-3 Ω^{-1} (12 hours) then decreases and remains stable in the range of (1.75E-4 to 2.29E-4) Ω^{-1} from 120 hours until 360 hours. A noticeable decrease up to 7.83E-5 Ω^{-1} is noted at the 480th hour of exposure. The $1/R_p$ value of the corrosion coupons in mixed bacteria inoculated cell is initially 6.51E-4 Ω^{-1} (12 hours) followed by a rapid decrease of 1.01E-4 Ω^{-1}, 4.39E-5 Ω^{-1}, and 2.86E-5 Ω^{-1} at the 120th hour, the 240th hour and the 360th hour, respectively. The $1/R_p$ value then increases significantly and reaches 1.48E-4 Ω^{-1} at 480 hours of exposure. The high initial $1/R_p$ value in all the four different conditions can be attributed to the time taken for the system to attain a steady state.[57]

Weight loss measurements give a more reliable result (Figure 5.10), but cannot provide comprehensive data unless the coupons are routinely retrieved from the cells. Hence weight loss only provides a historical average corrosion rate over the whole exposure period. The general results of the LPR, EIS and weight loss are in agreement: control cell show higher corrosion rate values compared to bacterial inoculated cells, which indicates corrosion inhibition by bacteria.

5.6 Corrosion inhibition

Bacterial inhibition of corrosion has been previously documented [48-51, 57, 59, 60]. The proposed corrosion inhibition mechanism could be that bacterial biofilms might prevent chloride attack on steel surfaces,[48, 51] the changes of the localised environmental chemistry by bacterial metabolites and oxygen depletion at metal surfaces by respiring cells.[57] In this experiment, it is proven by SEM that the bacteria formed biofilm on the steel surface (Figures 5.12 to 5.14). However, it is also mentioned in the literature that after bacteria die, the corrosion rate may increase.[48]

In the NRB inoculated cell, a low corrosion rate could be associated with the presence of nitrate and/or nitrite. Although from the thermodynamic point of view, both nitrate and nitrite could enhance corrosion by oxidation of Fe to Fe^{2+} under neutral conditions. However, in practice, nitrate is a less aggressive anion, compared to chloride.[39] In addition, nitrite is known as both oxidizing agent and corrosion inhibitor.[18, 39] It is generally believed that corrosion risk with nitrate addition may be induced by conversion of nitrate to nitrite by microbial activity.[39] In sufficient concentration, nitrite passivates mild steel, thus inhibiting corrosion. Nonetheless, insufficient nitrite concentration is believed to be associated with the increase in corrosion risk.[18, 39] This could be one of the reasons the corrosion rate increased after longer exposure time, because nitrate and nitrite were consumed by bacteria. However, nitrate and nitrite were not measured regularly to get enough data to make nitrate and nitrite profiles throughout the test. The low corrosion rate in the SRB inoculated cell could be related to the formation of FeS_x. The corrosion inhibition in the mixed bacteria inoculated cell could happen because of the bacterial biofilm. This is demonstrated by the SEM result that shows the bacteria form a compact biofilm on the steel surface (Figure 5.14c). However, as biofilm became mature, pits may grow underneath and promote localized corrosion (figure 5.14d). This localised attack may occur as the result of physiological activity of the microbes within the biofilm.[128]

5.7 Films surface analysis on carbon steel coupons by SEM and EDS

In general, the SEM images reveal the corrosion products formed on steel surfaces after 21 days of immersion time. Additionally, EDS spectra showed a phosphate (P) peak in all corrosion coupons under the four different conditions. This may happen because of contamination by the phosphate buffer solution (PBS), specially in the control corrosion coupons where a potassium (K) peak was found[129]; or precipitation from the production after being autoclaved. Figures 5.11a and 5.11b show that corrosion products uniformly covered the steel surface of the corrosion coupons in the control cell. No distinguishable pit could be found. It could be that the pit is covered by the corrosion product layer. The EDS spectra (Figure 5.11c and 5.11d) show that the corrosion products mainly consist of Fe and O. In the NRB inoculated cell, it can be seen that there is a layer formed on the steel surface, with corrosion products and bacteria colonies (Figure 5.12c). The bacteria formed a

porous biofilm on the surface (Figure 5.12a), and also embedded in the corrosion products (Figure 5.12b). There was also no distinguishable pit on the surface. The EDS spectra (Figures 5.12d and 5.12e) also show that the corrosion products consist

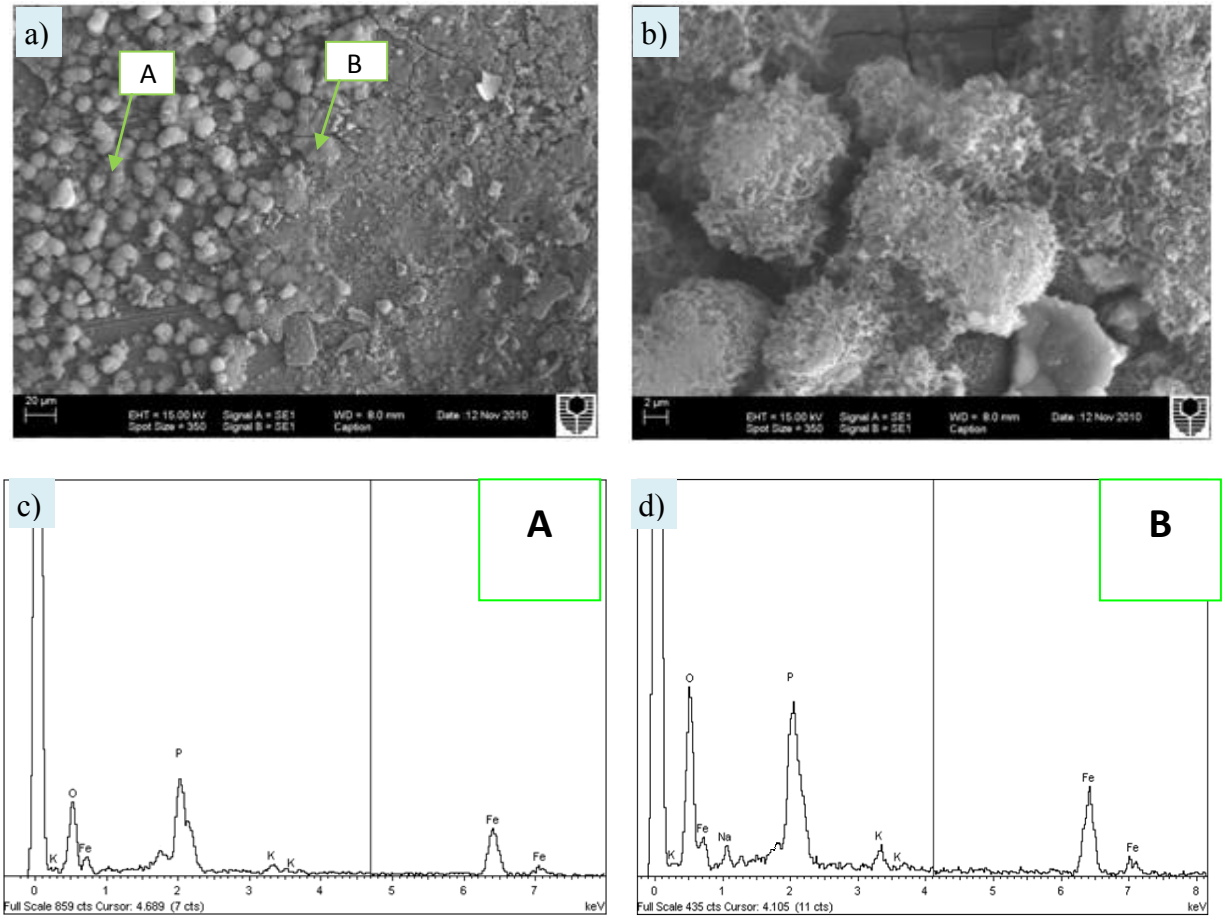

mainly of Fe and O.

Figure 5 .11 Representative SEM images of a corrosion coupon in control cell after 21 days of immersion time in production water + 10% (v/v) crude oil. (a, b) corrosion products on carbon steel surface, no distinguishable pit can be observed (c, d) A and B as seen by green frame represent EDS spectra taken from two different spots of corrosion products in (a).

In the SRB inoculated cell, corrosion product layers were found to be partially covering the steel surface (Figure 5.13b) and some small pits could be seen (Figure 5.13a). The bacteria formed patchy colonies on the steel surface (Figure 5.13e). The EDS spectra (Figure 5.13c and 5.13d) show the corrosion products consist of Fe and O. However S and Barium (Ba) precipitation are also found on the surface (Figure 5.13c), indicated FeS_x and/or barium sulphate, the latter most likely originating from the field brine solution.

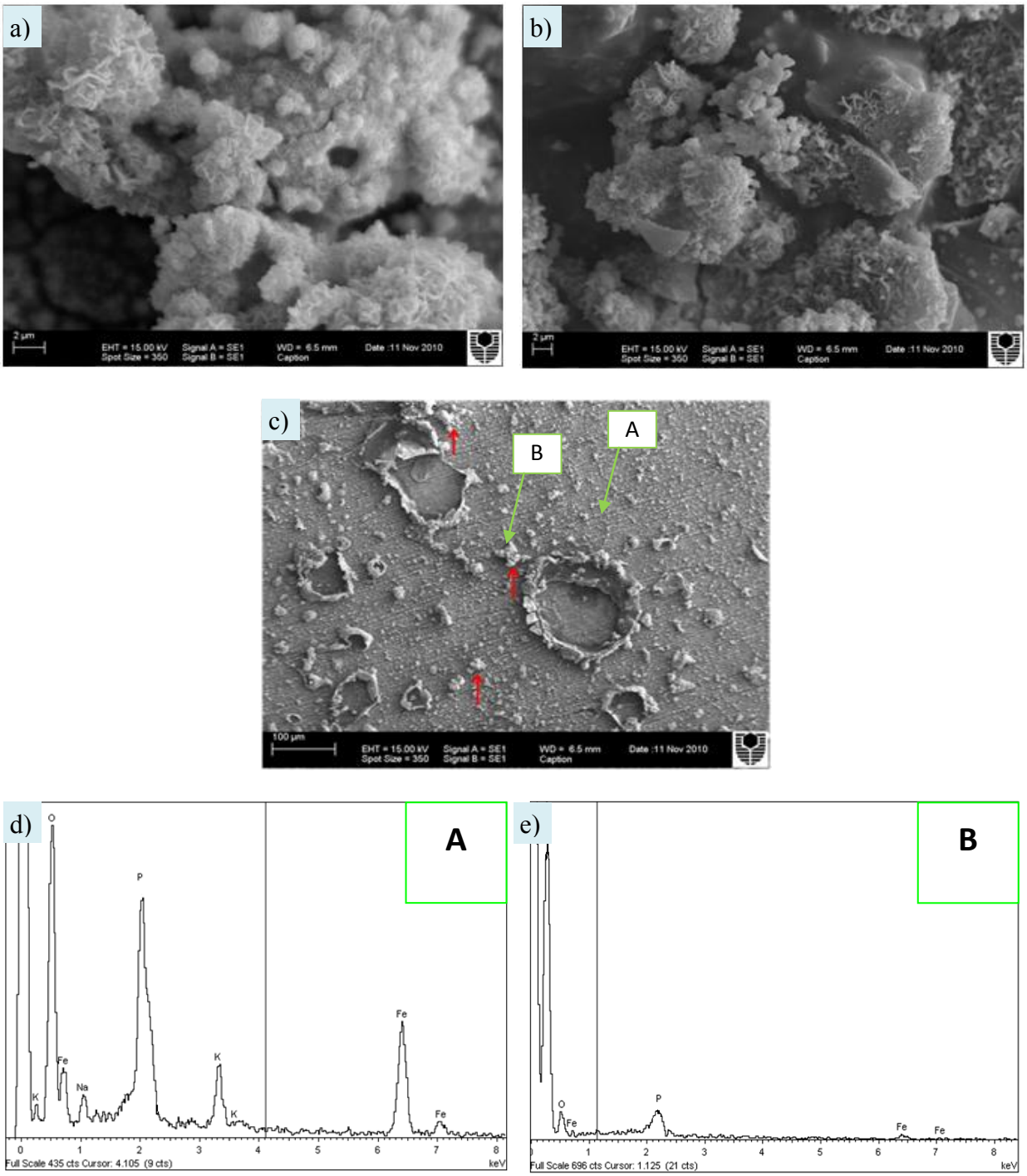

Figure 5.12 Representative SEM images of a corrosion coupon in the NRB inoculated cell after 21 days of immersion time in production water +10% (v/v) crude oil. (a) porous bacteria biofilm (b) bacteria cells embedded in corrosion products (c) patchy bacteria biofilm formed on carbon steel surface (red arrows). A and B as seen by green frame represent EDS spectra taken from 2 different spots in figure c: (d) corrosion product layer and (e) bacteria biofilm.

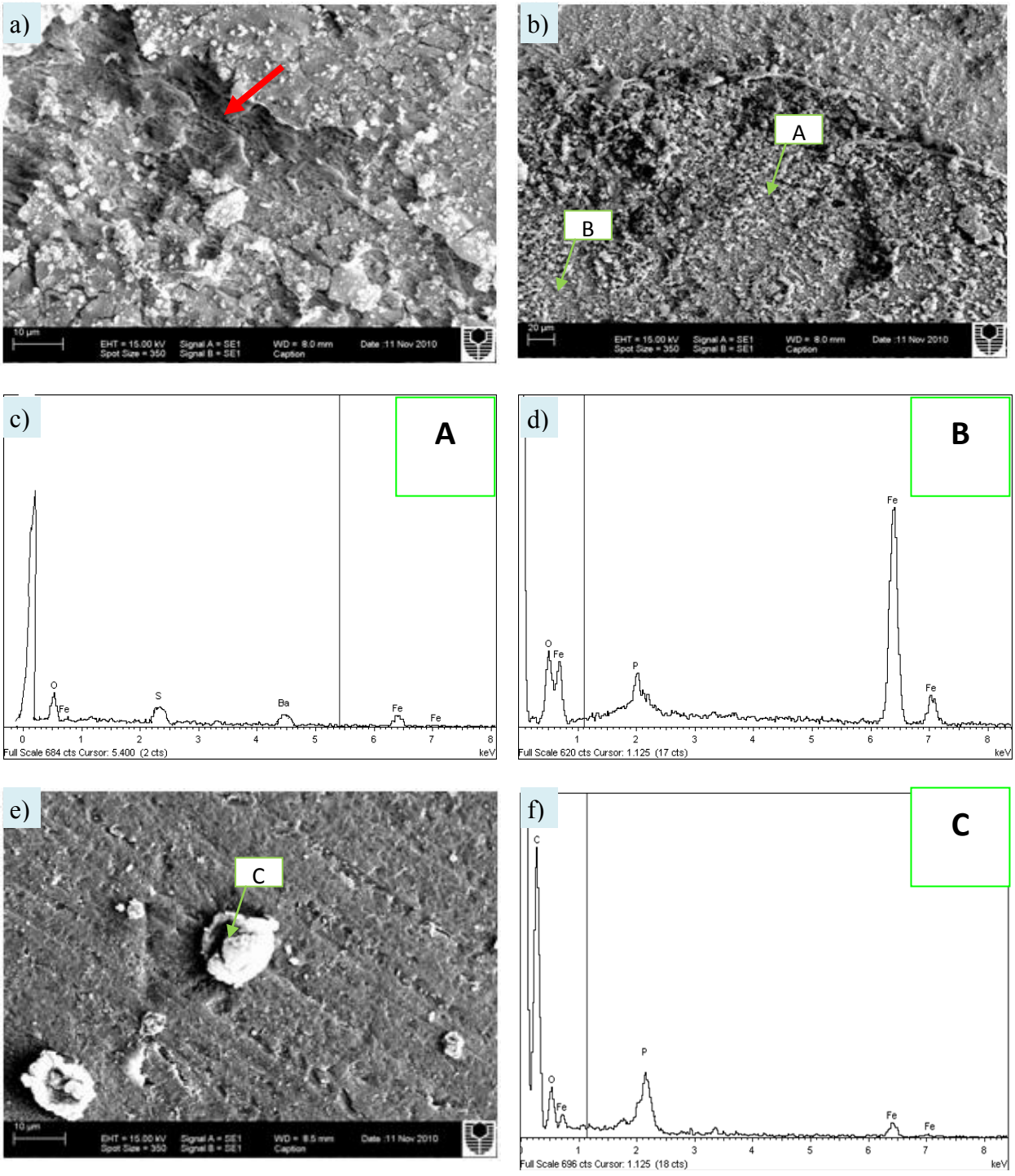

Figure 5.13 Representative SEM images of a corrosion coupon in the SRB inoculated cell after 21 days of immersion time in production water +10% (v/v) crude oil. (a) a small localized pit (red arrow); (b) corrosion product layer; (c, d) A and B represent EDS spectra taken from two different spots in (b); (e) SEM images of patchy bacteria biofilm on carbon steel surface; (f) EDS spectra of bacteria biofilm.

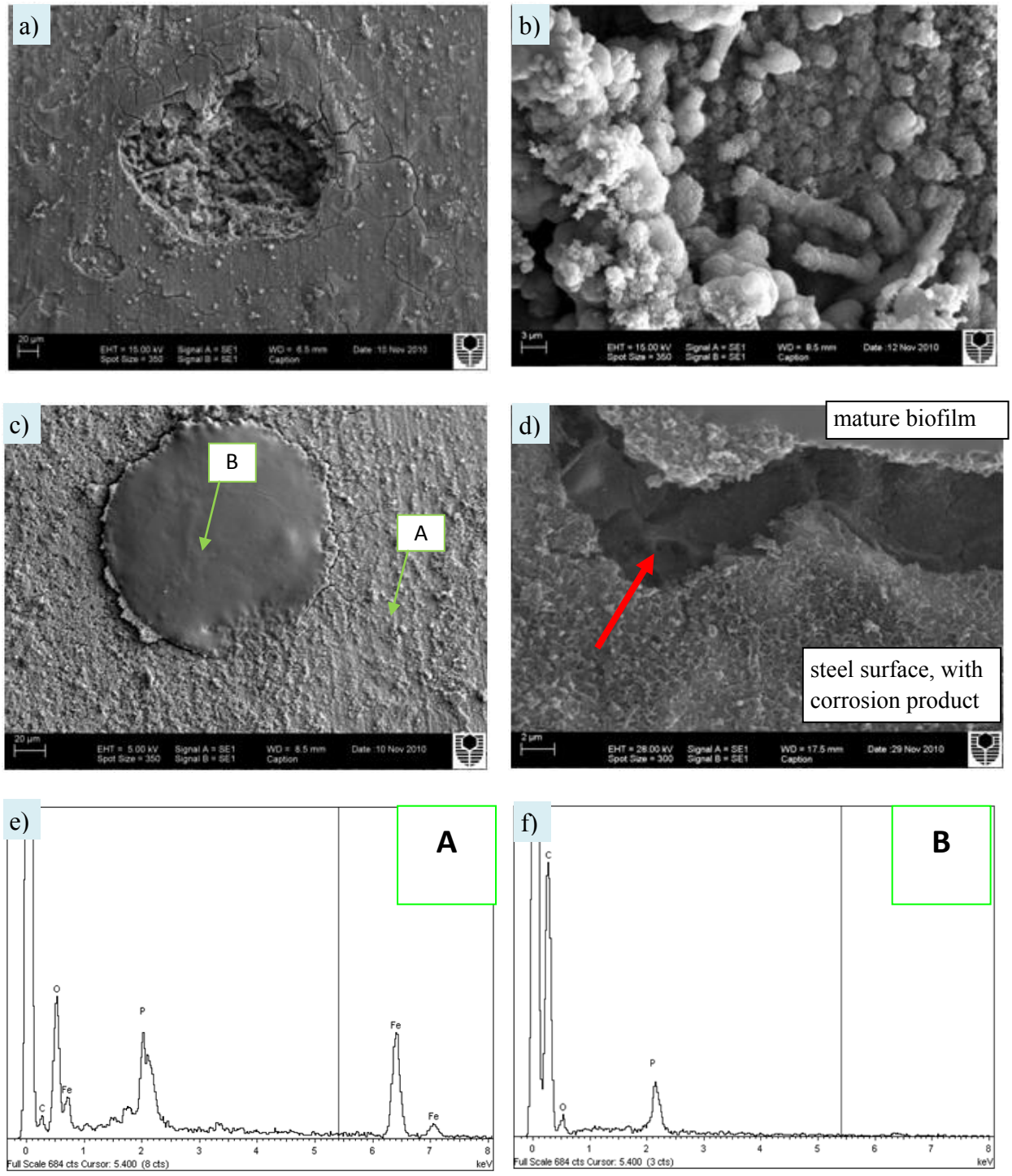

Figure 5.14 Representative SEM images of a corrosion coupon in the mixed bacteria (NRB+SRB) inoculated cell after 21 days of immersion time in production water +10% (v/v) crude oil. (a) pit formed on carbon steel surface; (b) various corrosion products; (c) mature biofilm, the bacterial cells are hidden underneath the extrapolymeric substances (EPS); (d) pit formation underneath mature biofilm (red arrow); (e) EDS spectra of corrosion product layer, (f)) EDS spectra of bacteria biofilm

In the mixed bacteria inoculated cell some mature biofilm can be seen. The bacterial colonies are covered by EPS (Figure 5.14c) and underneath the biofilm a pit formed (Figure 5.14d). It is postulated that, after the biofilm detached from the surface, the pit is exposed (Figure 5.14a), hence the biofilm induced the localized corrosion. Figure 5.14b showed various corrosion products formed on the steel surface. The EDS spectra (Figures 5.14e and 5.14f) also show that the corrosion products consist mainly of Fe and O.

5.8 Steel Surface Analysis by Visible Light Microscopy

5.8.1 2D Steel Surface Analysis by Visible Light Microscopy Before and After Samples Cleaning by Clarke's Solution

The steel surface before the samples are cleaned with Clarke's solution (Figures 5.15a-5.15d) show different corrosion products layers in the four different conditions. The control corrosion coupon (Figure 5.15a) shows a uniform black layer cover over almost all of the surface area. The NRB inoculated corrosion coupon (Figure 5.15b) and SRB inoculated corrosion coupon (Figure 5.15c) show different corrosion products as indicated by different colours. The mixed bacteria inoculated cell (Figure 5.15d) shows a mixture of green and black rust covering all the surface area almost evenly. The steel surfaces after the samples were cleaned with Clarke's solution were also studied (Figure 5.16a-5.16d) and surface 3D measurement was also performed.

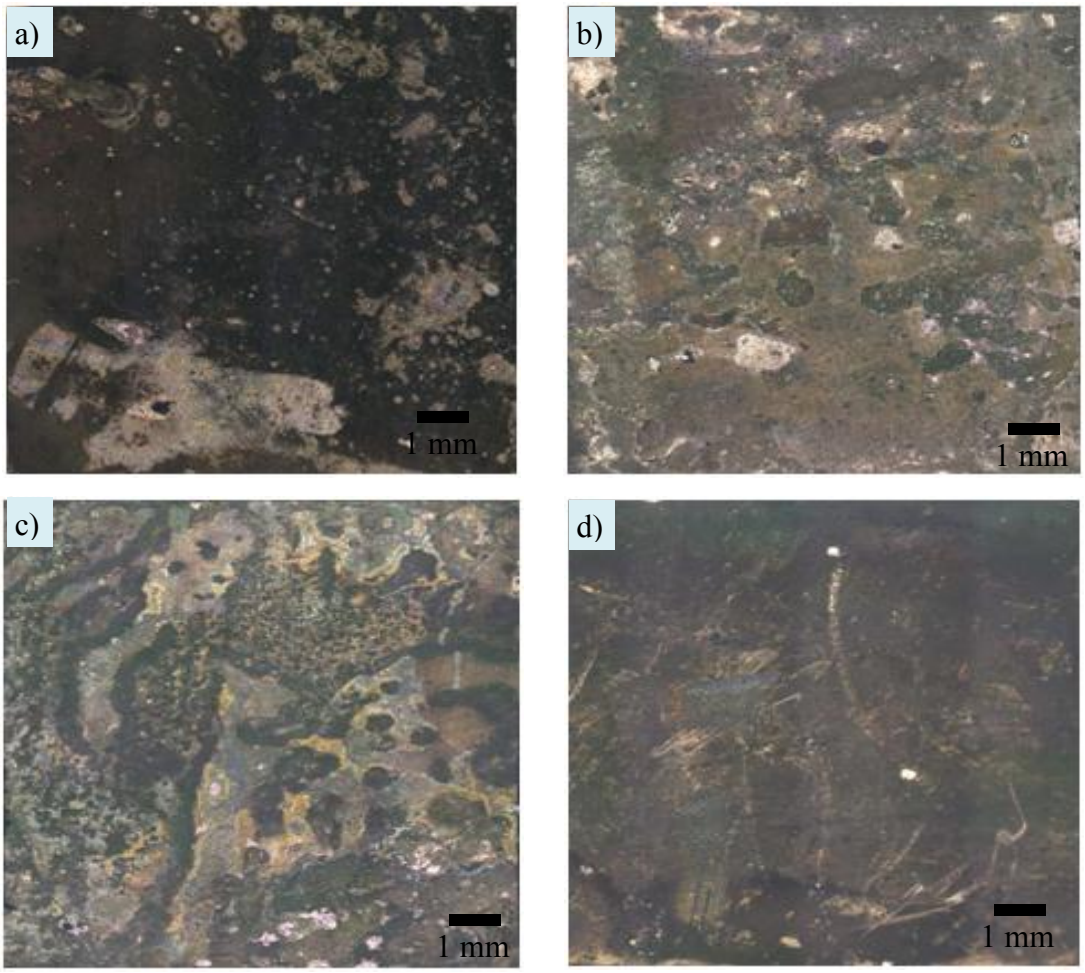

Figure 5.15 Representative images of the corrosion coupon surfaces under visible light microscopy after 21 days of immersion time in formation water and 10%(v/v) crude oil: (a) control cell; (b) NRB inoculated cell; (c) SRB inoculated cell; and (d) the mixed bacteria (NRB+SRB) inoculated cell. Pictures taken before corrosion products removal by Clarke's solution.

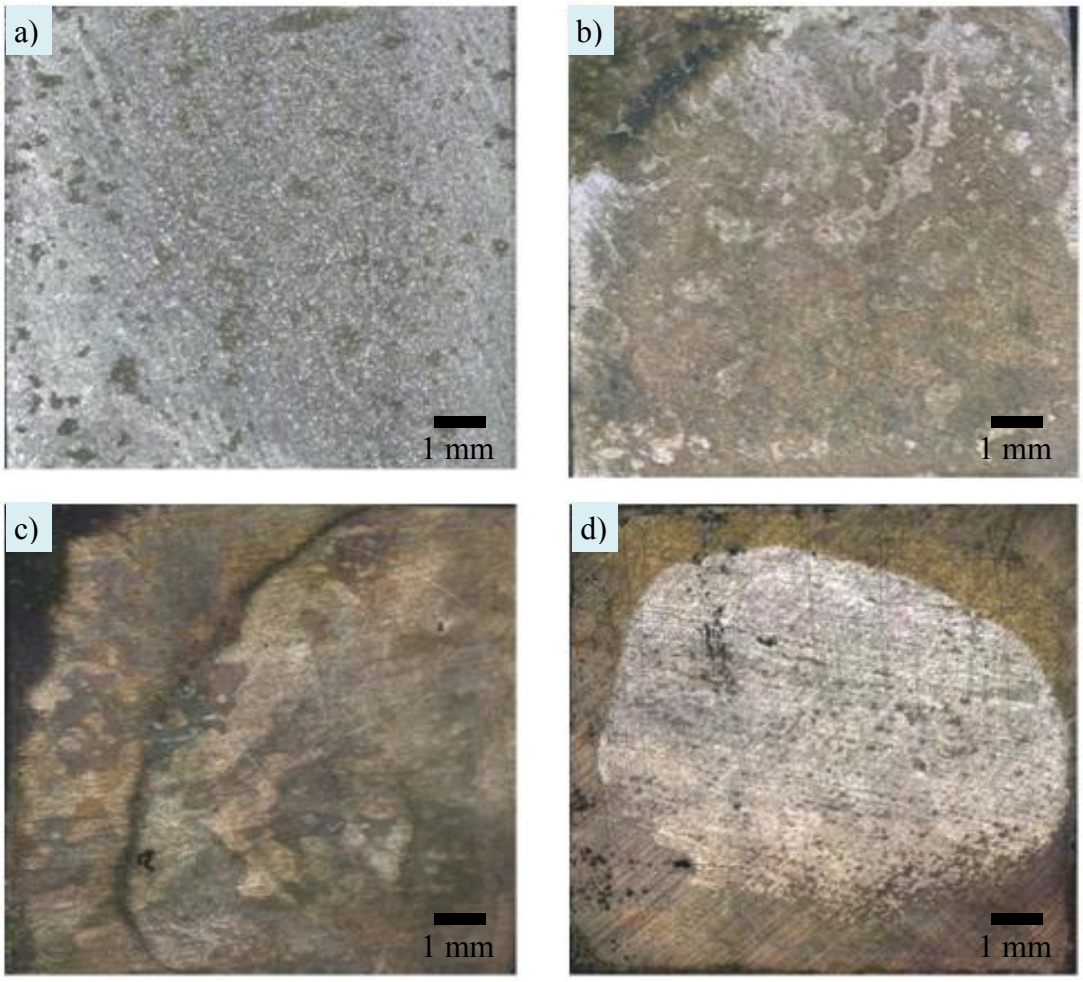

Figure 5.16 Representative images of the corrosion coupon surfaces under light microscopy after 21 days of immersion time in formation water +10%(v/v) crude oil: (a) control cell; (b) NRB inoculated cell; (c) SRB inoculated cell; and (d) the mixed bacteria (NRB+SRB) inoculated cell. Pictures taken after corrosion products removal by Clarke's solution.

5.9.1 3D and 2D Steel Surface Analysis by Light Microscopy after Samples Cleaning by Clarke's Solution

Figure 5.17a and 5.17b show 3D and 2D images of the blank or standard coupon (as received sample/without immersion). In the 3D images, it can be seen that the surface is smooth and the polishing marks can still be seen clearly. The 2D image revealed that the surface roughness is in the range of -0.5-1 μm. Uniform corrosion can be seen easily in the control corrosion coupon (Figures 5.18a and 5.18b). In both of the 3D (Figure 5.18a) and the 2D image (Figure 5.18b), the distribution of the surface roughness can be seen.

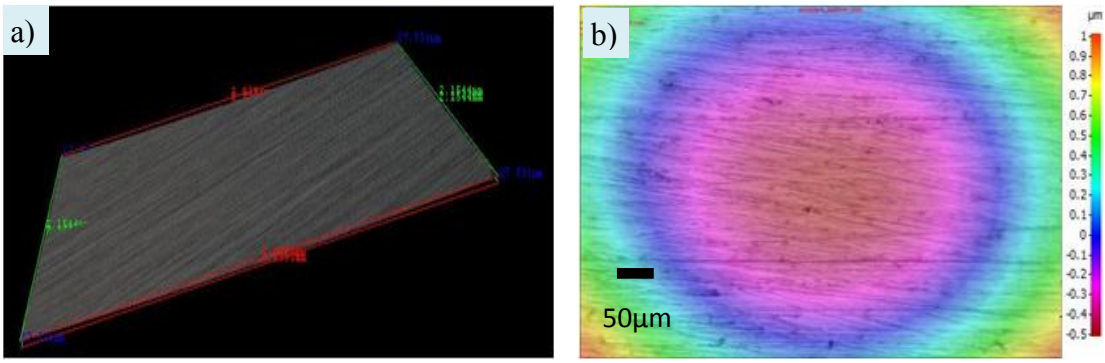

Figure 5.17 Representative images: (a) 3D and (b) 2D of the blank coupon (coupon as received sample/before immersion) under light microscopy.

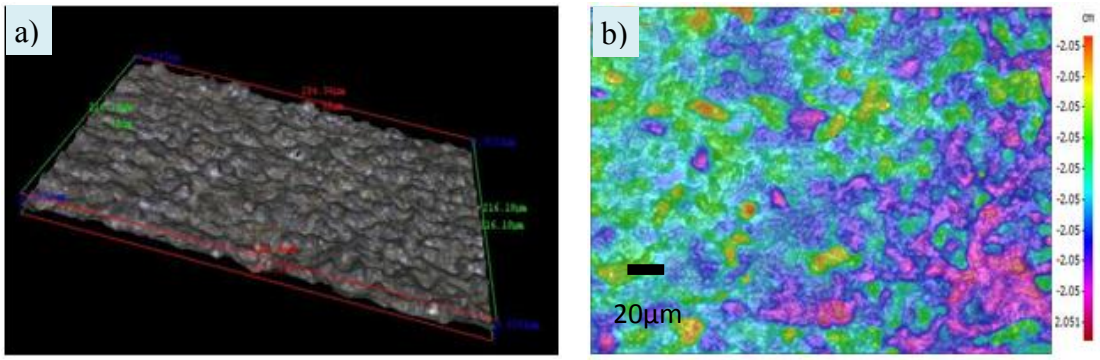

Figure 5.18 Representative images: (a) 3D and (b) 2D of the corrosion coupon in control cell under light microscopy after 21 days of immersion time in formation water +10% (v/v) crude oil.

The representative corrosion coupon in the NRB inoculated cell shows a smoother surface pattern (Figure 5.19a and 5.19b) compared to the corrosion coupon in the control cell. However, localised corrosion is observed in the form of narrow and deep pits (figure 5.19c). The pit depth is in the range of 51.17 µm - 144.04 µm and the pit volume was in the range of 1,027.40 µm³ -3,748.80 µm³.

The representative corrosion coupon in SRB inoculated cell (Figure 5.20a-5.20c) also show a smoother surface pattern compared to the corrosion coupon in the control cell. Localised corrosion is also observed. The pit characteristics are a narrow and shallow pit; and also a narrow and deep pit (Figure 5.20c). The pit depth is in the range of 1.43 µm - 107.83 µm and the pit volume was in the range of 568.06 µm³-1,028.40 µm³.

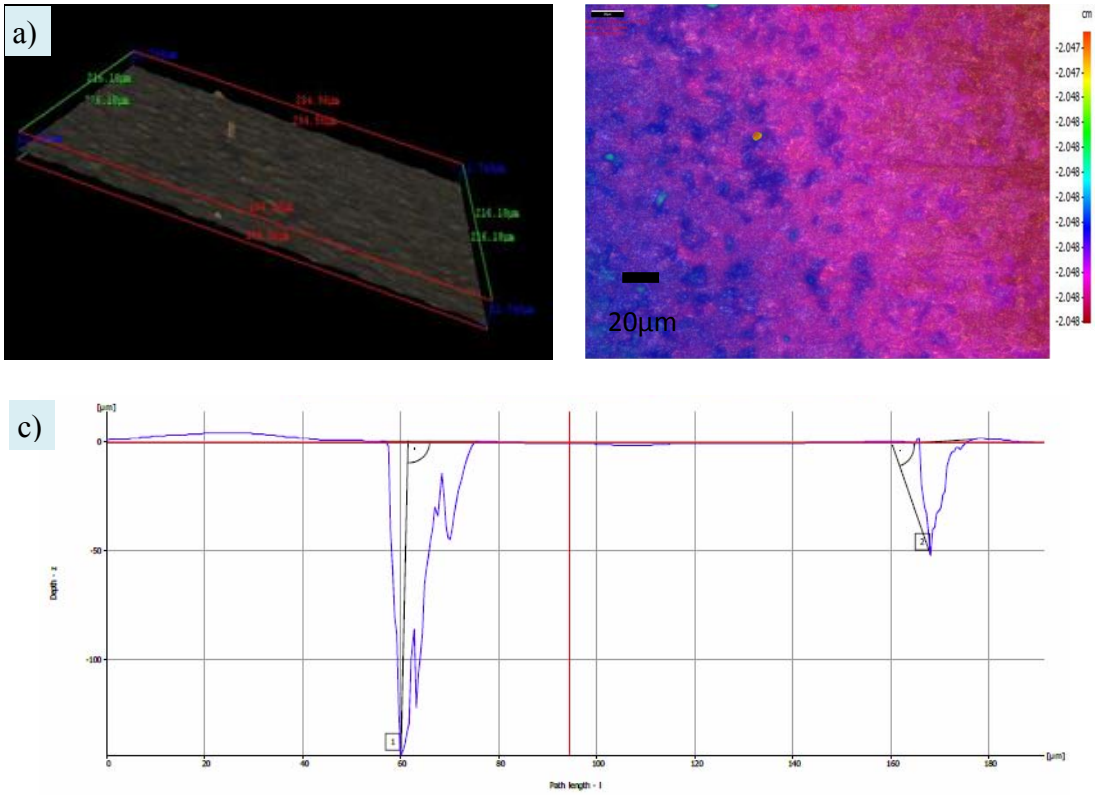

Pit depth: 51.17 µm
Pit volume: 1,027.40 µm³

Pit depth: 144.04 µm
Pit volume: 3,748.80 µm³

Figure 5.19 Representative images: (a) 3D and (b) 2D of the corrosion coupon in the NRB inoculated cell under light microscopy after 21 days of immersion time in formation water +10%(v/v) crude oil; (c) pit which formed on the surface

The representative corrosion coupon in the mixed bacteria inoculated cell also show a smoother surface pattern (Figure 5.21a and 5.21b) compared to the corrosion coupon in the control cell. Figure 5.21a shows a 3D image of a pit and figure 5.21b shows 3D image of corrosion products and/or bacteria biofilm attached to the surface. The localised corrosion is observed in the form of wide and deep pits (Figure 5.21c). The pit depth is in the range of 7.17 µm - 10.67 µm and the pit volume is in the range of 7,794.3 µm³ - 89,067 µm³.

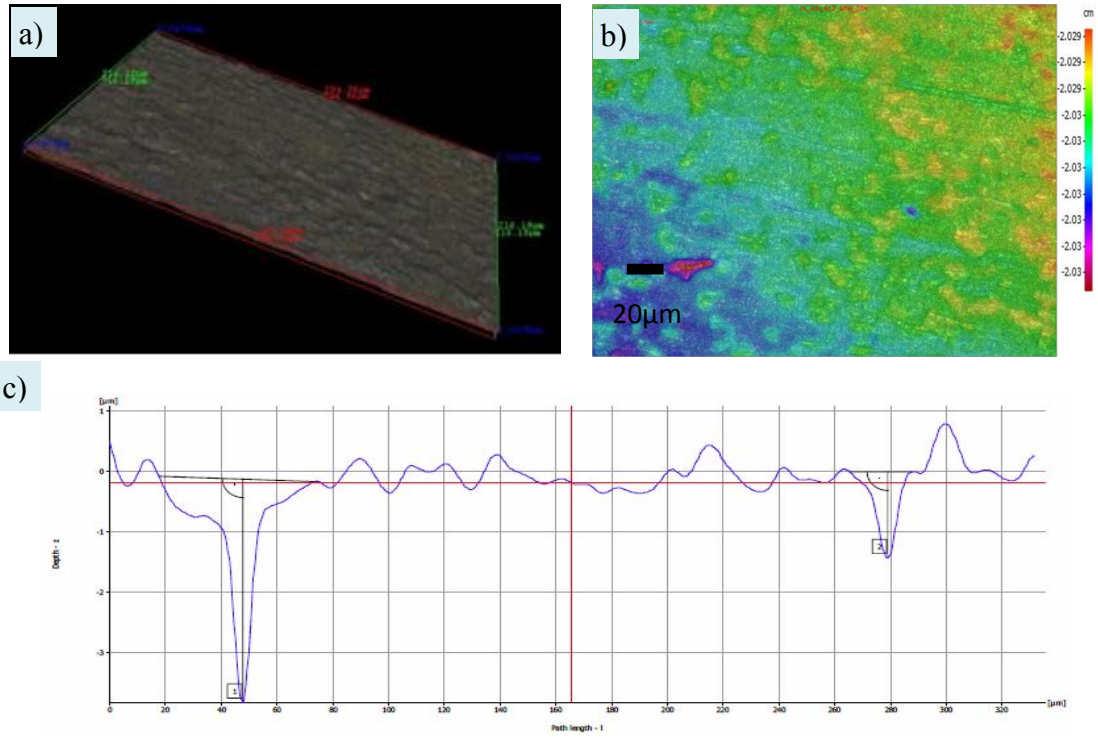

Figure 5.20 Representative images: (a) 3D and (b) 2D of the corrosion coupon in the SRB inoculated cell under light microscopy after 21 days of immersion time in formation water and 10%(v/v) crude oil; (c) pits which formed on the surface.

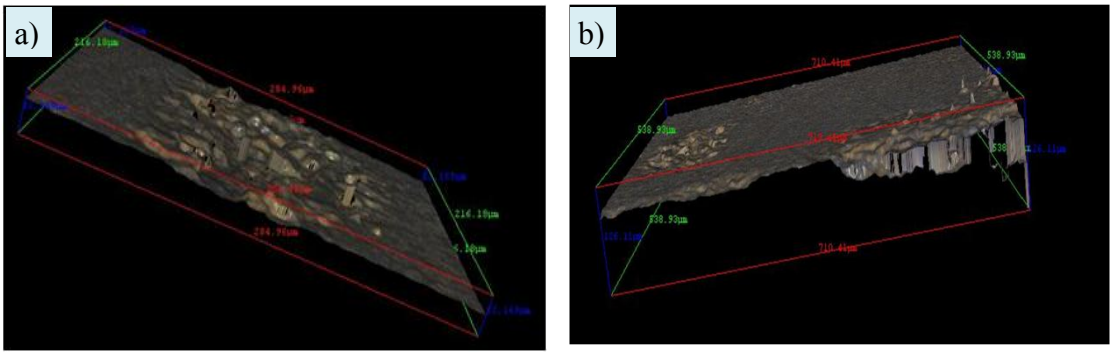

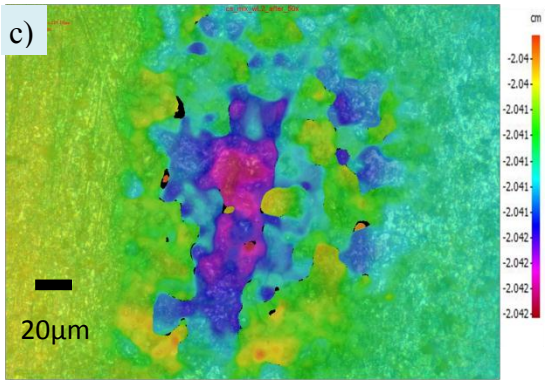

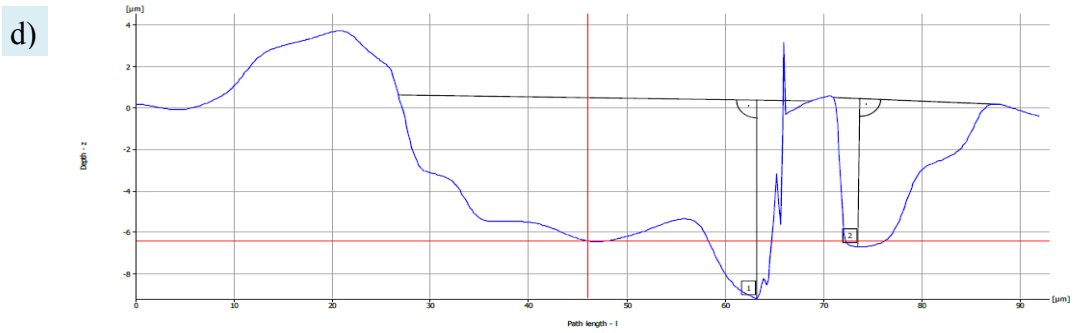

Pit depth: 9.60 µm and 7.17 µm
Total Pit volume:7,794.30 µm³

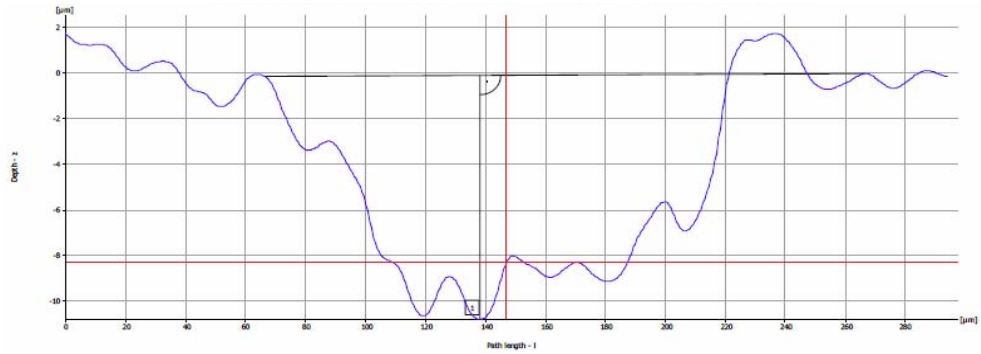

Pit depth: 10.67 µm
Pit volume: 89,067 µm³

Figure 5.21 Representative images: (a, b) 3D and (c) 2D of the corrosion coupon in mixed bacteria (NRB+SRB) inoculated cell under light microscopy after 21 days of immersion time in formation water +10% (v/v) crude oil; (d) pits which formed on the surface.

5.9 Concluding Remarks

The following conclusions can be made based on the results found:

- Addition of nitrate not only stimulates the growth of NRB, but also removes pre-existing sulphide.
- EIS is a useful electrochemical method to study film formation and/or corrosion products layer changes on the still surface. However, it will be beneficial to employ additional electrochemical tests, such as E_{corr}, LPR, and Potentiodynamic Tafel extrapolation in order to achieve more accurate results.
- These experiments prove that, in the pre-sour, corrosive (high chloride and sulphate) environment, bacteria may offer beneficial protection to carbon steel for a short immersion time. This is shown by a higher corrosion rate of corrosion coupons in control cell compared to corrosion coupons in the bacteria inoculated cell (NRB, SRB and mixed bacteria (NRB+SRB)).
- Localized corrosion in the presence of bacteria is inevitable. Therefore, the impact of bacterial biofilm over a longer time period and also the complex system of bacterial colonies and EPS for single cultures and a mixed bacteria culture need further study. The emphasis should be on the mixed bacteria population as it is the most likely occurring in the actual environment.

CHAPTER 6: Conclusions and Future Work

6.1 Conclusions

1. The NRB isolated from the production water and crude oil sample are able to suppress the growth of SRB, thus eliminating biogenic sulphide formation or H_2S gas production. Additionally, NRB are also able to oxidize the pre-existing sulphide.
2. In general, it is important to examine the corrosion effects of nitrate application on case by case basis because it is a complex mechanism and cannot be simply predicted based on electrochemical techniques alone.
3. It is proven that in corrosive, high chloride and sulphate media, bacteria may offer beneficial protection to both UNS S31603 and carbon steel for a short period of time. However, localized corrosion in the presence of bacteria is inevitable.
4. NRB decreased the critical pitting potential of the UNS S31603 to a greater extent than SRB; hence, increasing the risk of localised corrosion. However, it is also noted that the general corrosion rate of the UNS S31603 coupons in the SRB inoculated cell is higher than the corrosion rate of the UNS S31603 coupons in the NRB inoculated cell. Additionally, metastable pitting is found on the surface of the corrosion coupon in the SRB inoculated cell.
5. It is also noted that, in the presence of SRB, NRB does not grow aggressively on the UNS S31603; hence, the critical pitting potential can still be maintained at a "safe" level.
6. The corrosion rate of carbon steel corrosion coupons in this particular corrosive environment is more than 3 times higher compared to corrosion coupons in bacteria inoculated cell (NRB, SRB and mixed bacteria (NRB+SRB)).

6.2 Future Work

1. Investigations into the nitrate injection impact on steel materials in dynamic conditions that mimic the reservoir conditions should be conducted. This can be achieved by employing a sand packed bioreactor and placing the corrosion

coupons in the bioreactor inlet and outlet, simulating the injection pipe and the production pipe.

2. Further study on the dynamics of biofilm formation should be conducted to attain a better comprehension of the impact of the bacterial biofilm on corrosion, especially in the mixed bacteria culture as this is most likely what will naturally occur in any real situation.
3. Studies of the bacterial metabolism pathway and bacterial metabolite (such as nitrite and polysulphur) should be conducted to elucidate the uncertainty of the impact of nitrate injection on the corrosion of steel materials. Moreover, such studies can aid in understanding the fundamental biochemistry of nitrate injection, thus resulting in important information about the process and for the design of field applications.
4. A detailed study of the impact of nitrate and nitrite concentrations on the corrosion behaviour of UNS S31603 should be conducted in order to find the safe concentrations to avoid pitting corrosion.

Appendix 1

a)

b)

c)

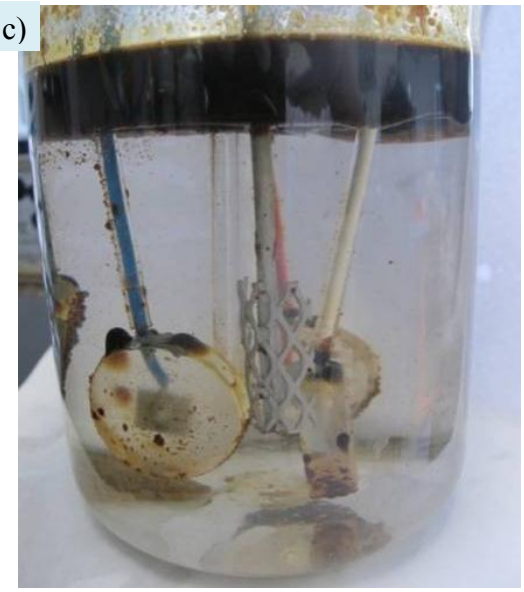

d)

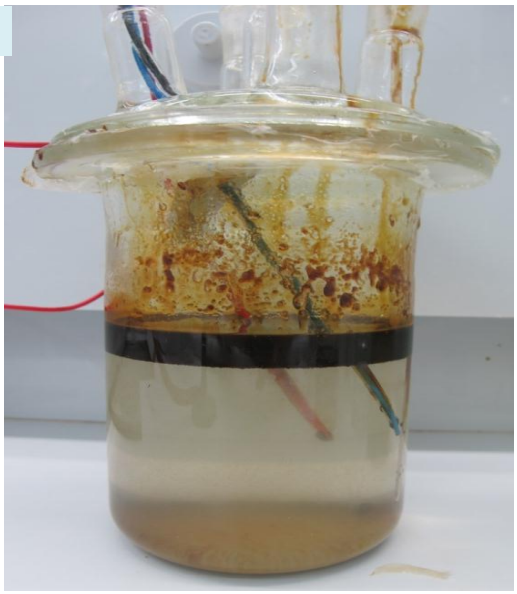

SRB inoculated cell (a) after 2 weeks of inoculation and immersion, the brine water starts to blacken; and (b) after 4 weeks of inoculation and immersion, sulphide precipitation can be easily seen on the bottom of the cell. Mixed bacteria (NRB+SRB) inoculated cell (c) after 2 weeks and (d) after 4 weeks of inoculation and immersion, no blackening occurs – NRB prevented sulphide formation

Appendix 2

a)

b)

c)

d)

SRB inoculated cell (a) after SRB inoculation, the brine water is black due to sulphide precipitation from inoculums, and (b) after 3 weeks of inoculation and immersion, the brine water was still black due to sulphide precipitation. Mixed bacteria (NRB+SRB) inoculated cell (c) after SRB and NRB inoculation, the brine water is black due to sulphide precipitation from the SRB inoculums; and (d) after 3 weeks of inoculation and immersion, no blackening – NRB oxidizes the sulphide.

References

1. Brown LR. Microbial Enhanced Oil Recovery (MEOR). Current Opinion in Microbiology. 2010;13(3):316-320.
2. Planckaert M. Oil Reservoir and Oil Production. In: Ollivier B, Magot M, editors. Petroleum Microbiology. Washington, DC: ASM Press; 2005. p. 3-19.
3. Donaldson EC, Chilingarian GV, Yen TF. Introduction : The Need for Microbial Enhanced Oil Recovery. In: Donaldson EC, Chilingarian GV, Yen TF, editors. Microbial Enhanced Oil Recovery. Amsterdam: Elsevier Science Publishing B.V.; 1989. p. 1-14.
4. Lazar I, Petrisor IG, Yen TF. Microbial Enhanced Oil Recovery (MEOR). Petroleum Science and Technology. 2007;25:1353-1366.
5. Magot M. Indigenous Microbial Communities in Oil Fields. In: Ollivier B, Magot M, editors. Petroleum Microbiology. Washington, DC: ASM Press; 2005. p. 21-33.
6. Magot M, Ollivier B, Patel BKC. Microbiology of Petroleum Reservoirs. Antonie van Leeuwenhoek. 2000;77:103-116.
7. Barnat IM. Biosurfactant Production and Possible Uses in Microbial Enhanced Oil Recovery and Oil Pollution Remediation : A Review. Bioresource Technology. 1995;51:1-12.
8. Portwood JT, editor. A Commercial Microbial Enhanced Oil Recovery Technology : Evaluation of 322 Projects. SPE/Production Operation Symposium; Oklahoma City, USA: Society of Petroleum Engineers, Inc ; 2-4 April 1995; SPE 29518.
9. Sen R. Biotechnology in Petroleum Recovery: The Microbial EOR. Progress in Energy and Combustion Science. 2008;34:714-724.
10. Gu JD, Moselio S. Corrosion, Microbial. Encyclopedia of Microbiology. Oxford: Academic Press; 2009. p. 259-269.
11. Stott JFD. Corrosion in Microbial Environments. In: Richardson TJA, editor. Shreir's Corrosion: Elsevier B.V; 2010. p. 1169-1190.
12. Little BJ, Lee JS. Microbiologically Influenced Corrosion. Revie RW, editor. New Jersey: John Wiley and Sons, Inc; 2007.

13. Jack TR. Microbial Enhancement of Oil Recovery. Current Opinion In Biotechnology. 1991;2:444-449.
14. McInerney MJ, Nagle DP, Knapp RM. Microbially Enhanced Oil Recovery : Past, Present and Future. In: Ollivier B, Magot M, editors. Petroleum Microbiology. Washington, DC: ASM Press; 2005. p. 215-237.
15. Anchliya A. New Nitrate Based Treatments-A Novel Approach to Control Hydrogen Sulfide in Reservoir and to Increase Oil Recovery. SPE/Europec/EAGE Annual Conference; 12-15 June 2006; Vienna, Austria: Society of Petroleum Engineers, Inc; 2006; SPE100337.
16. Hitzman DO, Dennis M, Hitzman DC. Recent Successes : MEOR Using Synergistic H_2S Prevention and Increased Oil Recovery Systems. SPE/DOE Fourteenth Symposium on Improved Oil Recovery; Tulsa, Oklahoma: Society of Petroleum Engineering, Inc; 17-21 April 2004; SPE 89453.
17. Hubert C. Microbial Ecology of Oil Reservoir Souring and Its Control by Nitrate Injection. In: K.N T, editor. Handbook of Hydrocarbon and Lipid Microbiology. Heidelberg: Springer-Verlag Berlin; 2010. p. 2754-2766.
18. Hubert C, Nemati M, Jenneman G, Voordouw G. Corrosion Risk Associated with Microbial Souring Control Using Nitrate or Nitrite. Applied Microbiology and Biotechnology. 2004;68:272-282.
19. Stott JFD, Dicken G, Rizk TY, editors. Corrosion Inhibition in PWRI System That Use Nitrate Treatment To Control SRB Activity and Reservoir Souring. Corrosion 2008 Conference and Expo; New Orleans, Lousiana, USA: NACE International; 16-20 March 2008; paper no 08507.
20. Bødtker G, Thorstenson T, Lillebø. B-L P, Thorbjørnsen BE, Ulvøen RH, Sunde E, et al. The Effect of Long-term Nitrate Treatment on SRB Activity, Corrosion Rate and Bacterial Community Composition in Offshore Water Injection Systems. Journal of Industrial Microbiology and Biotechnology. 2008;35:1625-1636.
21. Myhr S, Lillebo B-LP, Sunde E, Beeder J. Inhibition of Microbial H_2S Production in An Oil Reservoir Model Column by Nitrate Injection. Applied Microbiology and Biotechnology. 2001;58:400-408.

22. Reinsel MA, Sears JT, Stewart PS, McInerney MJ. Control of Microbial Souring by Nitrate, Nitrite or Glutaraldehyde Injection in A Sand Stone Column. Journal of Industrial Microbiology. 1996;17:128-136.
23. Voordouw G. Impact of Nitrate on The Sulfur Cycle in Oil Fields. In: Dahl CC, Friedrich CG, editors. Microbial Sulfur Metabolism. Berlin: Springer Berlin Heildelberg; 2008. p. 296-302.
24. An S, Tang K, Nemati M. Simultaneous Biodesulphurization and Denitrification Using an Oil Reservoir Microbial Culture: Effects of Sulphide Loading Rate and Sulphide to Nitrate Loading. Water Research. 2010;44:1531-1541.
25. Tang K, Baskaran V, Nemati M. Bacteria of The Sulphur Cycle : An Overview of Microbiology, Biokinetics and Their Role in Petroleum and Mining Industry. Biochemical Engineering Journal. 2009;44:73-94.
26. Hubert C, Nemati M, Jenneman G, Voordouw G. Containment of Biogenic Sulfide Production in Continuous Up-Flow Packed-Bed Bioreactors with Nitrate or Nitrite. Biotechnology Progress. 2003;19:338-345.
27. Nemati M, Jenneman G, Voordouw G. Impact of Nitrate-Mediated Microbial Control of Souring in Oil Reservoirs on The Extent of Corrosion. Biotechnology Progress. 2001;17:852-859.
28. Nemati M, Jenneman G, Voordouw G. Mechanistic Study of Microbial Control of Hydrogen Sulfide Production in Oil Reservoir. Biotechnology and Bioengineering. 2001;74:425-434.
29. de Lomas JG, Corzo A, Gonzalez JM, Andrades JA, Iglesias E, Montero MJ. Nitrate Promotes Biological Oxidation of Sulfide in Wastewater: Experiment at Plant-Scale. Biotechnology and Bioengineering. 2006;93(no 4):801-811.
30. Gardner LR, Stewart PS. Action of Glutaraldehyde and Nitrate Againts Sulfate-Reducing Bacterial Biofilms. Journal of Industrial Microbiology and Biotechnology. 2002;29:354-360.
31. Davidova I, Hicks MS, Fedorak PM, Suflita JM. The Influence of Nitrate on Microbial Processes in Oil Industry Production Waters. Journal of Industrial Microbiology and Biotechnology. 2001;27:80-86.
32. Dunsmore B, Youldon J, Thrasher DR, Vance I. Effects of Nitrate Treatment on Mixed Spesies, Oil Field Microbial Biofilm. Journal of Industrial Microbiology and Biotechnology. 2006;33:454-462.

33. Hubert C, Voordouw G, Mayer B. Elucidating Microbial Processes in Nitrate- and Sulfate-Reducing Systems Using Sulfur and Oxygen Isotope Ratios : The Example of Oil Reservoir Couring Control. Geochimica et Cosmochimica Acta. 2009;73:3864-3879.
34. Voordouw G, Nemati M, Jenneman G. Use of Nitrate-Reducing, Sulfide-Oxidizing Bacteria to Reduce Souring in Oil Field : Interactions with SRB and Effects on Corrosion. Corrosion 2002 Conference and Expo; Denver, Colorado, USA: NACE International; 7-11 April 2002; paper no 02034.
35. Schwermer CU, Lavik G, abed RMM, Dunsmore B, Ferdelman TG, Stoodley P, et al. Impact of Nitrate on Structure and Function of Bacterial Biofilm Communities in Pipelines Used for Injection of Seawater into Oil Fields. Applied and Environmental Microbiology. 2008;74(9):2841-2851.
36. Rempel CL, Evitts RW, Nemati M. Dynamics of Corrosion Rates Associated with Nitrite or Nitrate Mediated Control of Souring Under Biological Condition Simulating An Oil Reservoir. Journal of Industrial Microbiology and Biotechnology. 2006;33:878-886.
37. Voordouw G, Grigoryan A, Lambo A, Lin S, Park HS, Jack TR, et al. Sulfide Remediation by Pulsed Injection of Nitrate into a Low Temperature Canadian Heavy Oil Reservoir. Environmental Science and Technology. 2009;43(No 24):9512-9518.
38. Greene EA, Hubert C, Nemati M, Jenneman G, Voordouw G. Nitrate Reductase Activity of Sulphate-Reducing Bacteria Prevents Their Inhibition by Nitrate-Reducing, Sulphide Oxidizing Bacteria. Environmental Microbiology. 2003;5 607-617.
39. The Institute of Petroleum. The Stimulation of Nitrate Reducing Bacteria (NRB) in Oil Field System to Control Sulphate Reducing Bacteria (SRB), Microbiologically Influenced Corrosion (MIC) and Reservoir Souring : An Introduction Review. Hill G, Carberry P, Coleman M, Devine C, Dunsmore B, Herbert B, et al., editors. London: Energy Institute; 2003.
40. Videla HA, Herrera LK. Microbially Influenced Corrosion : Looking to The Future. International Microbiology. 2005;8:169-180.
41. Javaherdashti R. Microbiologically Influenced Corrosion. Derby B, editor. London: Springer; 2008.

42. Beech IB, Gaylarde CC. Recent Advances in The Study of Biocorrosion - An Overview. Revista de Microbiologia. 1999;30:177-190.
43. Sobrino FH, Monroy CR, Hernandez JK. Critical Analysis on Hydrogen as an Alternative to Fossil Fuels and Biofuels for Vehicles in Europe Renewable and Sustainable Energy Reviews. 2009;14(2):772-780.
44. Little BJ, Lee JS. Microbiologically Influenced Corrosion: John Wiley & Sons, Inc.; 2000.
45. Jayaraman A, Lee C-C, Chen MW, Mansfeld FB, Wood TK. I Inhibiting Sulphate-Reducing Bacteria in Biofilms by Expressing the Antimicrobial Peptides Indolicidin and Bactenecin. Journal of Industrial Microbiology. 1999;22:167-175.
46. Lewandowski Z, Wayne D, Lee W. Electrochemical Interactions of Biofilms with Metal Surfaces. WatSciTech. 1997;36 (no 1):295-302.
47. Zuo R. Biofilms: Strategies for Metal Corrosion Inhibition Employing Microorganism. Applied Microbiology and Biotechnology. 2007;76:1245-1253.
48. Iverson WP. Microbial Corrosion of Metals. Advances in Applied Microbiology. 1987;32:1-36.
49. Lee AK, Buehler MG, Newman DK. Influence of A Dual-spesies Biofilm on The Corrosion of Mild Steel. Corrosion Science. 2006;48:165-178.
50. Stadler R, Fuerbeth W, Harneit K, Grooters M, Woellbrink M, Sand W. First Evaluation of The Applicability of Microbial Extracellular Polimeric Substances for Corrosion Protection of Metal Substances. Electrochimica Acta. 2008;54:91-99.
51. Werner SE, Johnson CA, Laycock NJ, Wilson PT, Webster BJ. Pitting of Type 304 Stainless Steel in The Presence of Biofilm Containing Sulphate Reducing Bacteria. Corrosion Science. 1998;40(2-3):465-480.
52. Stoodley P, Boyle JD, DeBeer D, Lappin-Scott H. Evolving Perspectives of Biofilm Structure. Biofouling. 1999;14(1):75-90.
53. Denkhaus E, Maisen S, Telgheder U, Wingender J. Chemical and Physical Methods for Characterisation of Biofilms. Microchim Acta. 2007;158:1-27.
54. Videla HA. Manual of Biocorrosion. Florida: CRC Press, Inc; 1996.

55. Sanders P, Sturman PJ. Biofouling in The Oil Industry. In: Ollivier B, Magot M, editors. Petroleum Microbiology. Washington, DC: ASM Press; 2005. p. 171-198.
56. Yang L. Techniques for Corrosion Monitoring. Yang L, editor. Florida: Woodhead Publishing Limited; 2008.
57. Jayaraman A, Örneck D, Duarte DA, Lee C-C, Mansfeld FB, Wood TK. Axenic Aerobic Biofilms Inhibit Corrosion of Copper and Aluminum. Applied Microbiology and Biotechnology. 1999;52:787-790.
58. Örneck D, Jayaraman A, Syrett BC, Hsu C-H, Mansfeld FB, Wood TK. Pitting Corrosion Inhibition of Aluminum 2024 by Bacillus Biofilms Secreting Polyaspartate or γ-Polyglutamate. Applied Microbiology and Biotechnology. 2002;58:651-657.
59. Little BJ, Lee JS, Ray RI. A Review of 'Green' Strategies to Prevent or Mitigate Microbiologically Influenced Corrosion. Biofouling. 2007;23(2):87-97.
60. Videla HA. Understanding Microbial Inhibition of Corrosion. A Comprehensive Overview. International Biodeterioration and Biodegradation. 2009;63(7):896-900.
61. Moos O, Gumpel P. Comparison of the Microbiological Influenced on The Electro-Chemical Potential of Stainless Steel between Macro and Micro-areas of Specimens. Electrochimia Acta. 2008;54:53-59.
62. Almarshad AI, Jamal D. Electrochemical Investigations of Pitting Corrosion Behaviour of Type UNS S31603 Stainless Steel in Thiosulfate-Chloride Environment. Journal of Applied Electrochemistry. 2004;34:67-70.
63. Liou YM, Chiu SY, Lee CL, Shih HC. Electrochemical Pitting Behaviour of Type 321 Stainless Steel in Sulfide-Containing Chloride Solutions. Journal of Applied Electrochemistry. 1999;29:1377-1381.
64. Wilde BE, Williams E. The Use of Current/Voltage Curves for The Study of Localized Corrosion and Passivity Breakdown on Stainless Steels in Chloride Media. Electrochimica Acta. 1971;16(11):1971-1985.
65. Lopes FA, Morin P, Oliveira R, Melo LF. Interaction of *Desulfovibrio desulfuricans* Biofilm with Stainless Steel Surface and Its Impact on Bacterial Metabolism. Journal of Applied Microbiology. 2006;101:1087-1095.

66. Beech IB, Zinkevich V, Hanjangsit L, Gubner R. Modification of The Passive Layer on AISI 316 Stainless Steel in The Presence of *Pseudomonas* NCIMB 2021 Biofilm. 3rd Latin American Congress; 30 August - 4 September 1998; Cacun, Mexico: Houston, Tx : NACE International; 1998.
67. Migahed MA, Abd-El-Raouf M, Al-Sabagh AM, Abd-El-Bary HM. Effectiveness of Some Non Ionic Surfactants as Corrosion Inhibitors for Carbon Steel Pipelines in Oil Fields. Electrochimica Acta. 2005;50:4683-4689.
68. Race JM. Management of Corrosion of Onshore Pipelines. In: Tony JAR, editor. Shreir's Corrosion. Oxford: Elsevier; 2010. p. 3270-3306.
69. Chen G, Palmer RJ, White DC. Instrumental Analysis of Microbiologically Influenced Corrosion. Biodegradation. 1997;8(1997):189-200.
70. Mansfeld FB, Little BJ. A Technical Review of Electrochemical Techniques Applied to Microbiologically Influenced Corrosion. Corrosion Science. 1991;32(3):247-272.
71. Benetton XD. Biocomplexity and Electrochemical Influence of Biofilms in Carbon Steel Deterioration in Gasoline-Containing Environments [dissertation]. Mexico (America): Instituto Mexicano del Petroleo; 2007.
72. USGS. Reduction-Oxidation Potential (Electrode Method). Chapter 6 Field Measurement. USA: USGS; 2005.
73. Silverman DC. Tutorial on Cyclic Potentiodynamic Polarization Technique. Corrosion 1998 Conference and Expo; San Diego, California, USA: NACE International; 22-27 March 1998; paper no 98299.
74. Sheng X, Ting Y-P, Pehkonen SO. The Influence of Sulphate-Reducing Bacteria Biofilm on The Corrosion of Stainless Steel AISI 316. Corrosion Science. 2007;49:2159-2176.
75. Roberge PR. Handbook of Corrosion Engineering. New York: McGraw-Hill; 1999.
76. Szklarska Smialowska Z. Pitting and crevice corrosion. Houston: NACE International; 2005.
77. Beavers JA, Durr CL, Thompson NG. Unique Interpretation of Potentiodynamic Polarization Technique. Corrosion 1998 Conference and Expo; San Diego, California, USA: NACE International; 22-27 March 1998; paper no 98300.

78. Raetzer-Scheibe HJ, Tuck CDS. The Polarisation and Repassivation Behaviour of The Aluminium-Zinc-Magnesium-Copper Alloy 7010. Corrosion Science. 1994;36(6):941-56.
79. Mansfeld FB. he Use of Electrochemical Techniques for The Investigation and Monitoring of Microbiologically Influenced Corrosion and Its Inhibition- A Review. Materials and Corrosion. 2003;54:489-502.
80. Macdonald JR, Johnson WB. Fundamental of Impedance Spectroscopy. In: Barsoukov E, Macdonald JR, editors. Impedance Spectroscopy Theory, Experiment, and Application. Hoboken, New Jersey: John Wiley & Sons, Inc.; 2005. p. 1-20.
81. Scully JR. The Polarization Resistance Method for Determining of Instantaneous Corrosion Rates. In: Schweitzer PA, editor. Electrochemical Techniques in Corrosion Science and Engineering. New York: Marcel Dekker, Inc.; 2003. p. 124-150.
82. Gamry. Application Note : Basic of Electrochemical Impedance Spectroscopy. Gamry Instrument; 2010 [updated December 14, 2010; cited 2011 20 January]; Available from: http://www.gamry.com/App_Notes/EIS_Primer/Basics_Of_%20EIS.pdf.
83. Matsunami K, Kato T. Corrosion of Carbon Steel and its Estimation in Aqueous Solution Used in Petroleum Refineries. International Journal of Pressure Vessels and Piping 1991;45:179-197.
84. ASTM International. Standard Practice for Verification of Algorithm and Equipment for Electrochemical Impedance Measurements[1]. G 106-89. West Conshohocken, PA: ASTM International; 2010.
85. Bass. C, Sanders. P, Hilary L-S. Study of Biofilms of Sulfidogens from North Sea Oil Production Facilities Using Continous Flow Apparatus. Geomicrobiology Journal. 1998;15:101-120.
86. Wang. H, Fell. D, S B. Corrosion Inhibition Study for A H_2S Containing Water Injection System : A Field Investigation Using Electrochemical Techniques. Corrosion 2008 Conference and Expo; New Orleans, Lousiana, USA: NACE International; 16-20 March 2008; paper no 08644.
87. Kelland AM. Production Chemicals for the Oil and Gas Industry. Boca Raton: Taylor and Francis Group, LLC; 2009.

88. Hulecki. J.C, Foght. J.M, Gray. M.R, P.M F. Sulfide persistence in oil field waters amended with nitrate. Journal of Industrial Microbiology and Biotechnology. 2009;36:1499-1511.
89. Atlas RM. Handbook of Microbiological Media. Fourth Edition ed: Boca Raton : Taylor & Francis; 2010.
90. Gubner R. Biofilm and Accelerated Low-Water Corrosion of Carbon Steel Piling in Tidal Waters[disertation]. Portsmouth (United Kingdom): University of Portsmouth; 1998.
91. ASTM International. Standard Test Method for conducting potentiodinamic polarization resistance measurement. ASTM G 59-97. West Conshohocken, PA: ASTM International; 2009.
92. ASTM International. Standard Test Method for conducting Conducting Cyclic Potentiodynamic Polarization Measurements for Localized Corrosion Susceptibility of Iron-, Nickel-, or Cobalt-Based Alloys1. G 61-86. West Conshohocken, PA: ASTM International; 2009.
93. ASTM International. Standard Practice for calculation of corrosion rates and related information from electrochemical measurements. G102-89. West Conshohocken, USA: ASTM International; 2004.
94. ASTM International. Standard Practice for Preparing, Cleaning, and Evaluating Corrosion Test Specimens. G 1-03. West Conshohocken, USA: ASTM International; 2007.
95. APHA. Standard methods for the examination of water and wastewater/prepared and published jointly by American Public Health Association, American Water Work Association, and Water Environment Federation. 4500NO3-I. Washington D.C.: APHA-AWWA-WEF; 2005.
96. Ward OP, Singh A, Van Hamme JD, Voordouw G. Petroleum Microbiology. In: Moselio S, editor. Encyclopedia of Microbiology. Oxford: Academic Press; 2009. p. 443-456.
97. Grishchenkov VG, Townsend RT, McDonald TJ, Autenrieth RL, Bonner JS, Boronin AM. Degradation of Petroleum Hydrocarbons by Facultative Anaerobic Bacteria Under Aerobic and Anaerobic Conditions. Process Biochemistry. 2000;35(9):889-896.

98. Mechichi T, Patel BKC, Sayadi S. Anaerobic Degradation of Methoxylated Aromatic Compounds by Clostridium Methoxybenzovorans and A Nitrate-Reducing Bacterium *Thauera* sp. Strain Cin3,4. International Biodeterioration & Biodegradation. 2005;56(4):224-230.
99. Widdel F, Rabus R. Anaerobic Biodegradation of Saturated Aromatic Hydrocarbons. Current Opinion In Biotechnology. 2001;12:259-276.
100. Wilkes H, Boreham C, Harms G, Zengler K, Rabus R. Anaerobic Degradation and Carbon Isotopic Fractionation of Alkylbenzenes in Crude Oil by Sulphate-Reducing Bacteria. Organic Geochemistry. 2000;31(1):101-115.
101. Becerra HQ, Retamoso C, Macdonald DD. The Corrosion of Carbon Steel in Oil-in-Water Emulsions Under Controlled Hydrodynamic Conditions. Corrosion Science. 2000;42(3):561-575.
102. Nesic S. Key Issues Related to Modelling of Internal Corrosion of Oil and Gas Pipelines - A Review. Corrosion Science. 2007;49(12):4308-4338.
103. Zhang GA, Cheng YF. Electrochemical Corrosion of X65 Pipe Steel in Oil/Water Emulsion. Corrosion Science. 2009;51:901-7.
104. Bouazaze H, Huet F, Nogueira RP. A New Approach for Monitoring Corrosion and Flow Characteristics in Oil/Brine Mixture. Electrochimica Acta. 2005;50:2081-2090.
105. Willey JM, Sherwood LM, Woolverton CJ. Prescott, Harley, and Klein's Microbiology. 7th Edition ed. New york, USA: McGraw-Hill, Inc; 2008.
106. VanDemark PJ, Batzing BL. The Microbes: an introduction to their nature and importance. United States of America: Benjamin/Cummings Publishing Company, Inc; 1987.
107. Larsen J. Downhole Nitrate Application To Control Sulfate Reducing Bacteria Activity and Reservoir Souring. Corrosion 2002 Conference and Expo; Denver, Colorado, USA: NACE International; 7-11 April 2002; paper no 02025.
108. Dickinson WH, Lewandowski Z. Electrochemical Concepts and Techniques in the Study of Stainless Steel Ennoblement. Biodegradation. 1998;9:11-21.
109. Starosvetsky J, Starosvetsky D, Pokroy B, Hilel T, Armon R. Electrochemical Behaviour of Stainless Steels in Media Containing Iron-Oxidizing Bacteria (IOB) by Corrosion Process Modeling. Corrosion Science. 2008;50:540-547.

110. Starosvetsky D, Armon R, Yahalom J, Starosvetsky J. Pitting corrosion of carbon steel caused by iron bacteria. International Biodeterioration and Biodegradation. 2001;47:79-87.
111. Lewandowski Z, Beyenal H. Mechanism of Microbially Influenced Corrosion. In: Flemming HC, Murthy PS, Venkatesan R, Cooksey KE, editors. Marine and Industrial Biofouling. Berlin: Springerlink; 2008. p. 35-64.
112. Mansfeld F. The Interaction of Bacteria and Metal Surfaces. Electrochimia Acta. 2007;52:7670-7680.
113. Scotto V, Lai ME. Ennoblement of Stainless Steels in Seawater: A Likely Cxplanation Coming from The Field. Corrosion Science. 1998;40(6):1007-1018.
114. Little BJ, Lee JS, Ray RI. The Influence of Marine Biofilms on Corrosion : A Concise Review. Electrochimica Acta. 2008;54:2-7.
115. Shoesmith DW, Buchheit RG. Development of Corrosion Models Based on Electrochemical Measurements. In: Schweitzer PA, editor. Electrochemical Techniques in Corrosion Science and Engineering. New York: Marcel Dekker, Inc.; 2003.
116. Harrison PJ, Berges JA. Marine Culture Media. In: Andersen RA, editor. Algal Culturing Techniques. USA: Academic Press; 2005. p. 22.
117. Aminot A, Kerouel R. Autoclaved Sea Water as A Reference Material for The Determination of Nitrate and Phosphate in Sea Water. Analytica Chimica Acta. 1991;248(1):277-283.
118. Little B, Gerchakov S, Udey L. A Method for Sterilization of Natural Seawater. Journal of Microbiological Methods. 1987;7(4-5):193-200.
119. Starosvetsky D, Khaselev O, Starosvetsky J, Armon R, Yahalom J. Effect of Iron Exposure in SRB Media on Pitting Initiation. Corrosion Science. 2000;42:345-359.
120. Wilde BE. Critical Appraisal of Some Popular Laboratory Electrochemical Tests for Predicting the Localized Corrosion Resistance of Stainless Alloys in Sea Water. Corrosion. 1972;28(8):283-291.
121. Gayosso MJH, Olivares GZ, Ordaz NR, Ramirez CJ, Esquivel RG, Viveros AP. Microbial Consortium Influence upon Steel Corrosion Rate, Using Polarisation Resistance and Electrochemical Noise Techniques. Electrochimica Acta. 2004;49:4295–4301.

122. Da Silva S, Basseguy R, Bergel A. A New Definition of Cathodic Depolarization in Anaerobic Microbially Influenced Corrosion. Corrosion 2002 Conference and Expo; Denver, Colorado, USA: NACE International; 7-11 April 2002; paper no 02462
123. Yuan SJ, Pehkonen SO, Ting YP, Kang ET, Neoh KG. Corrosion Behaviour of Type 304 Stainless Steel in A Simulated Seawater-Based Medium in The Presence and Absence of Aerobic *Pseudomonas* NCIMB 2021. Ind Eng Chem Res. 2008;47:3008-3020.
124. Wu X, Ma H, Chen S, Xu Z, Sui A. General Equivalent Circuits for Faradaic Electrode Processes under Electrochemical Reaction Control. Journal of The Electrochemical Society. 1999;146(5):1847-1853.
125. Belkaid S, Ladjouzi MA, Hamdani S. Effect of Biofilm on Naval Steel Corrosion in Natural Seawater. Journal of Solid State Electrochemistry. 2011;15:525-537.
126. Yin Y, Cheng S, Chen S, Tian J, Liu T, Chang X. Microbiologically Influenced Corrosion of 303 Stainless Steel by Marine Bacterium *Vibrio natriegens*: (II) Corrosion Mechanism. Materials Science and Engineering C. 2009;29:756-760.
127. Gonzalez JEG, Santana FGH, Mirza-Rosca JC. Effect of Bacterial Biofilm on 316 SS Corrosion in Natural Seawater by EIS. Corrosion Science. 1998;40(12):2141-2154.
128. Beech IB. Corrosion of Technical Materials in The Presence of Biofilms - Current Understanding and State-of-The Art Methods of Study. International Biodeterioration and Biodegradation. 2004;53:177-183.
129. Castaneda H, Benetton XD. SRB-Biofilm Influenced in Active Corrosion Sites Formed at The Steel Electrolyte Interface When Exposed to Artificial Seawater Condition. Corrosion Science. 2008;50:1169-1183.